THREE-DIMENSIONAL COMPUTATIONAL ANALYSIS OF INLET AND FLOW CHARACTERISTICS IN PROTON EXCHANGE MEMBRANE FUEL CELL

KEERASUT SUTTANARAK

A THESIS SUBMITTED IN PARTIAL FULFILLMENT
OF THE REQUIREMENT FOR THE DEGREE OF
MASTER OF ENGINEERING IN AUTOMOTIVE ENGINEERING
(INTERNATIONAL PROGRAM) INTERNATIONAL COLLEGE
KING MONGKUT'S INSTITUTE OF TECHNOLOGY LADKRABANG
2010

KMITL-2010-IC-M-004-001

Thesis Title	Three-Dimensional Computational Analysis of Inlet and Flow Characteristics in Proton Exchange Membrane Fuel Cell
Student	Mr. Keerasut Suttanarak
Student ID.	50061925
Degree	Master of Engineering
Program	Automotive Engineering (International Program)
Year	2010
Thesis Advisor	Assoc.Prof.Dr. Jarruwat Charoensuk Dr. Nirut Naksuk Prof. Shuichiro Hirai

ABSTRACT

Fuel cells are electrochemical devices that rely on the transport of reactants (oxygen and hydrogen) and products (water and heat). These transports are coupled with electrochemistry and further complicated by phase change, porous media (gas diffusion electrodes) and a complex geometry. This research presents a three dimensional computational model of a proton exchange membrane fuel cell (PEMFC). It is the aim of this research to develop fundamental understanding of transport phenomena in PEMFC and to investigate the impact of inlet humidity at both anode and cathode sides. The mathematical model is limited to single phase flow with electrochemical reaction in porous media. The results show that at higher humidity condition, higher efficiency is achieved corresponding to the reaction heat source and water transport. This also includes higher effects of electro osmotic drag and water back diffusion. Moreover the effect of flow configurations (Co and Counter Flow) is studied by taking into account the concentration of hydrogen, oxygen and electrochemical reaction. At the operating potential, we have found that the effect of flow pattern at low current is insignificant. On the other hand, at high current condition, the Counter-flow pattern gives higher rate of water and heat sources thus yielding higher voltage than the Co-flow pattern apparently due to decrease in the concentration loss.

ACKNOWLEDGEMENT

This thesis could not be completed without the assistance of many persons to whom I would like to express my sincere appreciation.

First, I would like to sincerely thank my advisor, Assoc.Prof.Dr. Jarruwat Charoensuk, who has given me many helpful suggestions.

I would like to sincerely thank Dr. Nirut Naksuk for kind advising and helping, and Prof. Shuichiro Hirai for the suggestion of PEM Fuel Cell.

I would also like to thank Mr. Niwat Phoocharoen for well suggestion in using software and thank Electrochemical Materials and Systems Laboratory, National Metal and Materials Technology Center for the software package used in this research.

Moreover, I would like to show gratitude to National Metal and Materials Technology Center (MTEC), especially the Automation and Mechatronic laboratory for providing the high performance computer as well as financial supporting.

I am grateful to National Science and Technology Development Agency (NSTDA), which provided the full scholarship for studying in the master program.

Finally, I am very grateful to my family for all love, caring, understanding and motivation throughout my life.

Keerasut Suttanarak

CONTENTS

Page

ABSTRACT..... I

ACKNOWLEDGEMENT..... II

CONTENTS.....III

LIST OF TABLES.....VI

LIST OF FIGURES.....VII

CHAPTER 1 INTRODUCTION.....1

1.1 Significance and Background..... .1

1.2 Objectives.....1

1.3 Scopes.....1

1.4 Expected Benefits.....2

CHAPTER 2 THEORY AND LITERATURE REVIEWS.....3

2.1 Types of Fuel Cell.....3

2.1.1 Alkaline Fuel Cell (AFC).....3

2.1.2 Phosphoric Acid Fuel Cell (PAFC)..... 4

2.1.3 Molten Carbonate Fuel Cell (MCFC).....5

2.1.4 Solid Oxide Fuel Cell (SOFC)..... 6

2.1.5 Direct Methanol Fuel Cell (DMFC).....7

2.16 Polymer Electrolyte Membrane Fuel Cell (PEMFC).....7

2.2 Fuel Cell Components..... 8

2.2.1 Polymer Electrolyte Membrane.....8

2.2.2 Gas Diffusion Layers.....8

2.2.3 Catalyst Layers.....9

2.2.4 Bipolar Plates.....9

2.3 Fuel cell thermodynamic.....10

2.3.1Basic Reaction.....10

2.3.2 Heat of Reaction.....10

CONTENTS (CONT.)

Page

2.3.3 Higher and Lower Heating Value of Hydrogen.....11

2.3.4 Theoretical Electrical Work.....12

2.3.5 Theoretical Fuel Cell Potential.....12

2.3.6 Effect of Temperature.....13

2.3.7 Effect of Pressure.....13

2.4 Fuel cell Electrochemistry.....15

2.4.1 Electrode Kinetics.....15

2.4.2 Reaction Rate.....15

2.4.3 Reaction constants, transfer coefficient.....16

2.4.4 Current Potential Relationship—Butler-Volmer Equation.....17

2.4.5 Exchange Current Density.....18

2.4.6 Over-potentials and Crossover Losses in Fuel Cells.....20

2.4.6.1 Activation Polarization.....21

2.4.6.2 Ohmic Polarization.....22

2.4.6.3 Concentration Polarization.....23

2.5 Principle of Fluent 6.3.....24

2.6 Literature Reviews.....30

CHAPTER 3 INVESTIGATION PROCEDURES.....32

3.1 Computational Domain.....32

3.2 Computational Diagram.....33

3.3 Computational Grid.....34

3.4 Model Assumption.....36

3.5 Effect of inlet humidification to cell performance.....37

3.6 Effect of Co and Counter flow to cell performance.....38

CONTENTS (CONT.)

Page

CHAPTER 4 RESULTS AND DICUSSIONS.....39

4.1 Model validation.....39

4.2 Effect of inlet humidification on cell performance.....40

4.3 Effect of Co and Counter Flow on Cell Performance.....59

CHAPTER 5 CONCLUSION AND SUGGESTIONS.....68

5.1 Conclusion.....68

5.2 Suggestions.....68

REFERENCES.....69

BIOGRAPHY.....72

LIST OF TABLES

Table Page

3.1 Basic Parameter for all cases.....36

3.2 Model Dimension of all cases.....37

3.3 Different flow conditions used for different inlet humidity conditions.....37

LIST OF FIGURES

Figure Page

2.1 Schematic of a PEMFC....3

2.2 Schematic of an AFC....4

2.3 Schematic of a PAFC....5

2.4 Schematic of a MCFC....6

2.5 Schematic of a SOFC....7

2.6 Combustion of H_2+1/2O_2 in a calorimetric bomb-measurement of higher heating value....11

2.7 Combustion of H_2 with excess O_2 in a calorimetric bomb-measurement of lower heating value12

2.8 Schematic of PEM Fuel Cell....24

2.9 Boundary condition for ϕ_{sol} and ϕ_{mem} 26

3.1 Computational Domain....32

3.2 Cross section schematic of PEMFC.... 33

3.3 Computational Diagram 34

3.4 Computational Grid (Cross section view).... 35

3.5 Computation Grid (Perspective view)....36

3.6 Schematic of Co-Flow.... 38

3.7 Schematic of Counter-Flow.... 38

4.1 IV Polarization Curve between Simulation and Experiment....39

4.2 Temperature distribution along the channel for case of very low humidity....40

4.3 Temperature distribution along the channel for case of low humidity....41

4.4 Temperature distribution along the channel for case of high humidity....41

4.5 Temperature distribution along the channel for case of very high humidity....42

4.6 Reaction Heat Source for case of very low humidity.... 43

4.7 Reaction Heat Source for case of low humidity.... 43

4.8 Reaction Heat Source for case of high humidity.... 44

4.9 Reaction Heat Source for case of very high humidity.... 44

4.10 Osmotic Drag Source at the anode TPB for case of very low humidity....46

4.11 Osmotic Drag Source at the anode TPB for case of low humidity....46

4.12 Osmotic Drag Source at the anode TPB for case of high humidity....47

4.13 Osmotic Drag Source at the anode TPB for case of very high humidity....47

LIST OF FIGURES (CONT.)

Figure Page

4.14 Osmotic Drag Source at the cathode TPB for case of very low humidity..... 48

4.15 Osmotic Drag Source at the cathode TPB for case of low humidity..... 48

4.16 Osmotic Drag Source at the cathode TPB for case of high humidity..... 49

4.17 Osmotic Drag Source at the cathode TPB for case of very high humidity..... 49

4.18 Back Diffusion Mass Source at the anode TPB for case of very low humidity..... 50

4.19 Back Diffusion Mass Source at the anode TPB for case of low humidity..... 50

4.20 Back Diffusion Mass Source at the anode TPB for case of high humidity..... 51

4.21 Back Diffusion Mass Source at the anode TPB for case of very high humidity..... 51

4.22 Back Diffusion Mass Source at the cathode TPB for case of very low humidity..... 52

4.23 Back Diffusion Mass Source at the cathode TPB for case of low humidity..... 52

4.24 Back Diffusion Mass Source at the cathode TPB for case of high humidity..... 53

4.25 Back Diffusion Mass Source at the cathode TPB for case of very high humidity..... 53

4.26 Protonic conductivity at the anode TPB for case of very low humidity..... 54

4.27 Protonic conductivity at the anode TPB for case of low humidity..... 55

4.28 Protonic conductivity at the anode TPB for case of high humidity..... 55

4.29 Protonic conductivity at the anode TPB for case of very high humidity..... 56

4.30 Protonic conductivity at the cathode TPB for case of very low humidity..... 56

4.31 Protonic conductivity at the cathode TPB for case of low humidity..... 57

4.32 Protonic conductivity at the cathode TPB for case of high humidity..... 57

4.33 Protonic conductivity at the cathode TPB for case of very high humidity..... 58

4.34 IV Polarization Curve of Inlet humidification..... 59

4.35 IV Polarization Curve between Co-Flow and Counter-Flow..... 60

4.36 H_2 Mass fraction along the channel of Co-flow..... 62

4.37 H_2 Mass fraction along the channel of Counter-flow..... 62

4.38 O_2 Mass fraction along the channel of Co-flow..... 63

4.39 O_2 Mass fraction along the channel of Counter-flow..... 63

4.40 Molar Concentration of H_2O along the Channel of Co-flow..... 64

4.41 Molar Concentration of H_2O along the Channel of Counter-flow..... 64

4.42 Temperature distribution along the channel of Co-flow..... 65

LIST OF FIGURES (CONT.)

Figure Page

4.43 Temperature distribution along the channel of Counter-flow..... 66

4.44 Reaction Heat Source of Co-flow configuration..... 67

4.45 Reaction Heat Source of Counter-flow configuration..... 67

CHAPTER 1

INTRODUCTION

1.1 Significance and Background

Proton Exchange Membrane Fuel Cell (PEMFC), with its zero emission and numerous future commercial prospects, is a promising future energy technology. To develop an efficient fuel cell system, it is necessary to understand its underline mechanisms such as non-uniform concentration, current density distributions, high ionic resistance due to dry membrane, or high diffusive resistance due to the flooding on the cathode. These phenomena can cause performance loss. Water management is a key challenging problem in PEMFC design and operation. Effective water management is a critical requirement to operate PEMFC at high current density. Membrane in PEMFC needs to be fully hydrated to conduct ionic current thus low resistive loss. However, excessive water can result in flooding in the catalyst layer or the diffusion layer. In the worst case, water in liquid phase will block the reactant flow channels. Numerical simulation is the interesting tool to be used for this research. Although the model is limited to a single phase flow, it will be used to predict transport phenomena such as temperature distribution as well as investigate hydrogen, oxygen and water concentration along the channels, which are affected by the difference in flow distribution. Our investigation covers co-flow and counter-flow configuration at low and high current density and also covers a study on the effect of inlet humidification on the cell performance.

1.2 Objectives

1.2.1 To investigate transport phenomena of Proton Exchange Fuel Cell such as, temperature distribution, concentration of fuel, reactant and product, water source term, electro osmotic drag and water back diffusion by numerical simulation under different flow configuration and inlet humidity.

1.3 Scopes

1.3.1 Investigate the inlet humidification effect (anode and cathode) on cell performance.

1.3.2 Study the effect of flow configuration (Co-flow and Counter-flow) on cell performance.

1.4 Expected Benefits

1.4.1 To analyze the significance of inlet humidification to cell performance.

1.4.2 To understand the transport phenomena by comparing the result between co-flow and counter-flow configurations.

1.4.3 To determine the operation limit of the cell by looking at the water concentration level inside the flow channel. This could be an informative data for the direction of flow channel design and stack optimization in the further.

CHAPTER 2

THEORY AND LITERATURE REVIEWS

2 Fuel Cell Theory

In this chapter brings together, with certain degree of summary, the material from many sources including the introduction and theoretical review of Fuel cells as already seen in the literatures. For completeness of the content, readers should refer to the original manuscript at [1], [16].

2.1 Types of Fuel Cells

2.1.1 Alkaline Fuel Cell (AFC)

The electrolyte in this fuel cell uses a concentrated potassium hydroxide and can use a variety of non-precious metals as a catalyst at the anode and cathode. AFC high performance is due to the rate at which chemical reactions take place in the cell. They have also demonstrated high efficiencies in space applications. The reactions taking place in an AFC is,

$$Anode\ H_2 + 2(OH)^- \rightarrow 2H_2O + 2e^- \quad (2.1)$$

$$Cathode\ \frac{1}{2}O_2 + H_2O + 2e^- \rightarrow 2(OH)^- \quad (2.2)$$

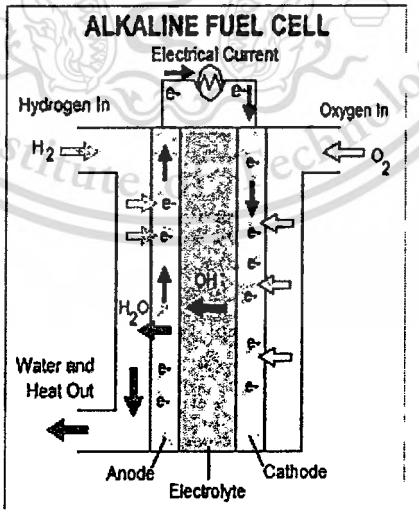

Figure 2.1 Schematic of an AFC [13]

The main problem encountered with AFC is that catalysts can easily be poisoned by CO_2. Even small amounts of CO_2 in the air can poison the catalyst. Thus, air and hydrogen must be purified before they enter the cell. However, this process is expensive. Fuel cell's life is affected

by the catalyst poisoning which will increase the costs. Up to 8000 hours of AFC stacks have maintained sufficiently stable operation. However, they need to sustain the operation for at least 40000 hours to become economically viable, but that long operation has been regarded as impossible for AFC due to material durability issues. This, being the most significant obstacle in commercializing this fuel cell technology, let AFC only be used proper applications.

2.1.2 Phosphoric Acid Fuel Cell (PAFC)

PAFC also use liquid electrolyte. Phosphoric acid is contained in a Teflon bonded silicon carbide matrix. As in PEMFC, the platinum catalyst is used to enhance the reaction. Chemical reactions taking place in PAFC is the same as those in PEMFC. PAFC is the first fuel cell type that is used commercially for its technological maturity. As stated before the first stationary power generation application was established with a PAFC. Apart from stationary applications, PAFC is used in heavy duty transportation like city busses.

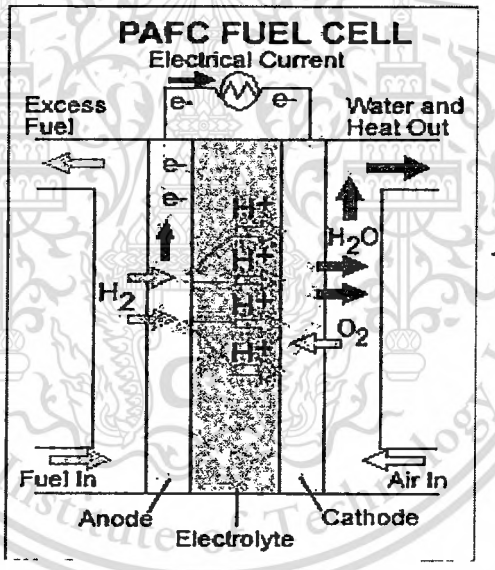

Figure 2.2 Schematic of a PAFC [13]

$$Anode\, 2H_2 \rightarrow 4H^+ + 4e^- \quad (2.3)$$

$$Cathode\, O_2 + 4H^+ + 4e^- \rightarrow 2H_2O \quad (2.4)$$

Effects of impurities in the fuel like CO poisoning are less in PAFC than that of PEMFC. Also, because the operating temperature is higher in this type of fuel cells, it is suitable for cogeneration applications thus PAFC can be utilized to be more efficient than PEMFC. However, the efficiency drops to 30 -40% when the stack is used standalone. The main disadvantage of this fuel cell is that the power density is less than those of other fuel cell types. As a result, these fuel

cells are typically large and heavy. PAFC is also expensive because like in PEMFC expensive platinum catalyst is used.

2.1.3 Molten Carbonate Fuel Cell (MCFC)

The electrolyte in this fuel cell is usually a combination of molten carbonate salt mixture suspended in a porous ceramic matrix of lithium aluminum oxide ($LiAlO_2$). Alkali carbonates form a highly conductive molten ionic transfer salt at high operating temperatures of 600 to 700 C. At these temperatures Ni anode and NiO cathode is sufficient to promote reactions without any requisite of noble catalyst metals, reducing the cost. The reactions taking place in this type of fuel cell is

$$Anode\ H_2 + CO_3^{-2} \rightarrow H_2O + CO_2 + 2e^- \quad (2.5)$$

$$Cathode\ \frac{1}{2}O_2 + CO_2 + 2e^- \rightarrow CO_3^{-2} \quad (2.6)$$

Efficiency improvement in MCFC is also another factor for cost reduction. Molten carbonate fuel cells can reach efficiencies approaching 60 percent, considerably higher than the 37-42 percent efficiencies of a phosphoric acid fuel cell plant. Cogeneration system efficiencies can rise up to 85%, by bleeding natural gas fuel to the exhaust of the fuel cell and feeding into a turbine.

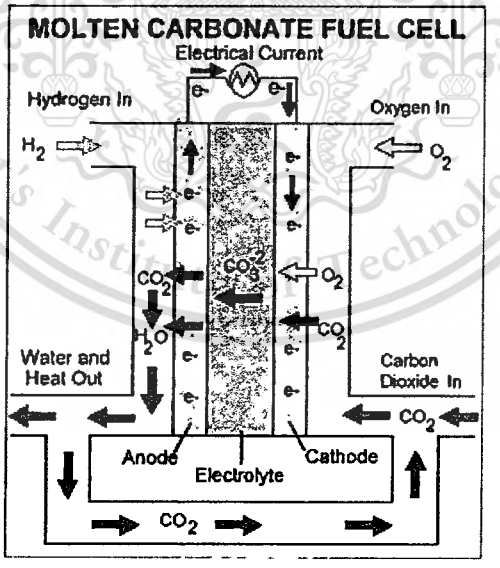

Figure2.3 Schematic of a MCFC [13]

In the previous fuel cell types external reforming must be employed to produce hydrogen. However, in MFCF, unlike alkaline, phosphoric acid, and polymer electrolyte membrane fuel cells, conversion to hydrogen can be carried out inside the fuel cell resulting in total cost reduction. MFCF is less sensitive to impurities in the fuel like CO and CO_2 than the

previous types. In fact, if the resistance of MCFC to other impurities such as sulfur is improved, even internal reforming of coal can be realized. The trade off coming with the high operation temperatures is that while the high temperature enhances the efficiency and reduces the cost thanks to preclusion of noble metals, the corrosion and breakdown of the cell components decrease cell life. Corrosion-resistant materials for components and fuel cell designs are great interests of the researchers to increase cell life without decreasing performance.

2.1.4 Solid Oxide Fuel Cell (SOFC)

The governing reactions are,

$$Anode\ H_2 + O^{-2} \rightarrow H_2O + 2e^- \tag{2.7}$$

$$Cathode\ \frac{1}{2}O_2 + 2e^- \rightarrow O^{-2} \tag{2.8}$$

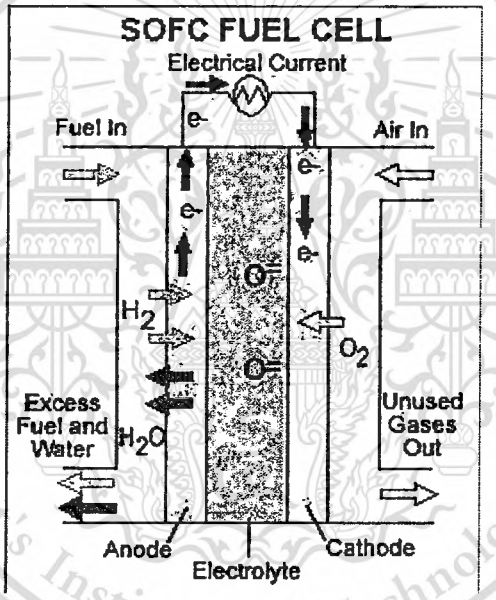

Figure 2.4 Schematic of a SOFC [13]

SOFC has the advantages of high operating temperatures such as high efficiencies, cogeneration capabilities and reduction of the cost due to the removal of the need for an expensive catalyst. Also the internal reforming capability should be appended in this perspective. In addition, the high resistance of SOFC to sulfur lets gases made of coal to be used within the fuel cell. Along with the disadvantages listed for MCFC, high temperature operation makes slow down of the SOFC start up. Also the safety requirements related to temperature makes SOFC not convenient for transportation and portable applications. However they are acceptable for utility applications. Scientists are currently exploring the potential for developing lower-temperature SOFC operating at or below 800°C that have fewer durability problems and less cost.

2.1.5 Direct Methanol Fuel Cell (DMFC)

Unlike the other types this type fuel cell does not use hydrogen as the fuel; methanol (CH_3OH) is fed directly to the anode where it is oxidized. DMFC usually utilize a polymer electrolyte similar to proton-exchange membrane (PEM) fuel cells. An acidic electrolyte is necessary to reject the CO_2 that is produced during the electro oxidation of methanol and because carbonate formation is a serious problem in alkaline solutions. The reactions in the cell are

$$Anode\ CH_3OH + H_2O \rightarrow CO_2 + 6H^+ + 6e^- \quad (2.9)$$

$$Cathode\ \frac{3}{2}O_2 + 6H^+ + 6e^- \rightarrow 3H_2O \quad (2.10)$$

Since methanol is easily provided and transported using the exist infrastructure, DMFC does not have fuel storage problems typical of the most types. Also the cost of the system is reduced because no reforming is needed though it operates at low temperatures and less catalyst is used. Direct methanol fuel cell technology is relatively new compared to hydrogen air fuel cell technology. However technological maturity is not sufficient for commercial use. The main problem with this fuel cell is the higher system complexity.

2.1.6 Polymer Electrolyte Membrane Fuel Cells (PEMFC)

PEMFC is a proton conductor membrane sandwiched between two electrodes. To have a good conduction of the ions, membrane must be well humidified. By product of the operation in this type is water mainly on the cathode side and heat. Since the operating temperatures are low due limitations imposed by the polymer membrane, produced heat cannot be used in cogeneration applications. Low temperature operation of PEMFC allows quick starts because of the shorter warm-up time and better durability due to less wear on system components. However, high Pt catalyst loadings are required to promote the reactions at the operating temperatures. Moreover, the catalyst is sensitive to CO poisoning, thus pure hydrogen fuel is required. The following chemical reactions take place in the electrodes.

$$Anode\quad H_2 \rightarrow 2H^+ + 2e^- \quad (2.11)$$

$$Cathode\ \frac{1}{2}O_2 + 2H^+ + 2e^- \rightarrow H_2O \quad (2.12)$$

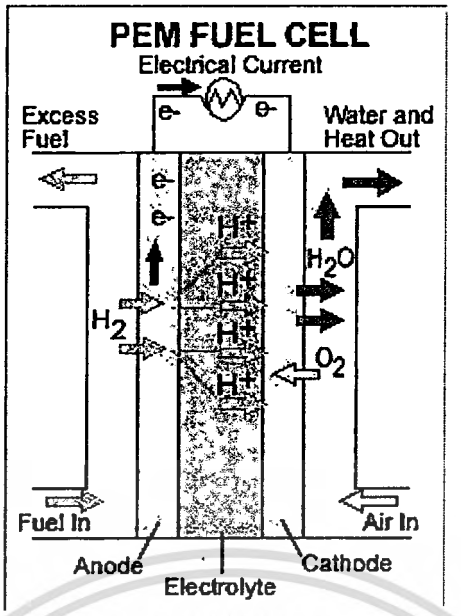

Figure 2.5 Schematic of a PEMFC [13]

Due to the fast start up time, low sensitivity to orientation, and favourable power to weight ratio, PEMFC is preferred to be used in transportation applications. Currently, hydrogen storage is one of the technology issues limiting the use of PEMFC in vehicles due to low energy density of hydrogen tanks (and other competing forms of on board storage) it is difficult for the vehicle to travel the same distance as the gasoline powered cars. In case of the utilization of hydrogen from liquids with high energy density like methanol or natural gas, onboard reformers must be used which increased cost, maintenance requirements and the complexity of the design.

2.2 Fuel Cell Components

2.2.1 Polymer Electrolyte Membrane

The Polymer electrolyte membrane (PEM) is probably the most complex and sensitive component of the PEMFC. At the core of a PEMFC is the polymer electrolyte membrane that separates the anode from the cathode. The desired characteristics of PEM is high proton conductivity, good electronic insulation, good separation of fuel in the anode side from oxygen in the cathode side, high chemical and thermal stability, and low production cost One type of PEM that meets most of these requirements is Nafion.

2.2.2 Gas Diffusion Layers

The typical materials for gas diffusion layers are carbon paper and carbon cloth. These are porous materials. The functions of the gas diffusion layers are to provide structural support for the catalyst layers, passages for reactant gases to reach the catalyst layers and transport of water to or from the catalyst layers, electron transport from the catalyst layer to the bipolar plate in the

anode side and from the bipolar plate to the catalyst layer in the cathode side, and heat removal from the catalyst layers. Gas diffusion layers are usually coated with Teflon to reduce flooding which can significantly reduce fuel cell performance due to poor reactant gas transport.

2.2.3 Catalyst Layers

The best catalyst material for both anode and cathode PEM fuel cell is platinum. Since the catalytic activity occurs on the surface of the platinum particles, it is desirable to maximize the surface area of the platinum particles. A common procedure for surface maximization is to deposit the platinum particles on larger carbon black particles. Several methods of applying the catalyst layer to the gas diffusion electrode have been reported. These methods are spreading, spraying, and catalyst power deposition. For the spreading method, a mixture of carbon support catalyst and electrolyte is spread on the GDL surface by rolling a metal cylinder on its surface. In the spraying method, the catalyst and electrolyte mixture is repeatedly sprayed onto the GDL surface until a desired thickness is achieved. A common problem of the anode catalyst is CO poisoning. Since platinum has a strong affinity for CO and CO exists in very small amount in the common reformed hydrogen fuel. Doping platinum with ruthenium has been shown to reduce the effect of CO poisoning.

2.2.4 Bipolar Plates

The functions of the bipolar plate are to provide the pathways for reactant gas transport and electron conduction paths from one cell to another in the fuel cell stack, separate the individual cells in the stack, carry water away from the cells, and provide cooling passages. Plate material and topologies facilitate these functions. Common plate topologies are straight, serpentine, or inter-digitated flow fields. Desirable material characteristics of bipolar plates are high electrical conductivity, impermeability to gases, good thermal conductivity, light weight, high corrosion resistance, and easy to manufacture. The common materials used in bipolar plates are graphite, metals such as stainless steel, aluminum, or composite materials. Graphite plates meet most of the requirements for optimal fuel cell performance however the disadvantage of graphite plates is the high cost of machining the flow fields. Metallic plates are cheap and easy to manufacture, but they have high contact resistance due to the metal oxide layer forming between the plate and the gas diffusion layer. Metallic plates also suffer high degradation from the corrosive fuel cell environment that leads to short life cycles. However, some coated metallic plates have been shown to produce performance comparable to graphite plates. Finally, composite

plates can offer the combined advantages of high electrical and thermal conductivity of graphite plates and low manufacturing cost of metallic plates.

2.3 Fuel cell thermodynamic

2.3.1Basic Reaction

The electrochemical reactions in fuel cells happen simultaneously on both sides of the membrane- the anode and the cathode. The basic fuel cell reactions are

At the anode

$$H_2 \rightarrow 2H^+ + 2e^- \tag{2.13}$$

At the cathode

$$\tfrac{1}{2}O_2 + 2H^+ + 2e^- \rightarrow H_2O \tag{2.14}$$

Overall

$$H_2 + \tfrac{1}{2}O_2 \rightarrow H_2O \tag{2.15}$$

2.3.2 Heat of Reaction

The overall reaction is the same as the reaction of hydrogen combustion. Combustion is an exothermic process, which means that there is energy released in the process:

$$H_2 + \frac{1}{2}O_2 \rightarrow H_2O + heat \tag{2.16}$$

The heat (or enthalpy) of a chemical reaction is the difference between the heats of formation of products and reactants. For the previous, this means:

$$\Delta H = (h_f)_{H_2O} - (h_f)_{H_2} - \frac{1}{2}(h_f)_{O_2} \tag{2.17}$$

Heat of formation of liquid water is -286kJmol (at 25°C) and heat of formation of elements is by definition equal to zero. Therefore

$$\Delta H = (h_f)_{H_2O} - (h_f)_{H_2} - \frac{1}{2}(h_f)_{O_2} = -286kJ/g - 0 - 0 = -286kJ.mol^{-1} \tag{2.18}$$

Note that the negative sign for enthalpy of a chemical reaction, by convention, means that heat is being released in the reaction, that is, this is an exothermic reaction may now be rewritten as:

$$H_2 + \frac{1}{2}O_2 \rightarrow H_2O(l) + 286\,kJ/mol \tag{2.19}$$

Here a positive sign is used because the enthalpy is placed on the right side of the reaction, clearly meaning a product of the reaction. This equation is valid at 25°C only, meaning that both the reactant gases and the product water are at 25°C. At 25°C, and atmospheric pressure, water is in liquid form.

2.3.3 Higher and Lower Heating Value of Hydrogen

The enthalpy of hydrogen combustion reaction is also called the hydrogen's heating value. It is the amount of heat that may be generated by a complete combustion of 1 mol of hydrogen. The measurement of a heating value is conducted in a calorimetric bomb. If 1 mol of hydrogen is enclosed in a calorimetric bomb with 72 mol of oxygen, ignited, fully combusted, and allowed to cool down to 25°C, at atmospheric pressure there will be only liquid water left in the bomb (Figure 2.6). The measurement should show that 286kJ of heat was released. This is known as hydrogen's higher heating value. However, if hydrogen is combusted with sufficient excess of oxygen (or air) and allowed to cool down to 25°C, the product water will be in the form of vapor mixed with unburned oxygen and/or nitrogen in case that air was used (Figure 2.7). The measurement should show that less heat was released, exactly 241 kJ. This is known as hydrogen's lower heating value.

$$H_2 + \frac{1}{2}O_2 \rightarrow H_2O(g) + 241kJ/mol^{-1} \qquad (2.20)$$

The difference between higher and lower heating value is the heat of evaporation of water (at 25°C)

$$H_{fg} = 286 - 241 = 45kJmol^{-1} \qquad (2.21)$$

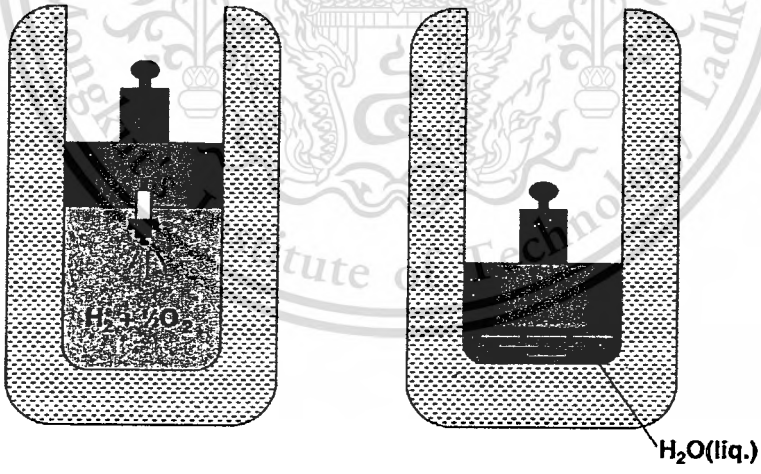

Figure 2.6 Combustion of H_2+1/2O_2 in a calorimetric bomb-measurement of higher heating value [1]

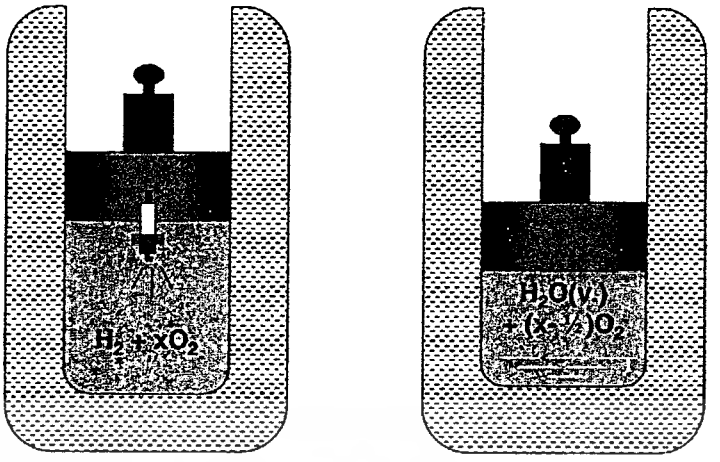

Figure 2.7 Combustion of H_2 with excess O_2 in a calorimetric bomb-measurement of lower heating value [1]

2.3.4 Theoretical Electrical Work

Hydrogen heating value is used as a measure of energy input in a fuel cell. This is the maximum amount of (thermal) energy that may be extracted from hydrogen. However, electricity is produced in a fuel cell. In every chemical reaction some entropy is produced, and because of that, a portion of the hydrogen's higher heating value cannot be converted into useful work-electricity. The portion of the reaction enthalpy (or hydrogen's higher heating value) that can be converted to electricity in a fuel cell corresponds to Gibbs free energy and is given by the following equation.

$$\Delta G = \Delta H - T\Delta S \tag{2.22}$$

In other words, there are some irreversible losses in energy conversion due to creation of entropy ΔS. Similarly, as ΔH for the reaction is the difference between the heats of formation of products and reactants ΔS is the difference between entropies of products and reactants

$$\Delta S = (S_f)_{H_2O} - (S_f)_{H_2} - \frac{1}{2}(S_f)_{O_2} \tag{2.23}$$

2.3.5 Theoretical Fuel Cell Potential

In general, electrical work is a product of charge and potential:

$$W_{el} = qE \tag{2.24}$$

Where

W_{el} = electrical work (Jmol^{-1})

q = charge (Coulombs mol^{-1})

E = potential (Volts)

The total charge transferred in a fuel cell reaction per mol of H_2 consumed is equal to:

$$q = nN_{Avg}q_{el} \tag{2.25}$$

n = number of electrons per molecule of H_2 = 2 electrons per molecule

N_{Avg} = number of molecules per mole (Avogadro's number) = 6.022 x10^{23} molecules/mol

Q_{el} = charge of 1 electron = 1.602 x 10^{-19} Coulombs/electron

The product of Avogadro's number and charge of 1 electron is known as Faraday's constant:

F = 96,485 Coulombs/electron-mol

Electrical work is therefore:

$$W_{el} = nFE \tag{2.26}$$

As mentioned previously, the maximum amount of electrical energy generated in a fuel cell corresponds to Gibbs free energy ΔG

$$W_{el} = -\Delta G \tag{2.27}$$

The theoretical potential of fuel cell is then:

$$E = -\frac{\Delta G}{nF} \tag{2.28}$$

Because ΔG, n, and F are all known, the theoretical fuel cell potential of hydrogen/oxygen can also be calculated:

$$E = \frac{-\Delta G}{nF} = \frac{237{,}340\ Jmol^{-1}}{296{,}485\ Asmol^{-1}} = 1.23\ Volts \tag{2.29}$$

At 25°C, the theoretical hydrogen/oxygen fuel cell potential is 1.23 Volts.

2.3.6 Effect of Temperature

The theoretical cell potential changes with temperature. Substituting Equation (2.22) into (2.28) yields:

$$E = -\left(\frac{\Delta H}{nF} - \frac{T\Delta S}{nF}\right) \tag{2.30}$$

Obviously, an increase in the cell temperature results in a lower theoretical.

In addition, both ΔH and ΔS are functions of temperature

$$h_T = h_{298.15} + \int_{298.15}^{T} c_p dT \tag{2.31}$$

$$S_T = S_{298.15} + \int_{298.15}^{T} \frac{1}{T} c_p dT \tag{2.32}$$

where c_p is specific heat of any gas, which is also a function of temperature

2.3.7 Effect of Pressure

All of the previous equations were valid at atmospheric pressure. However, a fuel cell may operate at any pressure, typically from atmospheric all the way up to 6-7 bar. For an

isothermal process, and with a little bit of basic thermodynamics, the change in Gibbs free energy may be shown to be:

$$dG = V_m dP \tag{2.33}$$

Where

V_m =molar volume, m^3 mol^{-1}

P =pressure. Pa

For an ideal gas:

$$PV_m = RT \tag{2.34}$$

Therefore:

$$dG = RT\frac{dP}{P} \tag{2.35}$$

After integration:

$$G = G_0 + RT\ln\left(\frac{P}{P_0}\right) \tag{2.36}$$

Where G_0 is Gibbs free energy at standard temperature and pressure (25°C and 1atm), and P_o is the reference or standard pressure (1atm).

For any chemical reaction

$$jA + kB \rightarrow mC + nD \tag{2.37}$$

The change in Gibbs free energy is the change between products and react ants

$$\Delta G = mG_C + nG_D - jG_A - kG_B \tag{2.38}$$

After substituting into Equation (2.35):

$$\Delta G = \Delta G_0 + RT\ln\left[\frac{\left(\frac{P_C}{P_0}\right)^m\left(\frac{P_D}{P_0}\right)^n}{\left(\frac{P_A}{P_0}\right)^j\left(\frac{P_B}{P_0}\right)^k}\right] \tag{2.39}$$

This is known as the Nernst equation, where P is the partial pressure of the reactant or product species and P_0 is the reference pressure (1 atm or 101.25kPa). For the hydrogen/oxygen fuel cell reaction, the Nernst equation becomes:

$$\Delta G = \Delta G_0 + RT\ln\left(\frac{P_{H_2 0}}{P_{H_2}P_{O_2}^{0.5}}\right) \tag{2.40}$$

By introducing Equation (2.30) into Equation (2.40):

$$E = E_0 + \frac{RT}{nF}\ln\left(\frac{P_{H_2}P_{O_2}^{0.5}}{P_{H_2O}}\right) \tag{2.41}$$

If air is used instead of pure oxygen, their partial pressure is proportional to their concentration and consequently the cell potential is lower. In case of air vs. oxygen, the theoretical voltage loss/gain is

$$\Delta E = E_{O_2} - E_{Air} = \frac{RT}{nF}\ln\left(\frac{P_{O_2}}{P_{Air}}\right)^{0.5} = \frac{RT}{nF}\ln\left(\frac{1}{0.21}\right)^{0.5} \quad (2.42)$$

2.4 Fuel cell Electrochemistry

2.4.1 Electrode Kinetics

A fuel cell is an electrochemical energy converter. Its operation is based on the following electrochemical reaction happening simultaneously on the anode and cathode.

At the anode

$$H_2 \rightarrow 2H^+ + 2e^- \quad (2.43)$$

At the cathode

$$\tfrac{1}{2}O_2 + 2H^+ + 2e^- \rightarrow H_2O \quad (2.44)$$

More precisely, the reactions happen on an interface between the ionically conductive electrolyte and electrically conductive electrode. Because there are gases involved in fuel cell electrochemical reaction, the electrodes must be porous allowing the gases to arrive to, as well as product water to leave the reaction sites. Note that these are the overall reactions and that in both cases there are several intermediary sequential and parallel steps involved.

2.4.2 Reaction Rate

Electrochemical reactions involve both a transfer of electrical charge and a change in Gibb energy. The rate of electrochemical reaction is determined by activation energy barrier that the charge must overcome in moving from electrolyte to a solid electrode or vice versa. The speed at which an electrochemical reaction proceeds on the electrode surface is the rate at which the electrons are released or consumed which is the electrical current. Current density is the current per unit area of the surface. From Faraday's Law it follows that current density is proportional to the charge transferred and the consumption of reactant per unit area.

$$i = nF_j \quad (2.45)$$

where nF is the charge transferred (coulombs mol^{-1}) and j is the flux of reactant per unit area ($mols^{-1}\ cm^{-2}$)

Therefore, the reaction rate may be easily measured by current-measuring device placed external to the cell. However, the measured current or current density is actually the net current,

that is, the difference between forward and reverse current on the electrode. In general, an electrochemical reaction involves either oxidation or reduction of the species.

$$red \rightarrow ox + ne^- \quad (2.46)$$

$$ox + ne^- \rightarrow red \quad (2.47)$$

In a hydrogen/oxygen fuel cell the anode reaction is oxidation of hydrogen, in which hydrogen is stripped of its electrons, and the products of this reaction are protons and electrons. The cathode reaction is oxygen reduction and water is generated as a product.

On an electrode at equilibrium conditions that is, when no external current is being generated, both process, oxidation and reduction, occur at equal rates.

$$ox + ne^- \leftrightarrow red \quad (2.48)$$

The consumption is proportional to their surface concentration. For the forward reaction, the flux is

$$j_f = k_f C_{ox} \quad (2.49)$$

where

k_f = forward reaction(reduction) rate coefficient

C_{ox} = surface concentration of the reacting species

Similarly for the backward reaction the flux is

$$j_b = k_b C_{rd} \quad (2.50)$$

where

k_b = backward reaction(oxidation) rate coefficient

C_{rd} = surface concentration of the reacting species

Each of these two reactions either releases or consumes electrons. The net current generated is the difference between the electrons released and consumed

$$i = nF\left(k_f C_{Ox} - k_b C_{Rd}\right) \quad (2.51)$$

At equilibrium the net current is equal to zero, although the reaction proceeds in both directions simultaneously. The rate at which these reactions proceed at equilibrium is called the exchange current density.

2.4.3 Reaction constants, transfer coefficient

From the transition state, it may be shown that the reaction rate coefficient for an electrochemical reaction is a function of the Gibbs free energy

$$k = \frac{k_b T}{h} \exp\left(\frac{-\Delta G}{RT}\right) \quad (2.52)$$

Where

k_b = Bolzmann's constant

h = planck's constant

The Gibbs free energy for electrochemical reactions may be considered to consist of both chemical and electrical terms. In that case, for a reduction reaction.

$$\Delta G = \Delta G_{ch} + \alpha_{Rd} FE \tag{2.53}$$

and for an oxidation reaction

$$\Delta G = \Delta G_{ch} + \alpha_{Ox} FE \tag{2.54}$$

The subscript *"ch"* denotes the chemical component of the Gibbs free energy, α is a transfer coefficient, F is the Faraday's constant, and E is the potential. There is a fair amount of confusion in the literature concerning the transfer coefficient, α, and the symmetry factor, β, that is sometimes used. The symmetry factor, β, may be used strictly for a single-step reaction involving a single electron (n = 1). Its value is theoretically between 0 and 1, but most typically for the reactions on a metallic surface it is around 0.5. The way in which β is defined requires that the sum of the symmetry factors in the anodic and cathodic direction be unity, if it is β for the reduction reaction it must be $(1-\beta)$ for the reverse, oxidation reaction.

However, both electrochemical reactions in a fuel cell, namely oxygen reduction and hydrogen oxidation, involve more than one step and more than one electron. In that case, at steady state, the rate of all steps must be equal, and it is determined by the slowest step in the sequence, which is referred to as the rate-determining step. In order to describe a multistep process, instead of the symmetry factor, β, a rather experimental parameter is used, which is called the transfer coefficient, α. Note that in this case $\alpha_{rd} + \alpha_{ox}$ does not necessarily have to be equal to unity. Actually, in general $(\alpha_{rd} + \alpha_{ox}) = n/\nu$, where n is the number of electrons transferred in the overall reaction and ν is the stoichiometric number defined as the number of times the rate-determining step must occur for the overall reaction to occur once .

The forward (reduction) and backward (oxidation) reaction rate coefficients in Equation (2.51) are then respectively.

$$k_f = k_{0,f} \exp\left[\frac{\alpha_{Rd} FE}{RT}\right] \tag{2.55}$$

$$k_b = k_{0,b} \exp\left[\frac{\alpha_{0x} FE}{RT}\right] \tag{2.56}$$

2.4.4 Current Potential Relationship—Butler-Volmer Equation

By introducing into Equation (2.50) the net current, density is obtained

$$i = nF\left\{k_{0,f}C_{Ox}\exp\left[\frac{\alpha_{Rd}FE}{RT}\right] - k_{0,b}C_{Rd}\exp\left[\frac{\alpha_{Ox}FE}{RT}\right]\right\} \quad (2.57)$$

At equilibrium, the potential is E_r, and the net current is equal to zero, although the reaction proceeds in both directions simultaneously. The rate at which these reactions proceed at equilibrium is called the exchange current density.

$$i_0 = nFk_{0,f}C_{Ox}\exp\left[\frac{\alpha_{Rd}FE_r}{RT}\right] = nFk_{0,b}C_{Rd}\exp\left[\frac{\alpha_{Ox}FE_r}{RT}\right] \quad (2.58)$$

By combining the Equations (2.57) and (2.58), a relationship between the current density and potential is obtained:

$$i = i_0\left\{\exp\left[\frac{-\alpha_{Rd}F(E-E_r)}{RT}\right] - \exp\left[\frac{\alpha_{Ox}F(E-E_r)}{RT}\right]\right\} \quad (2.59)$$

This is known as the Butler-Volmer equation, where E_r is the reversible or equilibrium potential. Note that the reversible or equilibrium potential at the fuel cell anode is O V by definition , and the reversible potential at the fuel cell cathode is 1.229 V (at 25°C and atmospheric pressure).The difference between the electrode potential and the reversible potential is called over potential. It is the potential difference required to generate current.

The Butler-Volmer Equation (2.59) is valid for both anode and cathode reaction in a fuel cell:

$$i_a = i_{0,a}\left\{\exp\left[\frac{-\alpha_{Rd,a}F(E_a-E_{r,a})}{RT}\right] - \exp\left[\frac{\alpha_{0x,a}F(E_a-E_{r,a})}{RT}\right]\right\} \quad (2.60)$$

And

$$i_c = i_{0,c}\left\{\exp\left[\frac{-\alpha_{Rd,c}F(E_c-E_{r,c})}{RT}\right] - \exp\left[\frac{\alpha_{0x,c}F(E_c-E_{r,c})}{RT}\right]\right\} \quad (2.61)$$

The over potential on the anode is positive($E_a > E_{r,a}$), which makes the first term of the Equation (2.60) negligible in comparison with the second term, that is, the oxidation current is predominant and the equation may be reduced to

$$i_a = -i_{0,a}\exp\left[\frac{\alpha_{Ox,a}(E_a-E_{r,a})}{RT}\right] \quad (2.62)$$

Note that the resulting current has a negative sign, which denotes that the electrons are leaving the electrode (net oxidation reaction).

Similarly, the over potential on the cathode is negative ($E_c < E_{rc}$), which makes the first term of the Equation (2.61) much larger than the second term, that is, the reduction current is predominant and the equation may be reduced to

$$i_c = -i_{0,c} \exp\left[\frac{\alpha_{Ox,c}\left(E_c - E_{r,c}\right)}{RT}\right] \tag{2.63}$$

2.4.5 Exchange Current Density

Exchange current density, i_0, in electrochemical reactions is analogous to the rate constant in chemical reactions. Unlike the rate constants, exchange current density is concentration dependent. It is also a function of temperature. The effective exchange current density (per unit of electrode geometrical area) is also a function of electrode catalyst loading and catalyst specific surface area. If the reference exchange current density (at reference temperature and pressure) is given per actual catalyst surface area, then the effective exchange current density at any temperature and pressure is given by the following equation

$$i_0 = i_0^{ref} a_c L_c \left(\frac{P_r}{p_r^{ref}}\right)^{\gamma} \exp\left[-\frac{E_c}{RT}\left(1 - \frac{T}{T_{ref}}\right)\right] \tag{2.64}$$

where

i_0^{ref} = reference exchange current density (at reference temperature and pressure, typically 25°C and 101.25 kPa) per unit catalyst surface area, Acm^2Pt,

a_c = catalyst specific area (theoretical limit for Pt catalyst is $2400cm^2\ mg^{-1}$, but state-of-the-art catalyst has about 600- 1000 $cm^2\ mg^{-1}$, which is further reduced by incorporation of catalyst in the electrode structures by up to 30%).

L_c = catalyst loading (state-of-the-art electrodes have 0.3- $0.5mgPtcm^{-2}$; lower loadings are possible but would result in lower cell voltages).

p_r = reactant partial pressure, kPa

p_r^{ref} = reference pressure, kPa

γ = pressure coefficient (0.5 to 1.0)

E_c = activation energy, $66kJmol^{-1}$ for oxygen reduction on Pt

R = gas constant, $8.314Jmol^{-1}\ K^{-1}$

T = temperature, K

T_{ref} = reference temperature, 298.15 K

The product $a_c L_c$ is also called electrode roughness, meaning the catalyst surface area, cm^2, per electrode geometric area, cm^2. Instead of the ratio of partial pressures, a ratio of concentrations at the catalyst surface may be used as well.

Exchange current density is a measure of an electrode's readiness to proceed with the electrochemical reaction. If the exchange current density is high, the surface of the electrode is

more active. In a hydrogen/oxygen fuel cell, the exchange current density at the anode is much larger (several orders of magnitudes) than at the cathode. The higher the exchange current density, the lower the energy barrier that the charge must overcome moving from electrolyte to the catalyst surface and vice versa. In other words, the higher the exchange current density, the more current is generated at any overpotential.

Because the anode exchange current density in hydrogen/oxygen fuel cells is several orders of magnitudes larger than the cathode current density, the overpotential on the cathode is much larger than the anode overpotential. For that reason, very often the cell potential current relationship is approximated solely by Equation (2.63).

2.4.6 Over-potentials and Crossover Losses in Fuel Cells

The reversible potential obtained from the Nernst equation corresponds to the thermodynamic equilibrium state of the electrochemical system. However, when current starts flowing through the cell, the cell potential drops below the reversible potential due to several types of over-potential including activation, ohmic, and concentration over-potential. In addition to these typical electrochemical over-potentials, PEM fuel cells also suffer from other losses such as internal currents and fuel crossover even at open circuit. The details of these potential losses are described in the sections below. Each hydrogen molecule that diffuses through the polymer electrolyte membrane and reacts with oxygen on the cathode side of the fuel cell results in two fewer electrons in the generated current of electrons that travels through an external circuit. These losses may appear insignificant in fuel cell operation, because the rate of hydrogen permeation or electron crossover is several orders of magnitude lower than hydrogen consumption rate or total electrical current generated. However, when the fuel cell is at open circuit potential or when it operates at very low current densities, these losses may have a dramatic effect on cell potential.

The total electrical current is the sum of external (useful) current and current losses due to fuel crossover and internal currents:

$$I = I_{ext} + I_{loss} \tag{2.65}$$

Current divided by the electrode active area, A, is current density, A/cm2:

$$i = \frac{I}{A} \tag{2.66}$$

Therefore

$$i = i_{ext} + i_{loss} \tag{2.67}$$

If this total current density is used in the equation that approximates the cell

$$E_{cell} = E_r - \frac{RT}{\alpha F}\ln(\frac{i_{ext} + i_{loss}}{i_0}) \quad (2.68)$$

Therefore, even if the external current is equal to zero, such as at open circuit, the cell voltage may be significantly lower than the reversible cell potential for given conditions. Indeed, open circuit potential of hydrogen/air fuel cells is typically below 1 V, most likely about 0.94 to 0.97 V (depending on operating pressure).

$$E_{cell} = E_r - \frac{RT}{\alpha F}\ln(\frac{i_{loss}}{i_0}) \quad (2.69)$$

Hydrogen crossover is a function of membrane permeability, membrane thickness, and hydrogen partial pressure (i.e., hydrogen concentration) difference across the membrane, as the main driving force. A very low open circuit potential (significantly below 0.9 V) may indicate either a hydrogen leak or an electrical short. As the fuel cell starts generating current, hydrogen concentration in the catalyst layer decreases, which reduces the driving force for hydrogen permeation through the membrane. That is one of the reasons these losses are mainly negligible at operation currents.

2.4.6.1 Activation Polarization

The activation over-potential is the potential loss to drive the electrochemical reactions from equilibrium state. Therefore, it is the potential loss when there is a net current production from the electrode, i.e. a net reaction rate. In PEM fuel cell, the activation over-potential at the anode is negligible compared to that of the cathode. Activation polarization depends on factors such as the material property of the electrode material, ion-ion interactions, ion-solvent interactions and characteristics of the electric double layer at the electrode-electrolyte interface. Activation polarization may be reduced by increasing operating temperature and by increasing the active surface area of the catalyst.

Some voltage difference from equilibrium is needed to get the electrochemical reaction going. This is called activation polarization, and it is associated with sluggish electrode kinetics. These losses happen at both anode and cathode; however, oxygen reduction requires much higher overpotentials, that is, it is a much slower reaction than hydrogen oxidation.

At relatively high negative overpotentials (i.e., potentials lower than the equilibrium potential), such as those at the fuel call cathode, the first term in the Butler-Volmer equation becomes predominant, which allows for expression of potential as a function of current density

$$\Delta V_{act,c} = E_{r,c} - E_c = \frac{RT}{\alpha_c F}\ln(\frac{i}{i_{0,c}}) \quad (2.70)$$

Similarly, at the anode at positive overpotentials (i.e., higher than the equilibrium potential) the second term in the Butler-Volmer equation becomes predominant:

$$\Delta V_{act,a} = E_{r,a} - E_a = \frac{RT}{\alpha_a F}\ln(\frac{i}{i_{0,a}}) \quad (2.71)$$

In electrochemistry, the reversible potential of the hydrogen oxidation reaction is zero at all temperatures. That is why the standard hydrogen electrode is used as a reference electrode. Therefore, for hydrogen anodes $E_{r,a}$ = 0 V. Activation polarization of the hydrogen oxidation reaction is much smaller than activation polarization of the oxygen reduction reaction.

A simplified way to show the activation losses is to use the so-called Tafel equation:

$$\Delta_{act} = a + b\log(i) \quad (2.72)$$

Where $a = -2.3\frac{RT}{\alpha F}\log(i)$ (2.73)

and $b = 2.3\frac{RT}{\alpha F}$ (2.74)

The constant b is called the tafel slope.

If these activation polarizations were the only losses in a fuel cell, the cell potential would be:

$$E_{cell} = E_c - E_a = E_r - \Delta V_{act,c} - \Delta V_{act,a} \quad (2.75)$$

$$E_{cell} = E_r - \frac{RT}{\alpha_c F}\ln(\frac{i}{i_{0,c}}) - \frac{RT}{\alpha_a F}\ln(\frac{i}{i_{0,a}}) \quad (2.76)$$

If anode polarization is neglected, the previous equation becomes

$$E_{cell} = E_r - \frac{RT}{\alpha F}\ln(\frac{i}{i_0}) \quad (2.77)$$

which has the same form as the Tafel Equation

2.4.6.2 Ohmic Polarization

Two types of ohmic losses occur in fuel cells. These are potential losses due to electron transport through electrodes, bipolar plates, and collector plates; and potential loss due to proton transport through the membrane. The magnitudes of these potential losses depend on the materials used in the construction of the fuel cells and the operating conditions of the cell. Membrane conductivity increases with membrane water content.

Ohmic losses occur because of resistance to the flow of ions in the electrolyte and resistance to the flow of electrons through the electrically conductive fuel cell components. These losses can be expressed by Ohm's law:

$$\Delta Vohm = iR_i \quad (2.78)$$

Where i = current density , A.cm^{-2} and

R_i = total cell internal resistance (which includes ionic, electronic, and contact resistance, Ω cm^2):

$$R_i = R_{i,i} + R_{i,e} + R_{i,c} \quad (2.79)$$

Electronic resistance is almost negligible, even when graphite or graphite/polymer composites are used as current collectors. Ionic and contact resistances are approximately of the same order of magnitude. Typical values for R_i are between 0.1 and 0.2 Ω cm^2.

2.4.6.3 Concentration Polarization

Mass transport loss becomes significant when the fuel cell is operated at high current density. This is created by the concentration gradient due to the consumption of oxygen or fuel at the electrodes. The mass transport loss at the anode can be negligible compared to the cathode. At the limiting current density, oxygen at the catalyst layer is depleted and no more current can be increased from the fuel cell. This is responsible for the sharp decline in potential at high current densities. To reduce mass transport loss, the cathode is usually run at high pressure.

Concentration polarization occurs when a reactant is rapidly consumed at the electrode by the electrochemical reaction so that concentration gradients are established. The electrochemical reaction potential changes with partial pressure of the reactants, and this relationship is given by the Nernst equation:

$$\Delta V = \frac{RT}{nF}\ln(\frac{C_B}{C_s}) \quad (2.80)$$

where C_B = bulk concentration of reactant, mol cm^{-3}

C_S = concentration of reactant at the surface of the catalyst, mol cm^{-3}

According to Fick's Law, the flux of reactant is proportional to concentration gradient:

$$N = \frac{D(C_B - C_S)}{\delta} A \quad (2.81)$$

where N = flux of reactants, mol s^{-1}

D = diffusion coefficient of the reacting species, cm^2 s^{-1}

A =electrode active area, cm^2

δ = diffusion distance, cm

In steady state, the rate at which the reactant species is consumed in the electrochemical reaction is equal to the diffusion flux:

$$I = \frac{N}{nF} \quad (2.82)$$

By combining Equations (2.79) and (2.80), the following relationship is obtained:

$$i = \frac{nF.D.(C_B - C_S)}{\delta} \tag{2.83}$$

The reactant concentration at the catalyst surface thus depends on current density-the higher the current density, the lower the surface concentration. The surface concentration reaches zero when the rate of consumption exceeds the diffusion rate-the reactant is consumed faster than it can reach the surface. Current density at which this happens is called the limiting current density. A fuel cell cannot produce more than the limiting current because there are no reactants at the catalyst surface. Therefore, for $C_S = 0$, $i = i_L$, and the limiting current density is then:

$$i_L = \frac{nFDC_B}{\delta} \tag{2.84}$$

By combining Equations (2.68), (2.73), and (2.74), a relationship for voltage loss due to concentration polarization is obtained

$$\Delta V_{conc} = \frac{RT}{nF}\ln(\frac{i_L}{i_L - i}) \tag{2.85}$$

2.5 Principle of Fluent 6.3

A fuel cell is energy conversion that converts the chemical energy of fuel into electrical energy. A schematic of PEM fuel cell is shown in figure 2.8.

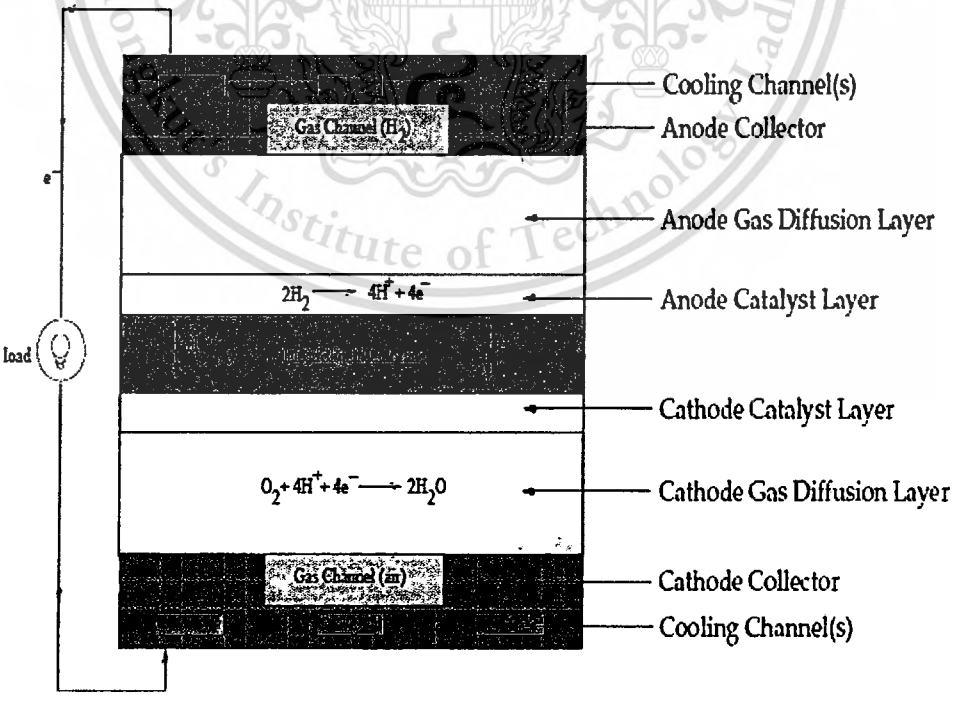

Figure 2.8 Schematic of PEM Fuel Cell [19]

Hydrogen flows into the fuel cell on the anode side. It diffuses through the porous gas diffusion layers and comes in contact with the catalyst layer. Here it forms hydrogen ions and electrons. The hydrogen ions diffuse through the polymer electrolyte membrane at the center, the electrons flow through the gas diffusion layer to the current collectors and into the electric load attached. Electrons enter the cathode side through the current collectors and the gas diffusion layer. At the catalyst layer on the cathode side, the electrons, the hydrogen ions and the oxygen combine to form water. In the PEM fuel cell model in FLUENT, two electric potential fields are solved. One potential is solved in the membrane and catalyst layers. The other is solved in the catalyst layers, the diffusion layers, and the current collectors. Surface reactions on the porous catalyst region are solved and the reaction diffusion balance is applied to compute the rates. Based on the cell voltage that you prescribe, the current density value is computed. Alternatively, a cell voltage can be computed based on a prescribed average current density.

2.5.1 Electrochemistry Modelling

At the center of the electrochemistry is the computation of the rate of the hydrogen oxidation and the rate of oxygen reduction. In the FLUENT PEM model, these electrochemical processes are treated as heterogeneous reactions that take place on the catalyst surfaces inside the two catalyst layers on both sides of the membrane.

The driving force behind these reactions is the surface over-potential: the difference between the phase potential of the solid and the phase potential of the electrolyte/membrane. Therefore, two potential equations are solved for in the PEM model: one potential equation (Equations 2.86) accounts for the electron transport e^- through the solid conductive materials (i.e., the current collectors and solid grids of the porous media); the other potential equation (2.87) represents the protonic (i.e., ionic) transport of H^+. The two potential equations read

$$\nabla.(\sigma_{sol}\nabla\phi_{sol}) + R_{sol} = 0 \quad (2.86)$$

$$\nabla.(\sigma_{mem}\nabla\phi_{mem}) + R_{mem} = 0 \quad (2.87)$$

where

σ = electrical conductivity (1/ohm-m)

ϕ = electric potential (volts)

R = volumetric transfer current (A/m^3)

The following figure illustrates the boundary conditions that are used to solve for ϕ_{sol} and ϕ_{mem}

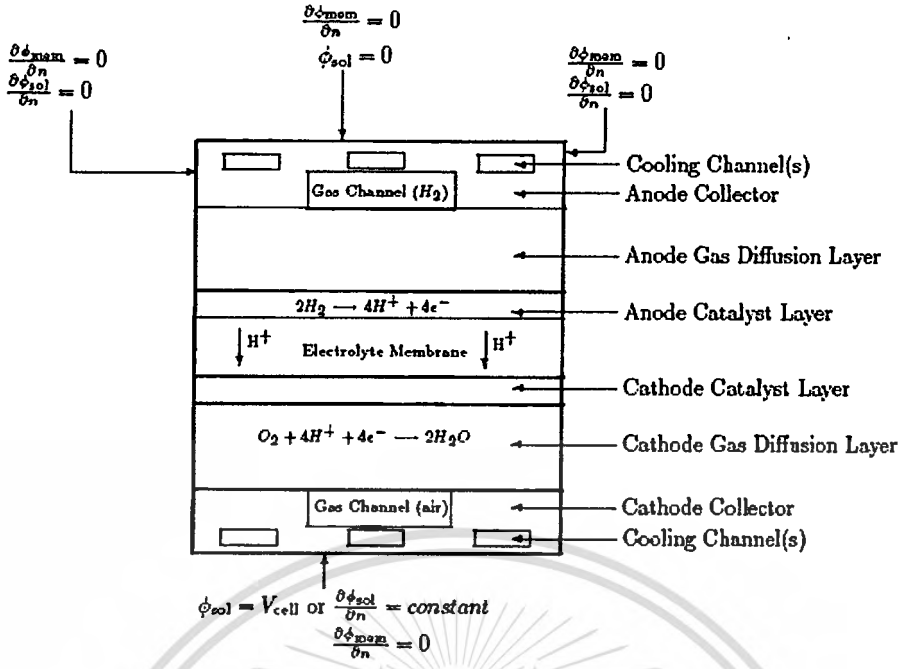

Figure 2.9 Boundary condition for ϕ_{sol} and ϕ_{mem} [19]

There are two types of external boundaries. Those through which there passes an electrical current and those through which there passes no current.

As no protonic current leaves the fuel cell through any external boundary, there is a zero flux boundary condition for the membrane phase potential, ϕ_{mem}, on all outside boundaries.

For the solid phase potential, ϕ_{sol}, there are external boundaries on the anode and the cathode side that are in contact with the external electric circuit and only through these boundaries passes the electrical current generated in the fuel cell. On all other external boundaries there is a zero flux boundary condition for ϕ_{sol}.

The transfer currents, or the source terms in Equations 2.86 and 2.87, are non-zero only inside the catalyst layers and are computed as

For the solid phase, $R_{sol} = -R_{an}(<0)$ on the anode side and $R_{sol} = +R_{cat}(>0)$ on the cathode side.

For the membrane phase, $R_{mem} = +R_{an}(>0)$ on the anode side and $R_{mem} = -R_{cat}(<0)$ on the cathode side.

The source terms in Equations 2.86 and 2.87 are also called the exchange current density (A/m^3), and have the following general definitions:

$$R_{an} = j_{an}^{ref}\left(\frac{[H_2]}{[H_2]_{ref}}\right)^{\gamma_{an}}\left(e^{\alpha_{an}F\eta_{an}/RT} - e^{-\alpha_{cat}F\eta_{an}/RT}\right) \qquad (2.88)$$

$$R_{cat} = j_{cat}^{ref}\left(\frac{[O_2]}{[O_2]_{ref}}\right)^{\gamma_{cat}}\left(e^{-\gamma_{cat}F\eta_{cat}/RT}\right) \quad (2.89)$$

By default, the Butler-Volmer function is used in the FLUENT PEM model to compute the transfer currents inside the catalyst layers.

The driving force for the kinetics is the local surface over-potential also known as the activation loss. It is generally the difference between the solid and membrane potentials, ϕ_{sol} and ϕ_{mem}

The gain in electrical potential from crossing from the anode to the cathode side can then be taken into account by subtracting the open-circuit voltage V_{oc} on the cathode side.

$$\eta_{an} = \phi_{sol} - \phi_{mem} \quad (2.90)$$

$$\eta_{cat} = \phi_{sol} - \phi_{mem} - V_{oc} \quad (2.91)$$

From Equations 2.86 through 2.91, the two potential fields can be obtained

Mass conservation

$$\nabla.(\varepsilon\rho u) = s_m \quad (2.92)$$

where ε is porosity ρ is mixture density and u is velocity vector.

The s_m denotes source terms corresponding to the consumption of hydrogen and oxygen in the anode and cathode, and the production of water in the cathode

$$s_m = s_{H2} + s_{aw} \quad : Anode\ side \quad (2.93)$$

$$s_m = s_{O2} + s_{cw} \quad : Cathode\ side \quad (2.94)$$

Momentum conservation

$$\nabla(\varepsilon\rho uu) = -\varepsilon\nabla p + \nabla(\varepsilon\mu\nabla u) + s_u \quad (2.95)$$

where subscript 'a' and 'c' refer to the anode and cathode respectively.

Where p is pressure, μ is dynamic viscosity

$S_{.}$ denote source term based on Darcy's law

$$s_{ux} = -\frac{\mu u}{\beta_x} \quad s_{uy} = -\frac{\mu u}{\beta_y} \text{ and } s_{uz} = -\frac{\mu u}{\beta_z} \quad (2.96)$$

where β is the permeability And the energy conservation relation can be written as

$$\frac{\partial}{\partial t}(\varepsilon\rho h) + \nabla.(\varepsilon\rho uh) = \nabla.q + \varepsilon\frac{dp}{dt} - j_T\eta + \frac{i.i}{\sigma} + S_h \quad (2.97)$$

where h is mixture static enthalpy i is current density J_T is the transfer current η is electrode over potential σ is electrical conductivity S_h is latent heat of phase change and q is heat flux due to thermal conductivity. The species diffusion equation above can be written as

$$q = k\nabla T + \sum J_i h_i \quad (2.98)$$

where k is the thermal conductivity; T is the mixture temperature and J_i is species diffusion flux. The species conservation equation can be written as

$$\nabla(\varepsilon\mu C_k) = \nabla(D_k^{eff}\nabla C_k) + s_k \tag{2.99}$$

where C_i is Molar concentration of chemical species

D_k^{eff} is the effective diffusion coefficient and S_i denotes source term

$$S_i = -\frac{I(x,y)}{2F} M_{H2} A_{CV} \qquad S_{H_2} \tag{2.100}$$

$$-\frac{\alpha(x,y)}{F} I(x,y) M_{H2O} A_{CV} \qquad S_{ow} \tag{2.101}$$

$$-\frac{I(x,y)}{4F} M_{O2} A_{CV} \qquad S_{o_2} \tag{2.102}$$

$$-\frac{1+2\alpha(x,y)}{2F} I(x,y) M_{H2O} A_{CV} \qquad S_{cw} \tag{2.103}$$

where M_{H2}, M_{H2O} and M_{O2} are the molecular weight of hydrogen, water and oxygen respectively and $I(x,y)$ is the local current density F is Faradays constant $\alpha(x,y)$ is the local net water transfer coefficient per proton and A_{cv} is the specific surface area of control volume element in the domain.

The water management is a critical issue for the performance of a proton electrolyte membrane fuel cell. The transport phenomena of water can be described as follows.

First, the water molecules are transported through the polymer electrolyte membrane by the hydrogen protons and this process is called electro-osmotic drag. In addition to the molecular diffusion and electro-osmotic drag, water is generated in the cathode catalyst layer due to electrochemical reaction.

1) Electro-osmotic water flux going through the membrane can be calculated from the proton flux going through the membrane, given by the specified current density and Faraday law as

$$j_{H_2O} = 2 x n_d \frac{I(x,y)}{2F} \tag{2.104}$$

n_d is Electro-osmotic drag coefficient which depend on water activity as follow

$$n_d = 0.029\lambda^2 + 0.05\lambda - 3.4x10^{-19} \tag{2.105}$$

where λ represents water content of the membrane described as

$$\lambda = 0.043 + 17.81a_k - 39.85a_k^2 + 36a_k^3 \qquad 0 < a_k < 1 \tag{2.106}$$

$$\lambda = 14 + 1.4(a_i - 1) \qquad 1 < a_i < 3 \tag{2.107}$$

where a_k is water activity

$$a_k = \frac{x_{wk} p(x,y)}{p_{wk}^{sat}} \qquad k = Anode\ or\ Cathode \tag{2.108}$$

where x_{wk}, p^{sat} are water mole fraction and saturation pressure at each electrode respectively therefore

$$\log_{10} p^{sat} = -2.1794 + 0.02953T - 9.1837x10^{-5}T^2 + 1.4454x10^{-7}T^3 \tag{2.109}$$

2) For the back diffusion flux, the water formation at the cathode results in a gradient in the water content between the cathode side and anode side of the membrane. For PEMFC, this gradient causes a water flux back to anode side, which is superimposed to the electro-osmotic flux. This back diffusion is expressed as following water flux as

$$J_{H2O} = -\frac{\rho}{M} x D_w x \frac{d\lambda}{dz} \tag{2.110}$$

where ρ is the dry density of electrolyte, M is electrolyte equivalent weight, z is the direction through the membrane thickness and D_w is water diffusion coefficient therefore

$$D_w = D_\lambda \exp(2416x(\frac{1}{303} - \frac{1}{T_{cell}})) \tag{2.111}$$

where

$$D_\lambda = 10^{-10} \qquad \lambda < 2 \tag{2.112}$$

$$D_\lambda = 10^{-10}(1 + 2(\lambda - 2)) \qquad 2 \le \lambda \le 3 \tag{2.113}$$

$$D_\lambda = 10^{-10}(3 - 1.67(\lambda - 3)) \qquad 3 < \lambda < 4.5 \tag{2.114}$$

$$D_\lambda = 1.25x10^{-10} \qquad \lambda \ge 4.5 \tag{2.115}$$

And Protonic Conductivity is presented

$$\sigma = (0.514 - 0.326)e^{1268\left(\frac{1}{303} - \frac{1}{T}\right)} \tag{2.116}$$

Where σ is Protonic Conductivity (1/ohm.m)

Moreover, heat source is combined

$$s_h = h_{react} - R_{an,cat}\eta_{an,cat} + I^2 R_{Ohm} + h_L \tag{2.117}$$

where h_{react} is net enthalpy change due to electrochemical reaction , $R_{an,cat}\eta_{an,cat}$ is the product of transfer current and over potential in anode or the cathode TPB, R_{ohm} is the ohmic resistivity of the conducting media and h_L is enthalpy change due to phase change.

2.6 Literature reviews

There have been several researchers working in the area of computational fluid dynamic for PEMFC analysis. The researchers' names and their findings are summarized below.

S.Shimpalee et.al. (1999) showed that the effect of inlet humidity had a significant influence on the performance of PEMFC and indicated that the ionic resistivity of the electrolyte membrane depended on the activity of water at the membrane surface. Water flux and activities changed along the flow direction.

A.kumar et. al. (2003) studied the effect of channel dimension on the hydrogen consumption at the anode. This work was done ranging from 0.5 to 4 mm. for different channel width, land(rib) width and channel depth. For high hydrogen consumption (80 %) the optimum dimension for channel width, land width, and channel depth were close to 1.5, 0.5 and 1.5 mm respectively. The effect of channel shape was also studied. The result showed that the triangular and hemispherical cross-section of land or collector rib had resulted in an increase in hydrogen consumption by around 9 % at the anode.

T.Berning et.al. (2005) presented a three dimensional model of PEMFC. The model accounted for all major transport phenomena in the flow channel, electrode and electrolyte membrane. Results were physically consistent and in good agreement with experiment and also had the capability to provide water transport mechanism and mass transport limitation for parametric studies of interest in design and prototyping.

F.B. Weng et.al. (2005) presented a 3-D mathematical model for prediction and analysis of proton exchange membrane fuel cells(PEMFC) species concentration and current density distribution in different flow field patterns and operating conditions. The mode is based on the solution of the conservation equation of mass, momentum, species and electric current in a fully integrated finite-volume solver using the CFDRC commercial code. The polarization curve of serpentine flow pattern is well correlated with experimental data. The cell performance with parallel straight, serpentine and interdigitated flow patterns are calculated and compared. The simulation results revealed that serpentine and interdigitated flow patterns show strong convection and high mass transfer. However, they also have larger pressure loss. In addition, the effects of operating temperature and relative humidity were also studied. Non-uniform distributions of concentration and current density appeared at high temperature, high current density and low humidity operation, which could lead to an unstable cell performance.

D.Hasan et. al. (2006) investigated the performance of Proton Exchange Membrane Fuel Cell (PEMFC). The investigation was done on different channel geometries at high operating current density including rectangular, trapezoidal and parallelogram. The simulation result showed that a channel with rectangular cross section gave high cell voltage compared with trapezoidal and parallelogram cross sections. However, the trapezoidal cross-section facilitates reactant diffusion. This led to more uniform reactant and local current density distribution over the reacting area. They also recommended that the shoulder width was one of the most influential in terms of its impact on cell performance by ohmic losses significantly increasing with decreasing shoulder width. In contrast, a small shoulder width facilitates the distribution of reactants and helps to reduce concentration losses.

P.T.Nguyen et. al. (2006) presented a three dimension computational model of PEMFC with serpentine flow field channel. The comprehensive model accounted for all important transport phenomena in fuel cell such as heat transfer, mass transfer, electrode kinetics and potential fields in the membrane and gas diffusion layers. The coupling between local current density, oxygen concentration and activation over potential was fully implemented by using a new algorithm to solve for the potential losses across the cell. Moreover the simulation showed that the counter current flow gave higher performance than co flow for stationary condition but had larger potential drop for case of automotive condition.

P.H.Lee et.al. (2008) presented a single-phase, fully three dimensional simulation model for PEMFC. The results showed that hydrogen and oxygen were solely supplied to the membrane by diffusion mechanism rather than convection transport, and the higher pressure drop at cathode side was thought to be caused by higher flow rate of oxygen at cathode. It was also found that the amount of water in cathode channel was determined by water formation due to electrochemical reaction plus electro-osmotic mass flux directing toward the cathode side. They had emphasized that it was very important to model the back diffusion and electro-osmotic mass flux accurately since the two fluxes were closely correlated each other and greatly influenced for determination of ionic conductivity of the membrane which directly affects the performance of fuel cell.

CHAPTER 3

INVESTIGATION PROCEDURES

3.1 Computational Domain

The Computation Domain including single straight channel, which is a house of flow domain in bipolar plate, is shown in figure 3.1. A cross section schematic in figure 3.2 shows anode and cathode current collector, gas diffusion layer, catalyst layer and polymer electrolyte membrane.

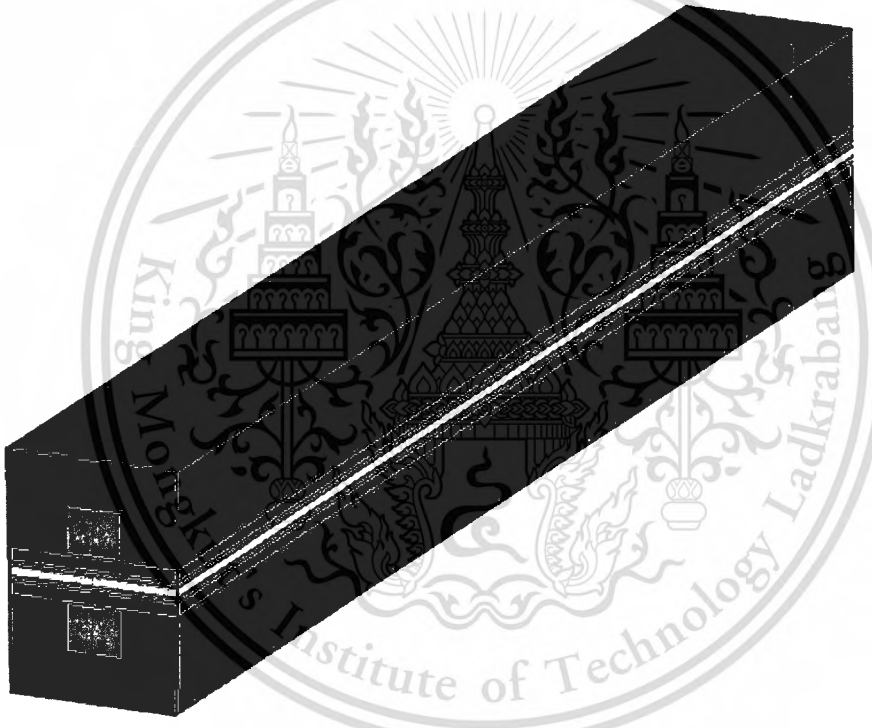

Figure 3.1 Computational Domain

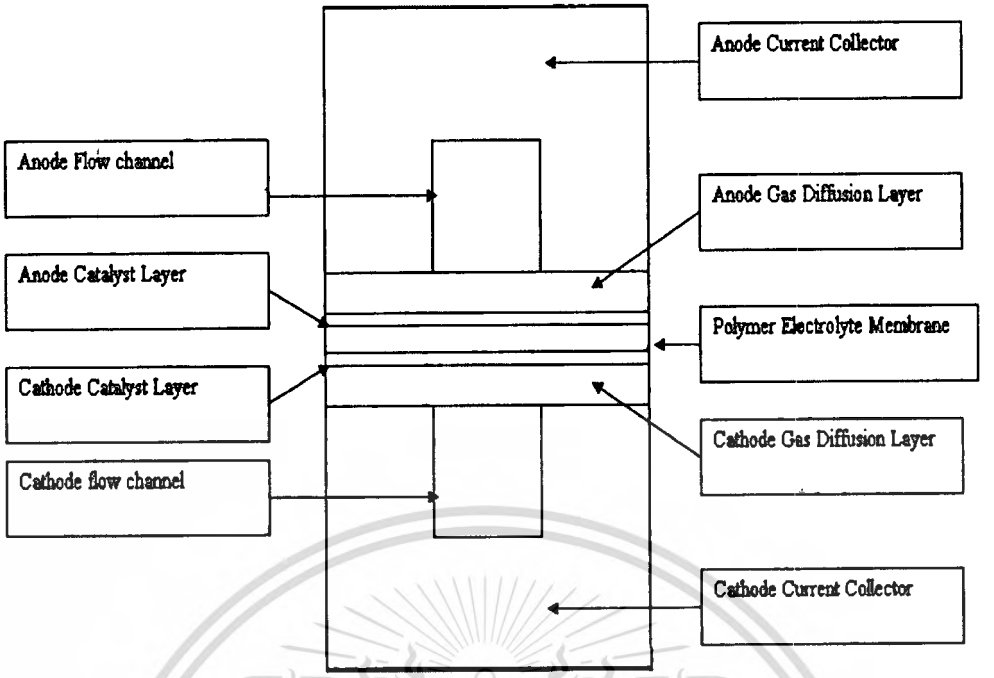

Figure 3.2 Cross section schematic of PEMFC

3.2 Computational Diagram

The numerical simulation model is based on SIMPLE (semi-implicit method for pressure linked equations consistent) algorithm using Segregated solver of Fluent (version 6.3). Uniform flow velocity and reactant concentration at the inlet are given as the inlet condition. Source terms generated by the electrochemical reaction are inserted into mass and species conservation equation using the User Define Function (UDF). The coupled set of equations is solved iteratively until the relative error in each field reaches a specific convergent standard (usually 10^{-6}). The flow diagram for this numerical algorithm is represented in figure 3.3

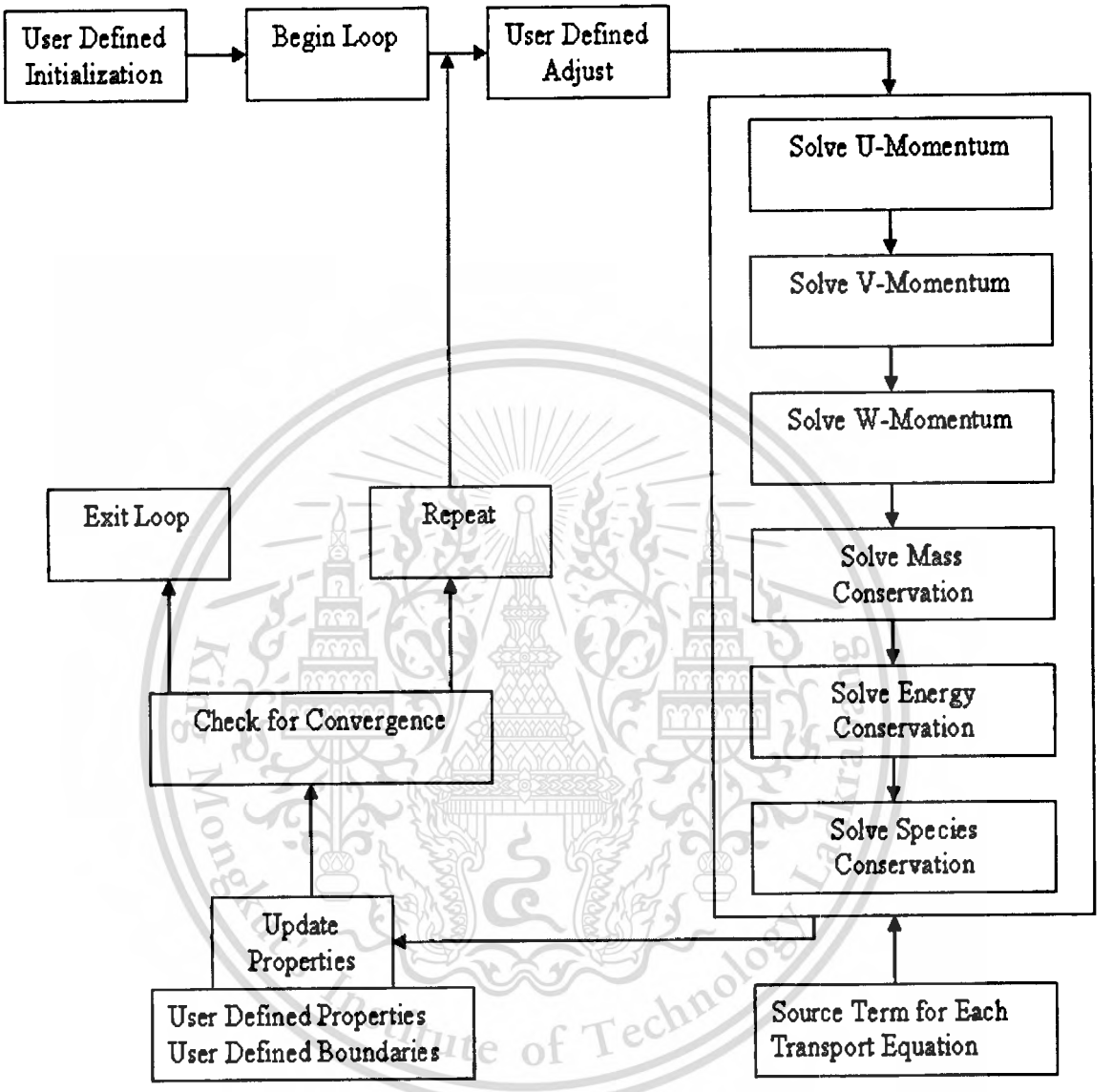

Figure 3.3 Computational Diagram

3.3 Computational Grid

The computational grid is use with total number of grid 15x52x160, 124800 cells. This is relatively sufficient when considering the grid independent of the solution at the location of interest, i.e.; the contour of the species and others importance properties at the triple–phase boundary, etc. In this research, species distribution in the Membrane Electrode Assembly (MEA) is investigated. As a result, fine meshes are applied in the reaction area to achieve more detailed result, as shown in figures 3.4 and 3.5

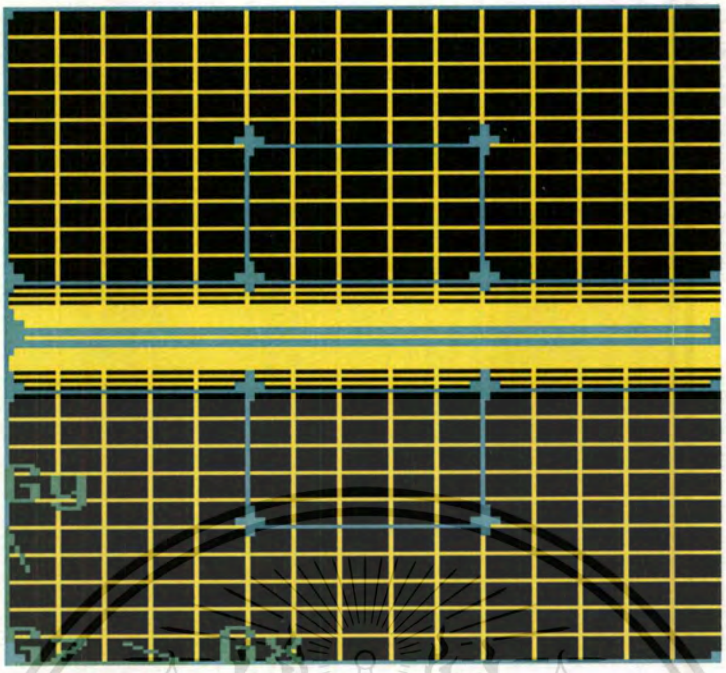

Figure3.4 Computational Grid (Cross section view)

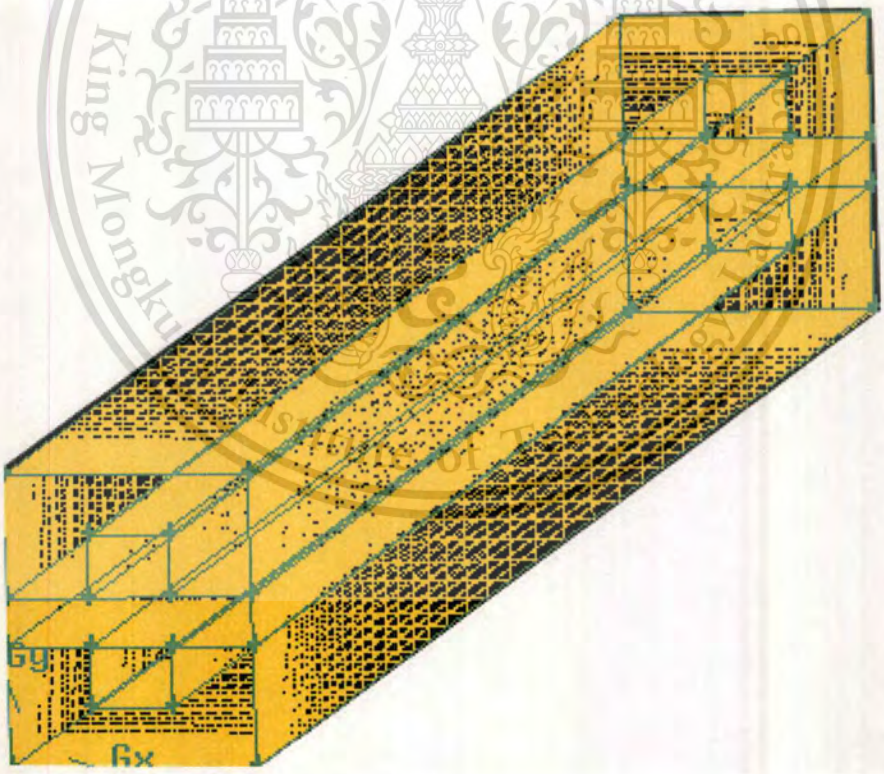

Figure 3.5 Computation Grid (Perspective view)

For boundary condition, the domain is divided into solid and fluid types. The interface between solid and fluid is defined as "wall" whereas those between fluids are defined as "interior".

3.4 Model Assumption

1) Steady state

2) Laminar flow

3) Isothermal

4) Incompressible fluid

5) Butler-volmer equation is used to describe electrochemical reaction.

6) Reactant species include H_2, O_2, N_2 and H_2O (vapour) are considered.

7) The volume of liquid H_2O is assumed negligible in the domain.

8) The gravity effect is negligible

Table 3.1 Basic Parameter for all cases [12]

Parameters	Anode	Cathode
Ref. Current Density (A/m^2)	$1.5e^9$	$1.5e^9$
Ref. Concentration ($kmol/m^3$)	1	1
Concentration Exponent	0.5	2
Exchange Coefficient	2	2
GDL Porosity	0.5	0.5
GDL Permeability (m^2)	$1e^{-12}$	$1e^{-12}$
CL Porosity	0.5	0.5
CL Permeability (m^2)	$1e^{-12}$	$1e^{-12}$
Cell Temperature (K)	353	
Operating Pressure (Mpa)	0.1	

Table 3.2 Model Dimension of all cases [12]

Dimensions	Value
Channel width (*mm*)	0.8
Channel high (*mm*)	0.6
Channel length (*mm*)	40
Rip width (*mm*)	0.8
GDL thickness (*mm*)	0.21
Catalyst thickness (*mm*)	0.012
Membrane thickness (*mm*)	0.036

3.5 Effect of inlet humidification to cell performance

In this work, the amount of water is varied at inlet for both anode and cathode sides which include very low humidity, low humidity, high humidity and very high humidity as shown in table 3.3.

Table 3.3 Different flow conditions used for different inlet humidity conditions [8]

Flow Conditions		Very low humidity	Low humidity	High humidity	Very High humidity
Anode gas inlet	H_2 mass fraction	0.96	0.94	0.86	0.79
	H_2O mass fraction	0.04	0.06	0.14	0.21
Cathode gas inlet	O_2 mass fraction	0.2	0.193	0.18	0.15
	H_2O mass fraction	0.037	0.072	0.13	0.29

3.6 Effect of Co and Counter flow on cell performance

This section, the flow configuration is investigated which is described as follow, the characteristic of "Co-flow" is where the fuel and the reactant gas are fed in the same direction as shown in figure 3.6. Conversely, the configuration where both fuel and reactant gas are fed from different direction is termed as "Counter-flow" as shown in figure3.7.

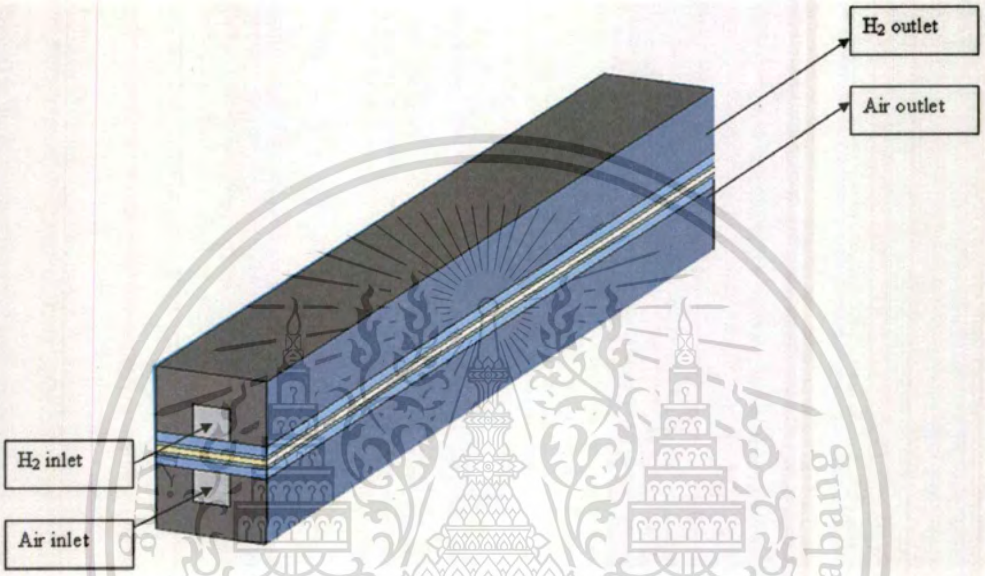

Figure 3.6 Schematic of Co-Flow configuration

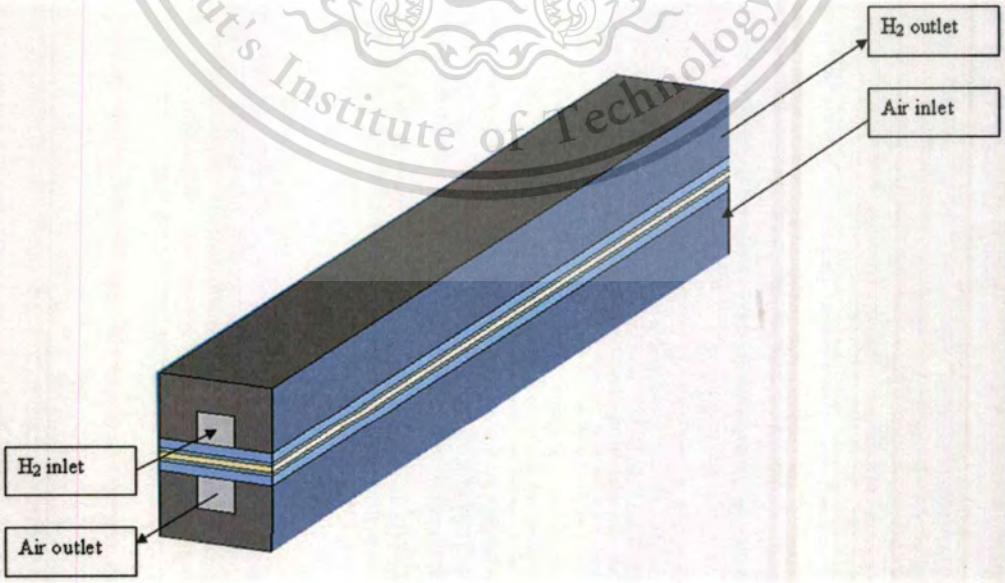

Figure 3.7 Schematic of Counter-Flow configuration

CHAPTER 4

RESULTS AND DICUSSIONS

4.1 Model validation

To validate the numerical simulation model used in this study, the IV Polarization Curve of cell voltage and current density with the experiment data under the same condition [12] is used as a reference.

The result shows that at low and medium current density, the simulated performance agrees reasonably well with the experimental result. However, at high current density the simulation overestimates the cell voltage. This is because of the emerging liquid water in the cathode channel that result in diffusion loss on the cell performance as shown in figure 4.1

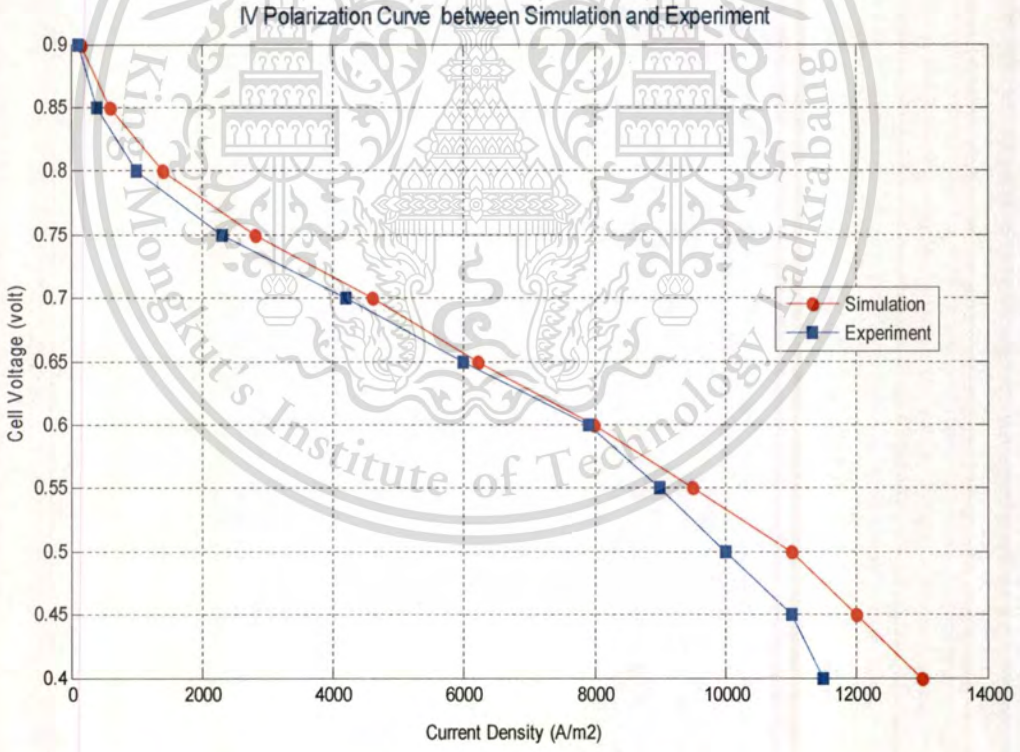

Figure 4.1 IV Polarization Curve between Simulation and Experiment

Although currently, there are some researches about PEMFC simulation which related to the effect of humidity and flow configuration (co flow and counter flow) on the cell performance

but those works only presented an overview of transport phenomena such as concentration, current density and temperature distribution. To gain better understanding on the interactions of physical and chemical processes, the source/sink terms of transported properties should be taken into account in the analyses of the simulation results. It is hoped that such information will be useful for future work of other researchers in this field.

4.2 Effect of inlet humidification on cell performance

Figures 4.2-4.5 show the temperature distribution along the channel in 4 cases of inlet humidity (very low, low, high and very high humidity). We have found that the increasing in humidity at channel inlet affects directly to the temperature distribution. High temperature occurs at the cathode side due to the presence of water, especially the highest temperature is observed in case of very high inlet humidity see in figure 4.5

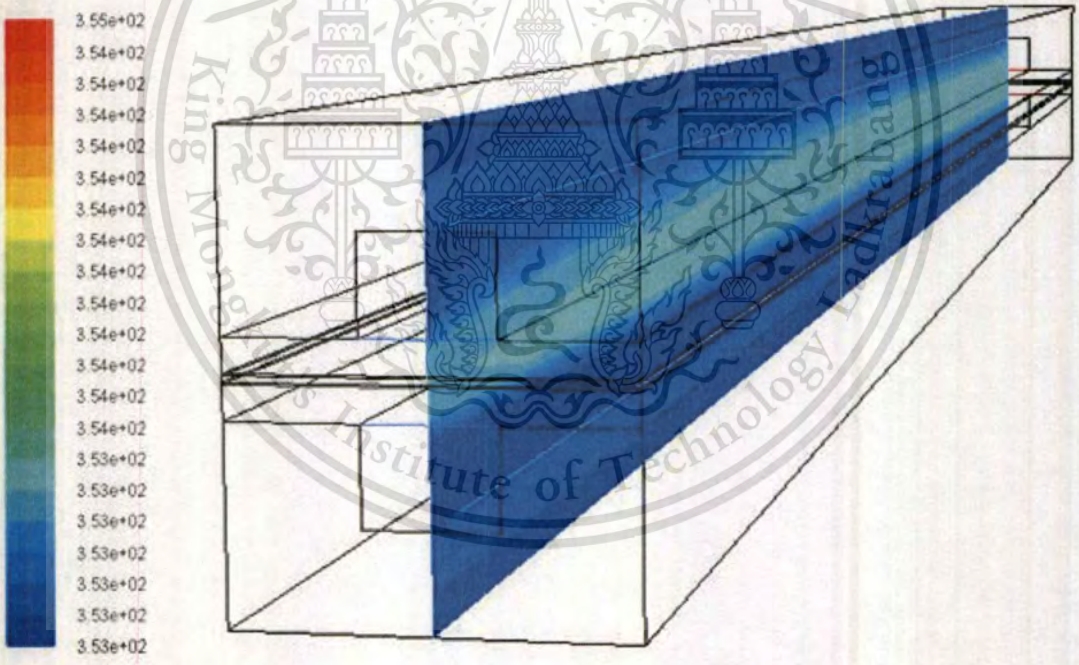

Figure 4.2 Temperature distribution along the channel for the case of very low humidity

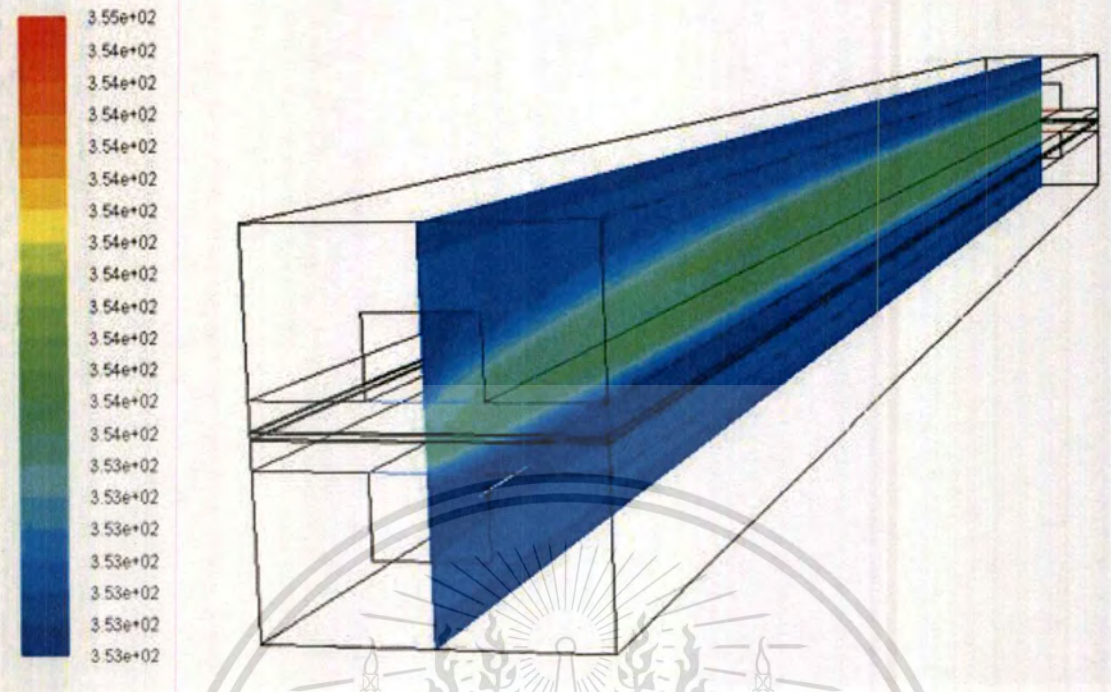

Figure 4.3 Temperature distribution along the channel for the case of low humidity

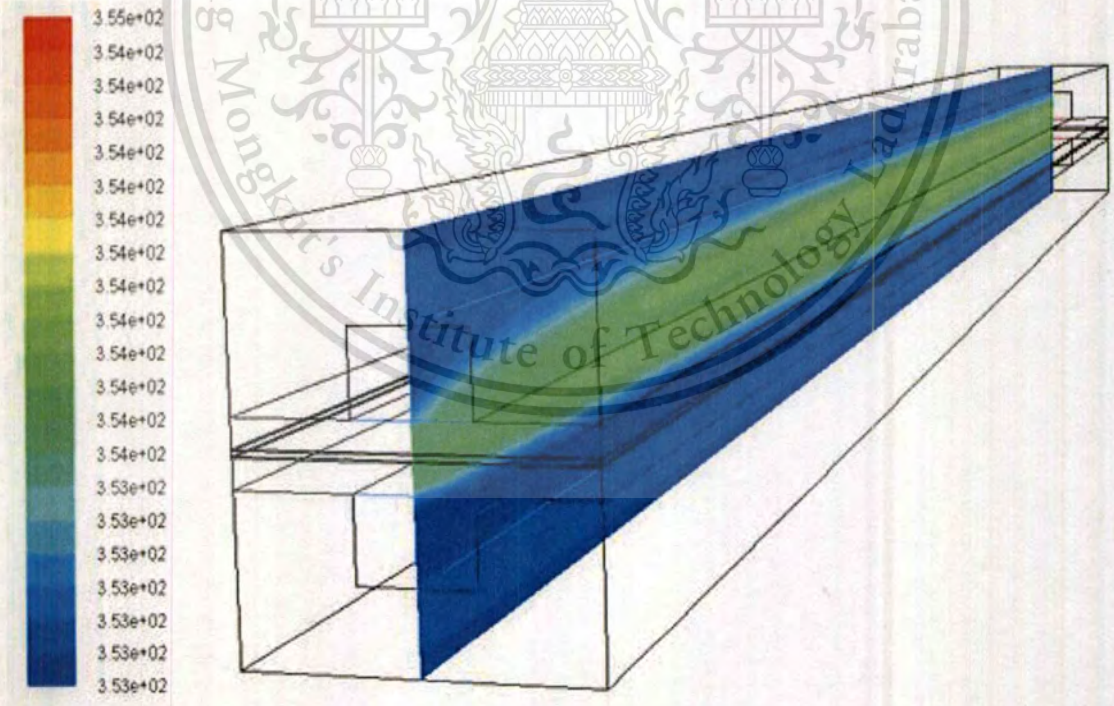

Figure 4.4 Temperature distribution along the channel for the case of high humidity

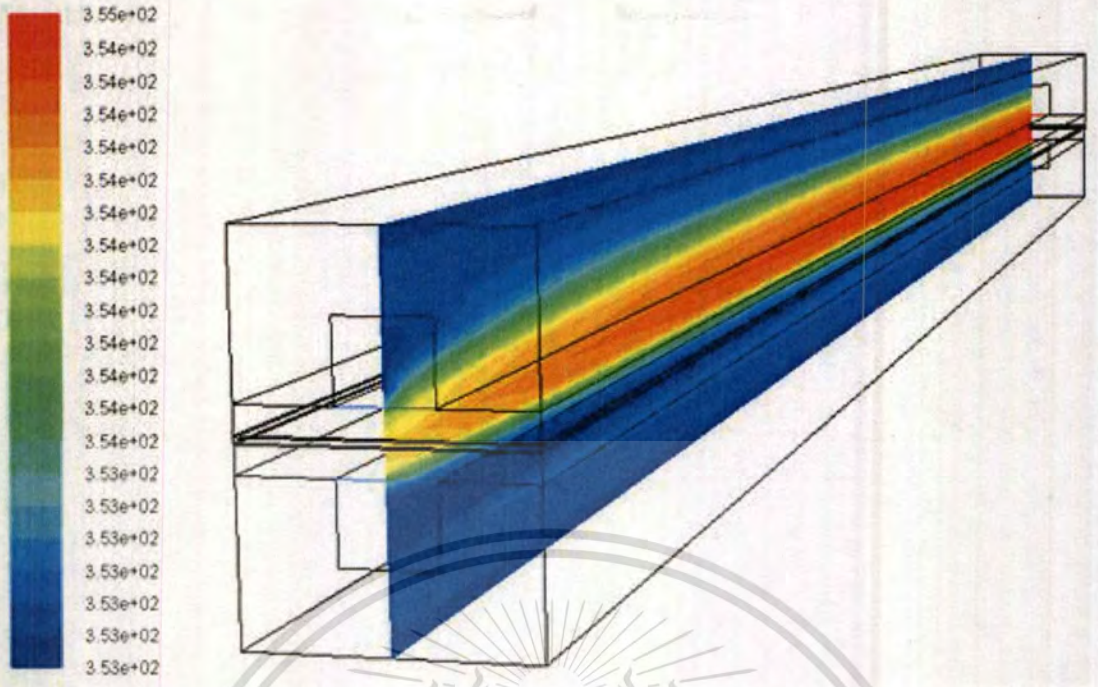

Figure 4.5 Temperature distribution along the channel for the case of very high humidity

One of heat sources Eq. 2.117. in PEMFC which has a significant effect on the electrochemical reaction rate is the reaction heat source (w/m^3) . Note that in this research, heat source from phase change is neglected due to the assumption of single phase flow. The ohmic heat source is regarded as minority, as compared to the reaction heat source.

The reaction heat source is observed at cathode TPB and we have found that the heat generation rate increase gradually along the channel as shown in figures 4.6-4.9 with the highest value observed for case of very high humidity as seen in figure 4.9. This is due to the positive effect of humidity on photonic conductivity which will be explained in effect of inlet humidity in protonic conductivity section. Moreover, high temperature also promotes the electrochemical reaction leading to greater chemical reactivity.

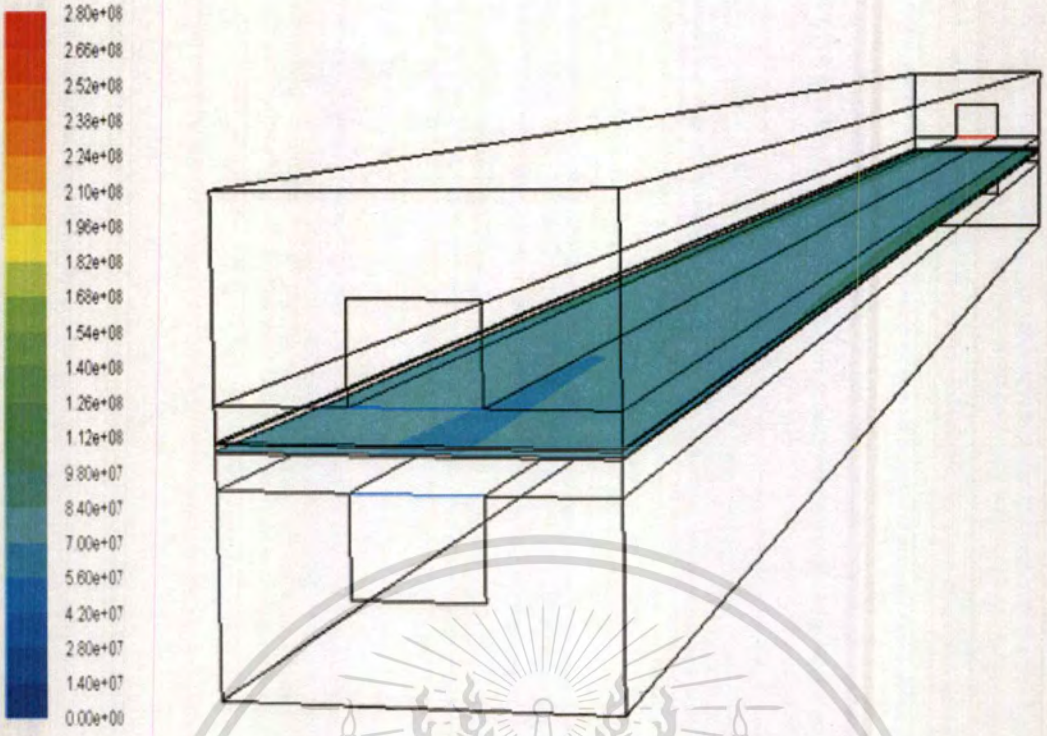

Figure 4.6 Reaction Heat Source for the case of very low humidity

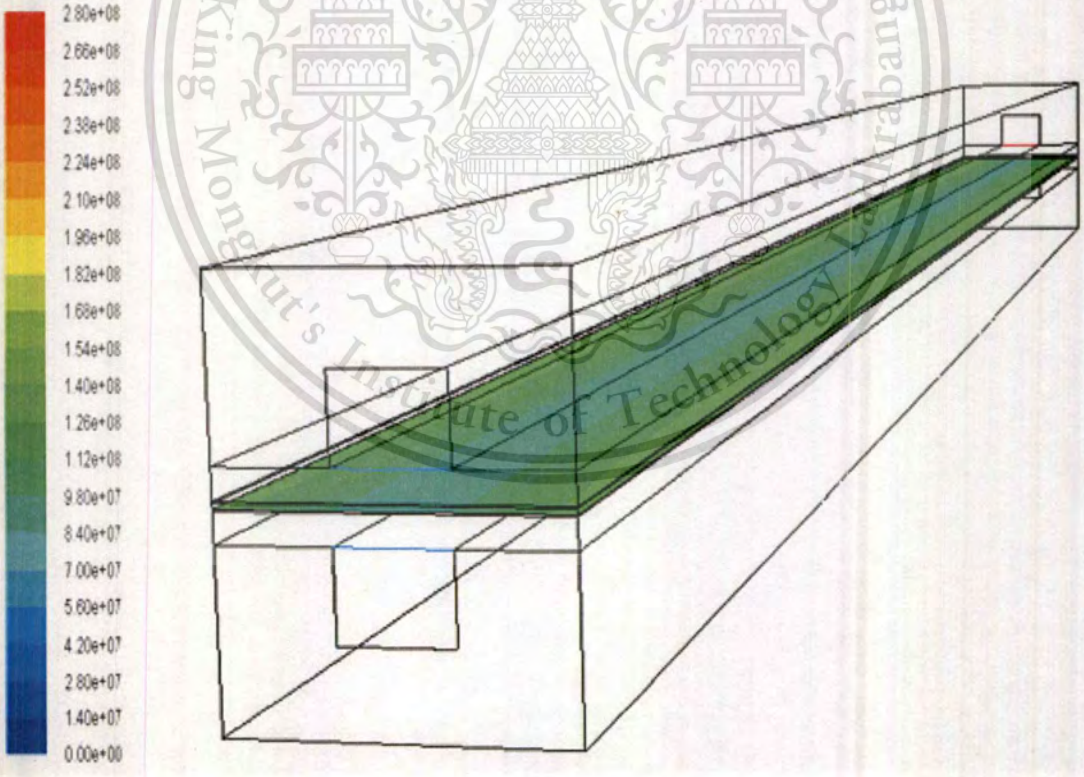

Figure 4.7 Reaction Heat Source for the case of low humidity

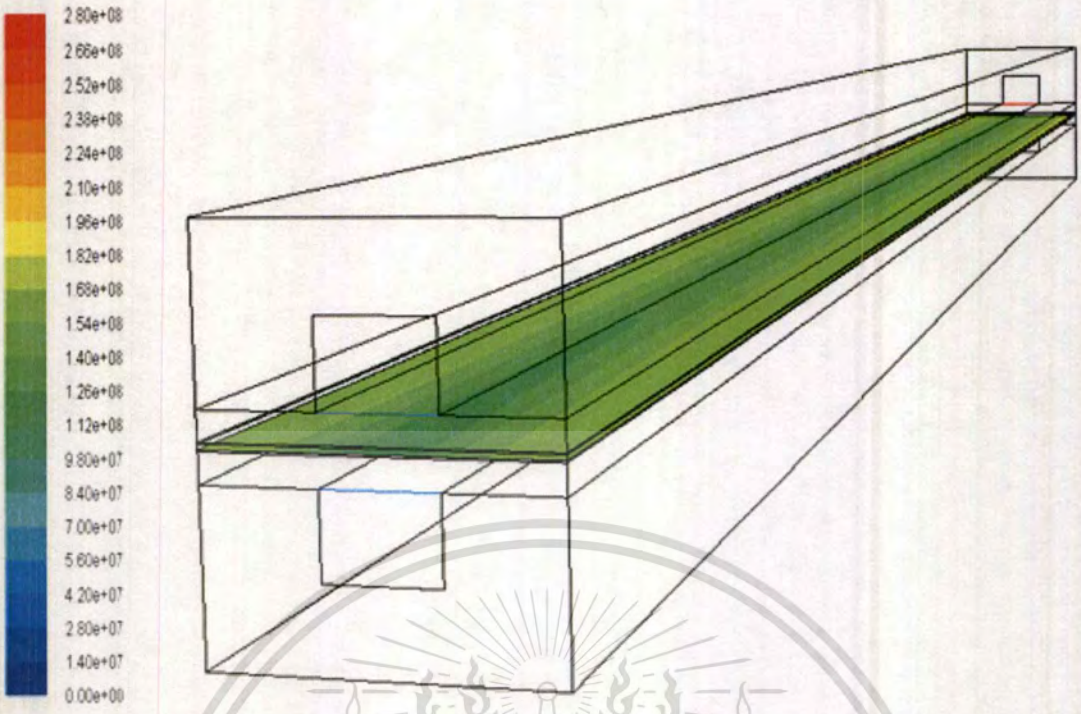

Figure 4.8 Reaction Heat Source for the case of high humidity

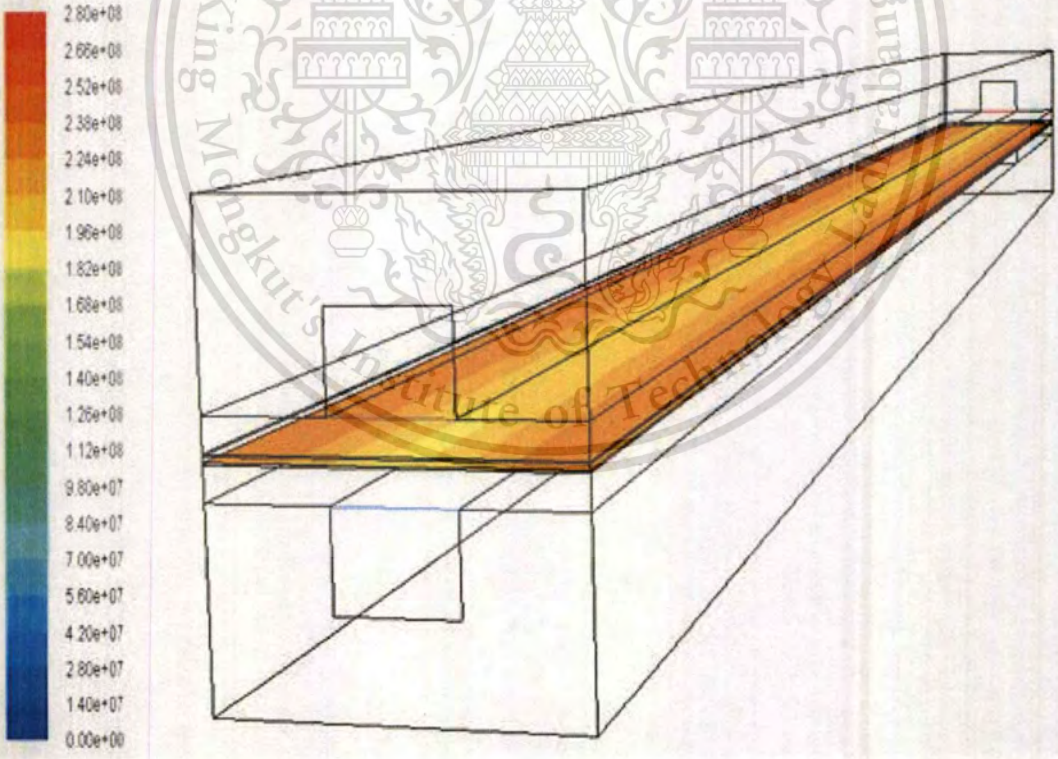

Figure 4.9 Reaction Heat Source for the case of very high humidity

The water management is a critical issue for the performance of PEM fuel cell. The water product is generated at Cathode side with certain amount diffuses back to the anode layer by

water back diffusion. The osmotic drag force also create significant amount of mass transfer of water from the anode side to the electrolyte layer as described in the literature [12]. The water molecules are transported through the polymer electrolyte membrane by the hydrogen protons and this process is called electro-osmotic drag. In addition to the water influx to the cathode side by electro-osmotic drag, water is generated in the cathode catalyst layer due to electrochemical reaction. This creates high water content on the cathode side and consequently leads to molecular back diffusion flux associated with the gradient of water concentration. For PEMFC, this is an important issue for research and development work nowadays as it is necessary to create an environment where the amount of water carried by the photon is counter-balanced by water transport due to the back diffusion [18]

Electro osmotic flux going through the membrane can be calculated from proton flux (Electro-osmotic drag coefficient) through the membrane see in Eq 2.104. This coefficient depends on water content of the membrane, see Eq 2.105.

Figures 4.10-4.17 show osmotic drag source, having the unit of kg per sec per unit volume, in 4 cases which are observed at both anode and cathode TPBs. When consider distribution along the channel we have found that this source term increases along the channel due to the transported proton. Particularly, for the case of very high humidity at inlet channel this source term is the highest as well as the back diffusion mass source. as shown in figure 4.18-4.25. This correspond to the distribution of heat source as already mentioned in figures 4.6-4.9. This is due to the electrochemical reaction is exothermic having protons as one of the reactant. For high humidity case proton could travel with relatively less resistance thus greater amount of proton per unit of time is available at the Triple Phase Boundary leading to greater rate of reaction. When consider the distribution along the channel, this back diffusion mass source increases from inlet to outlet channel due to an increasing in gradient of water content between the cathode side and anode side of the membrane as seen in Eq 2.110. Moreover we have noticed that the highest value of this source term at both anode and cathode TPBs occur at very high inlet humidity condition see in figure 4.21 and 4.25 respectively

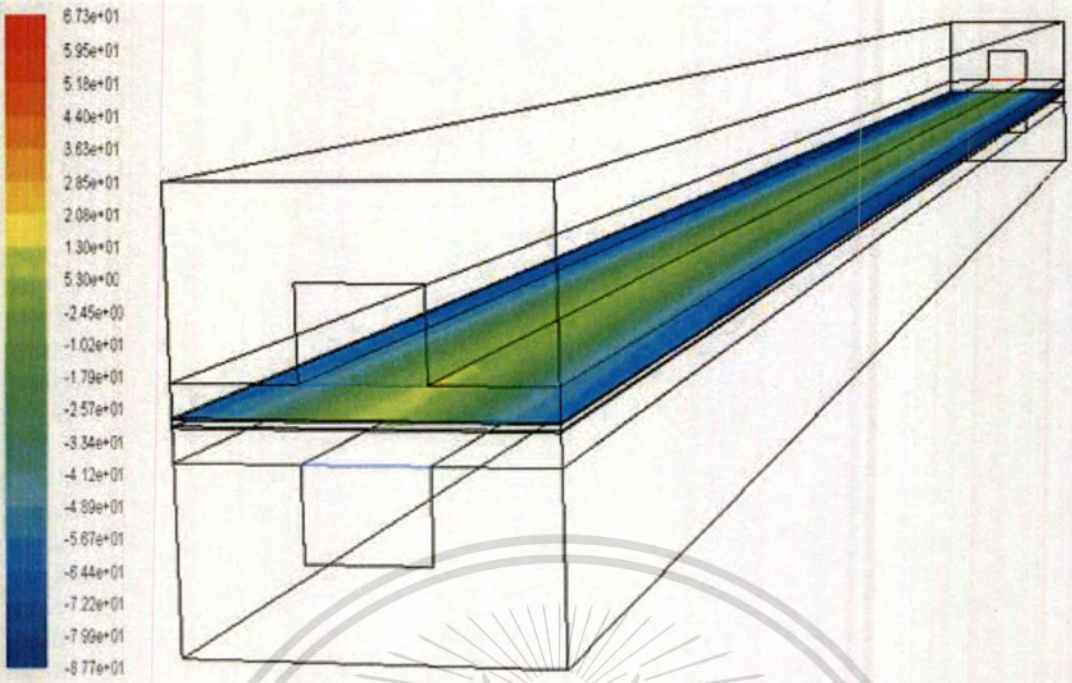

Figure 4.10 Osmotic Drag Source at the Anode TPB for the case of very low humidity

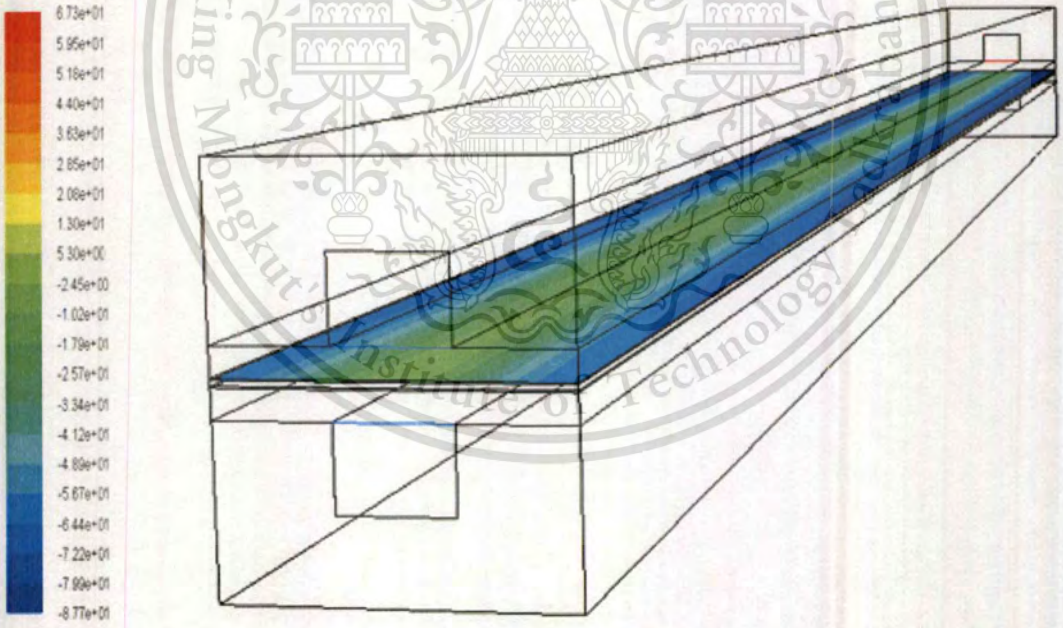

Figure 4.11 Osmotic Drag Source at the Anode TPB for the case of low humidity

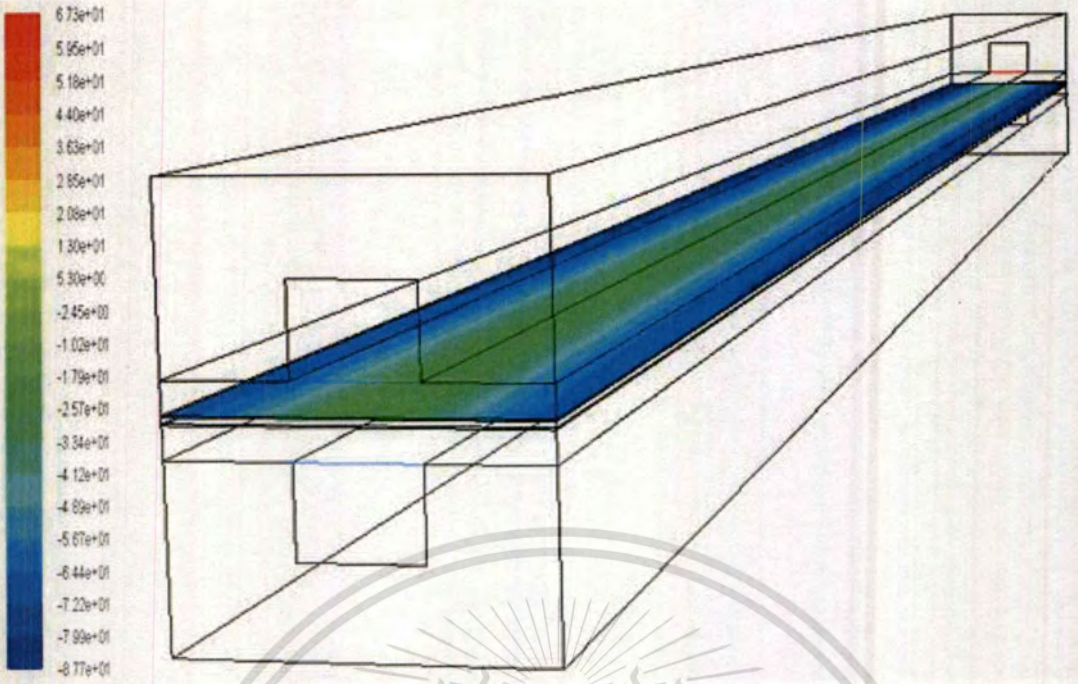

Figure 4.12 Osmotic Drag Source at the Anode TPB for the case of high humidity

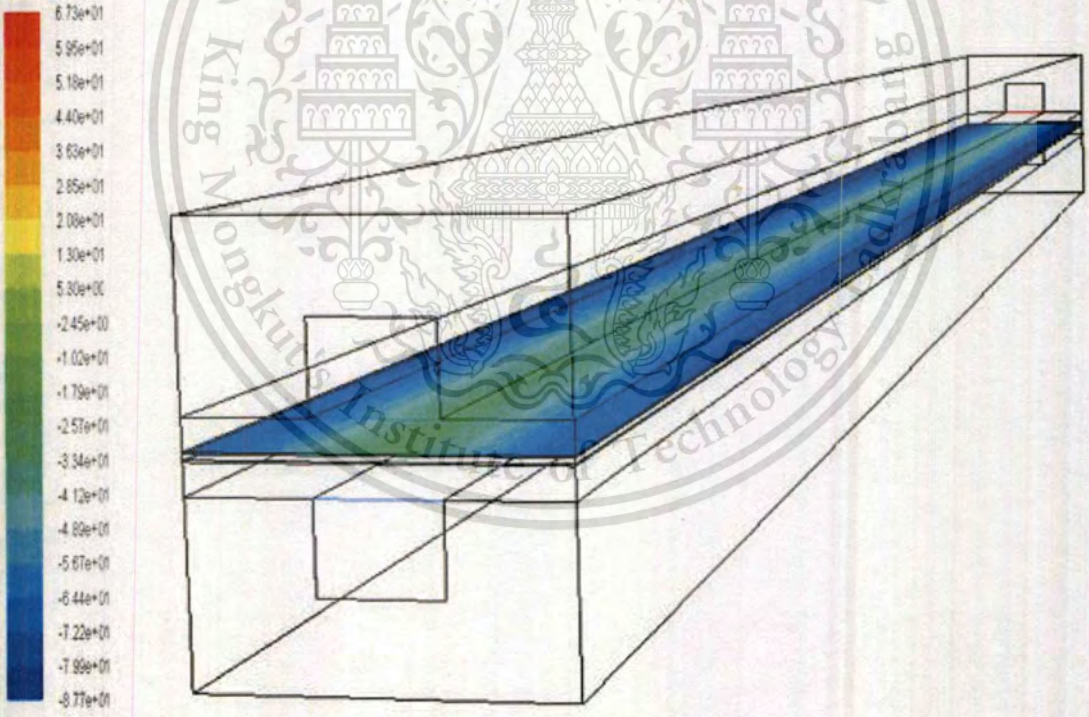

Figure 4.13 Osmotic Drag Source at the Anode TPB for the case of very high humidity

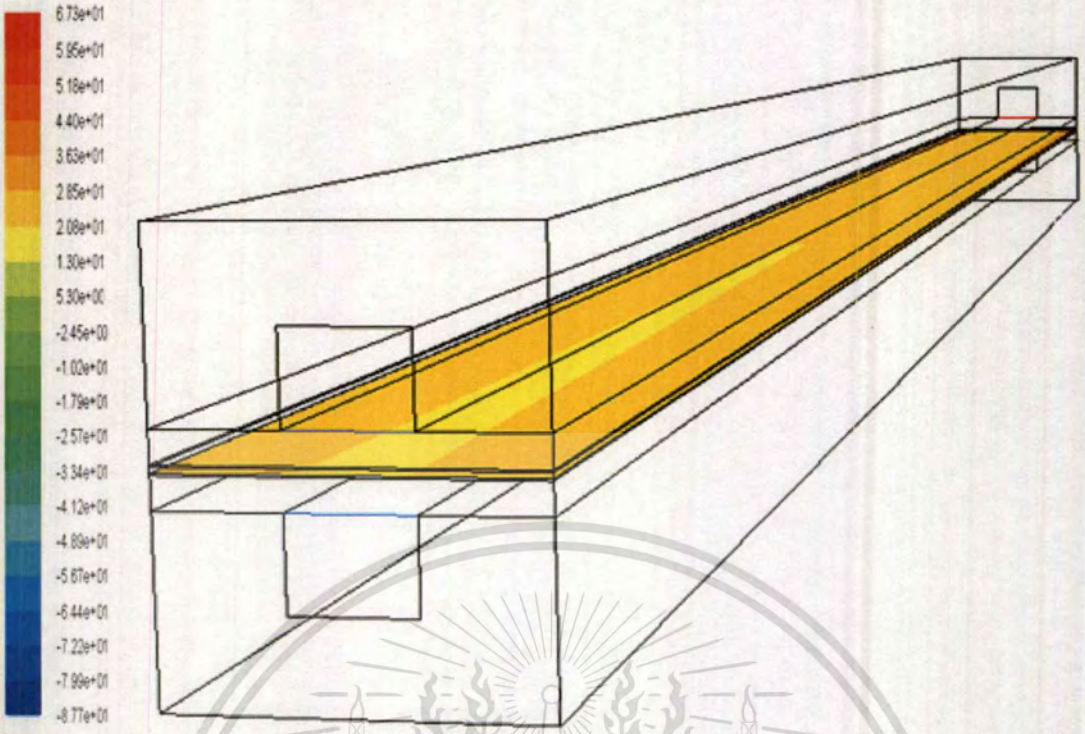

Figure 4.14 Osmotic Drag Source at the Cathode TPB for the case of very low humidity

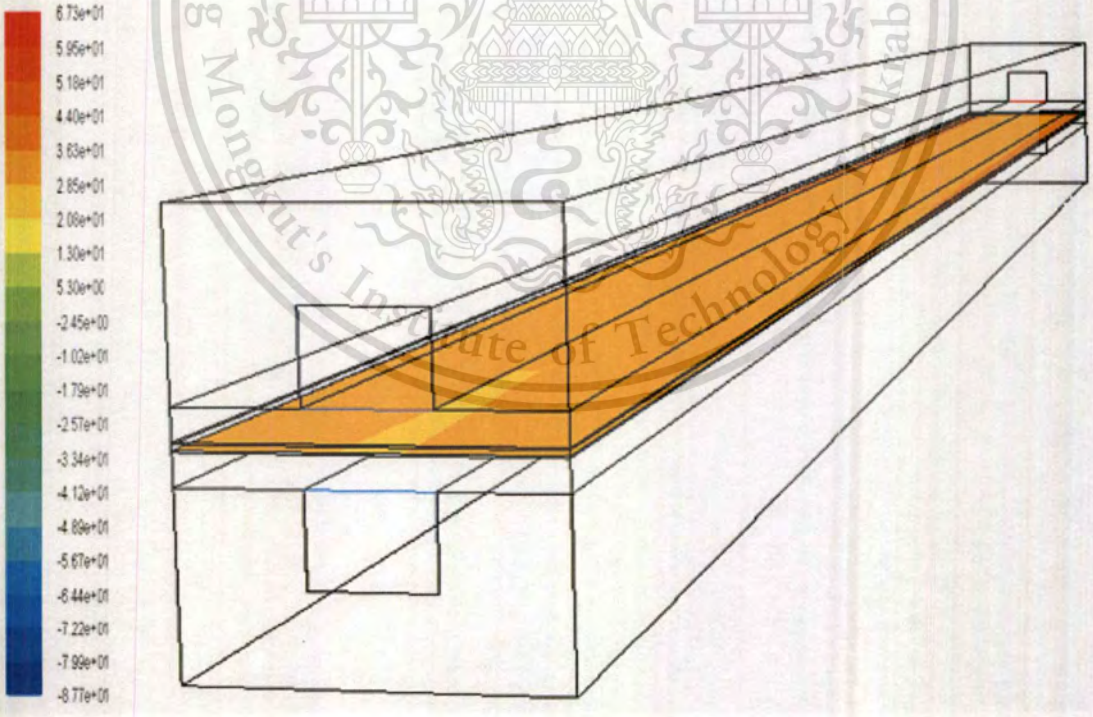

Figure 4.15 Osmotic Drag Source at the Cathode TPB for the case of low humidity

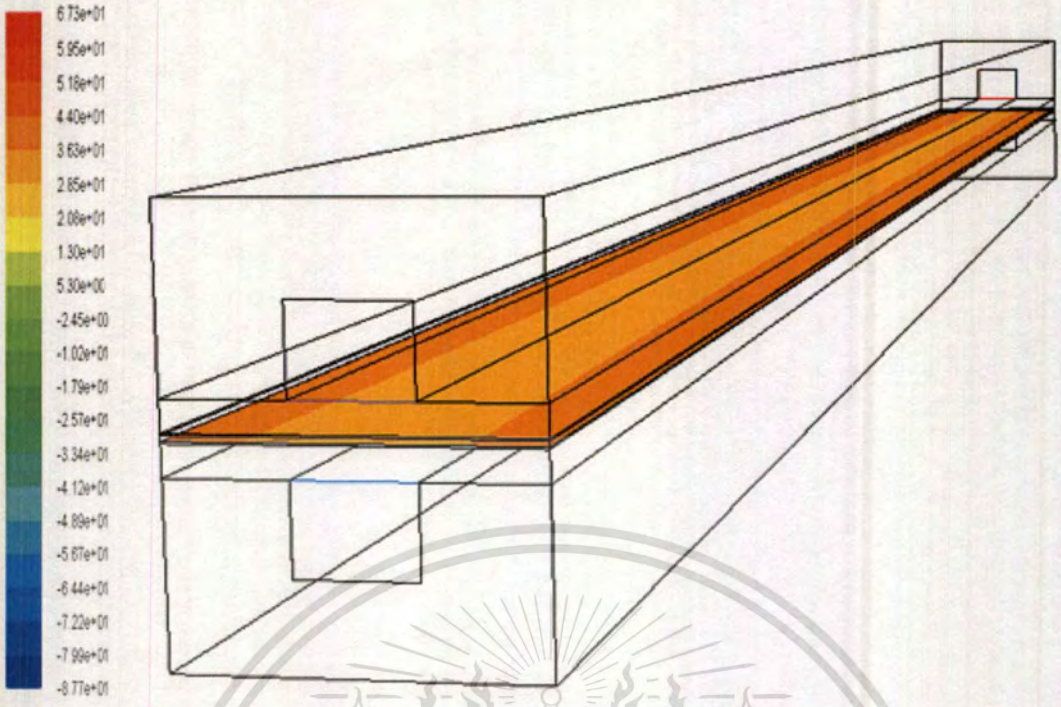

Figure 4.16 Osmotic Drag Source at the Cathode TPB for the case of high humidity

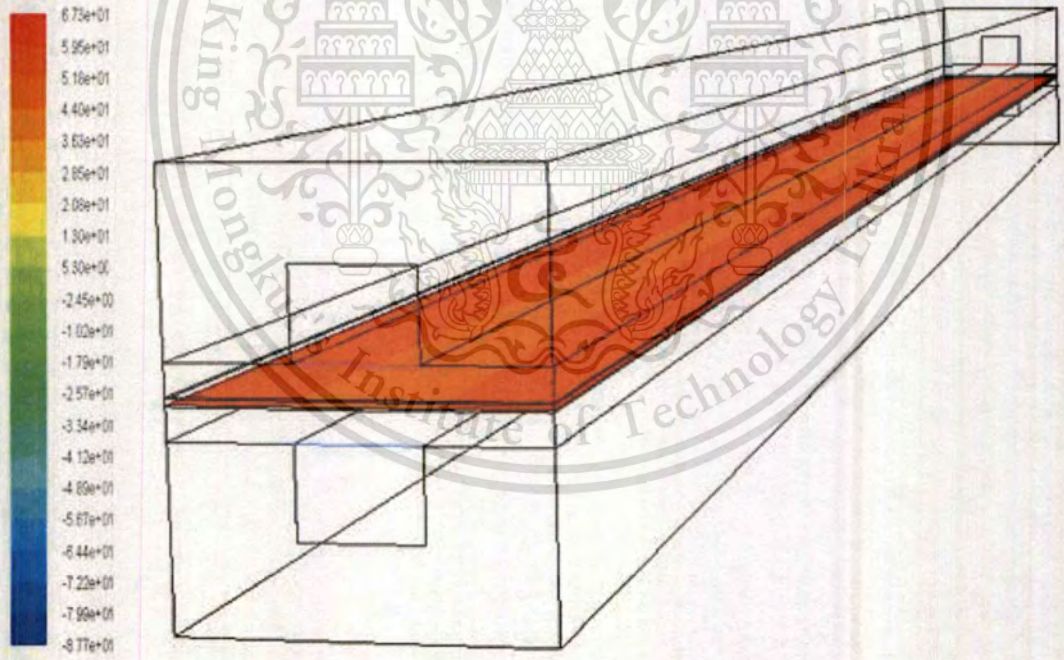

Figure 4.17 Osmotic Drag Source at the Cathode TPB for the case of very high humidity

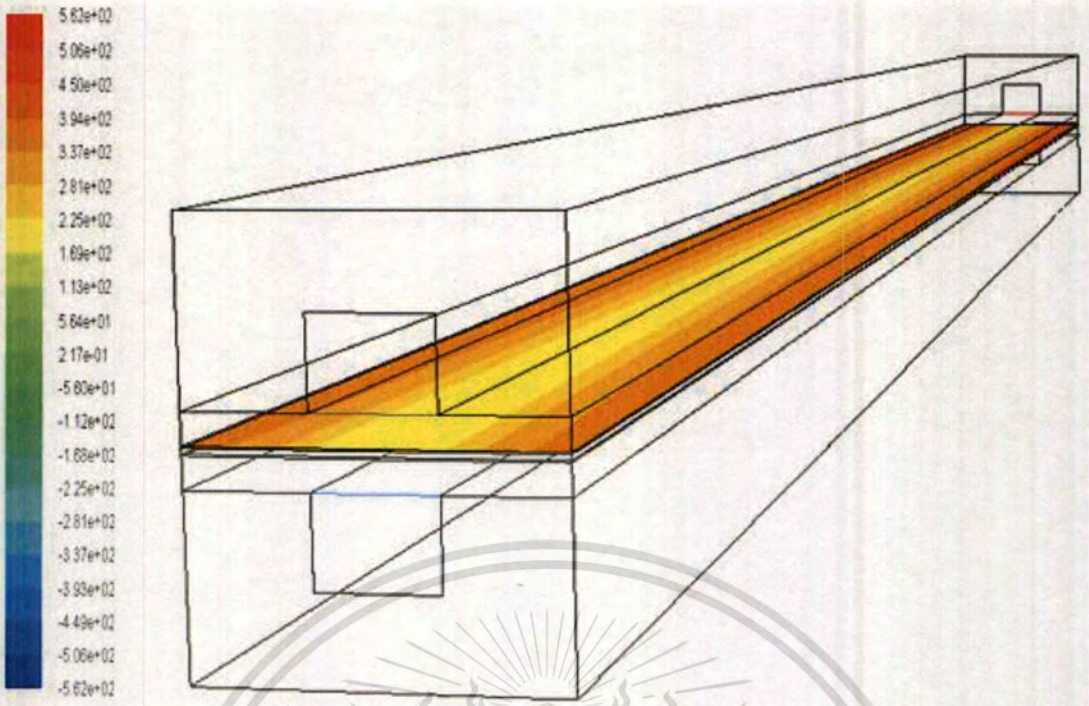

Figure 4.18 Back Diffusion Mass Source at the Anode TPB for the case of very low humidity

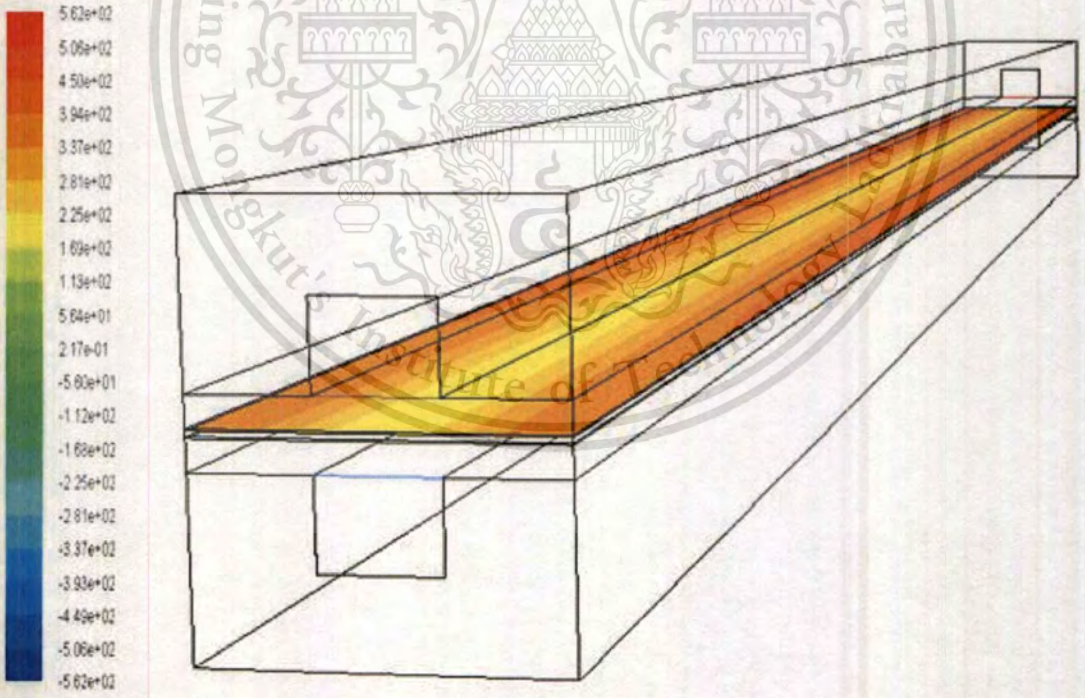

Figure 4.19 Back Diffusion Mass Source at the Anode TPB for the case of low humidity

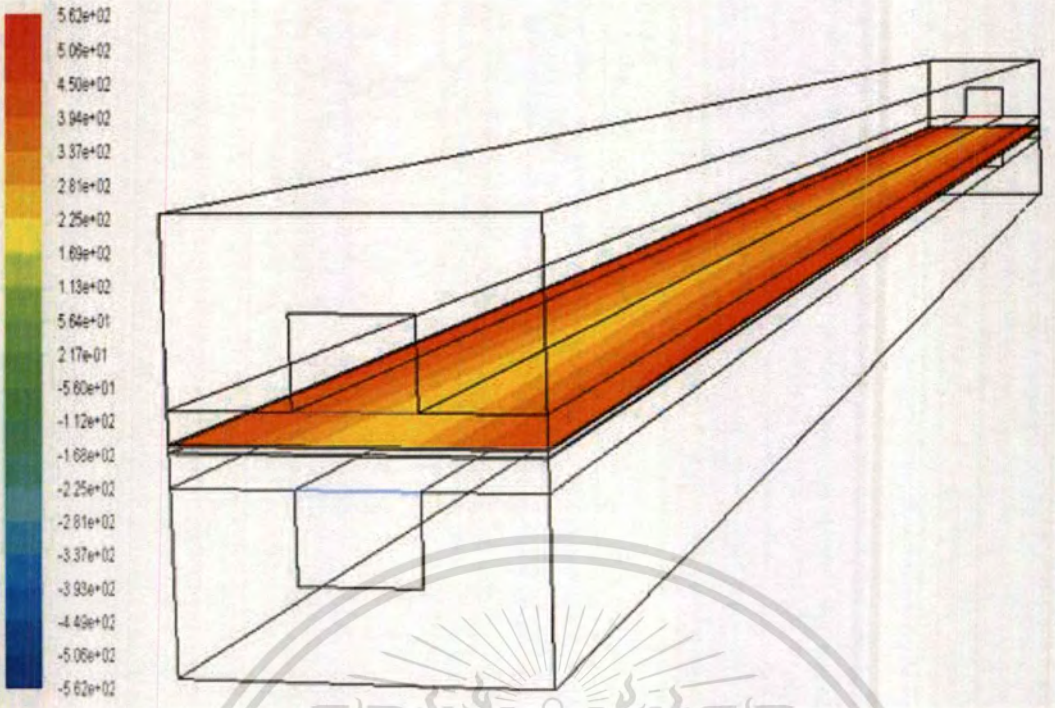

Figure 4.20 Back Diffusion Mass Source at the Anode TPB for the case of high humidity

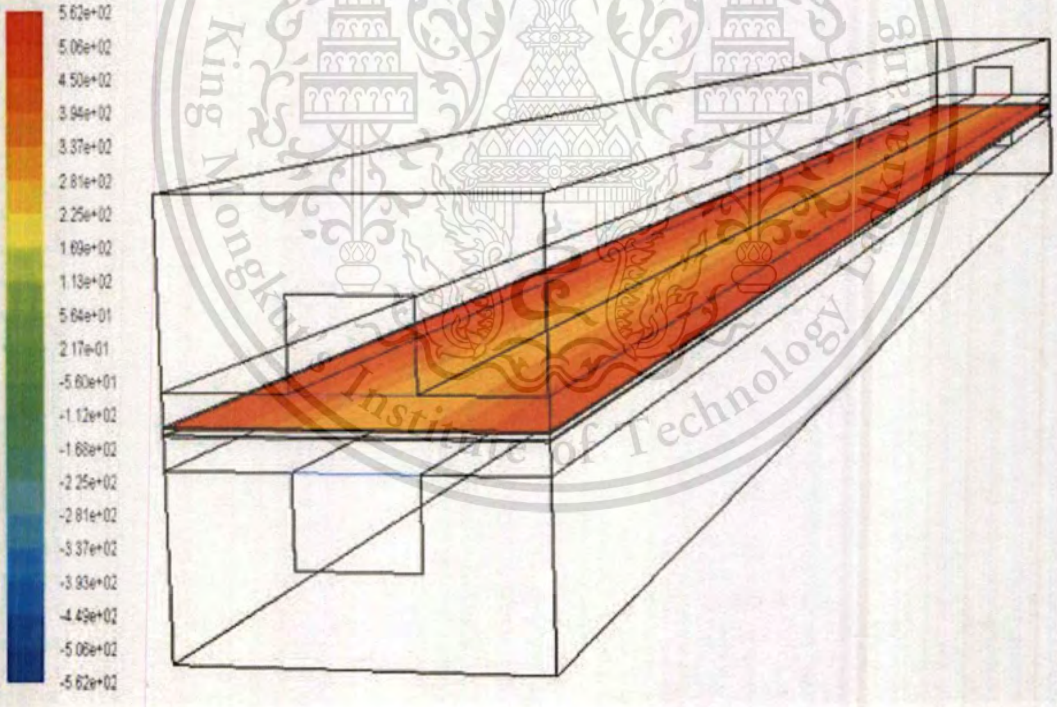

Figure 4.21 Back Diffusion Mass Source at the Anode TPB for the case of very high humidity

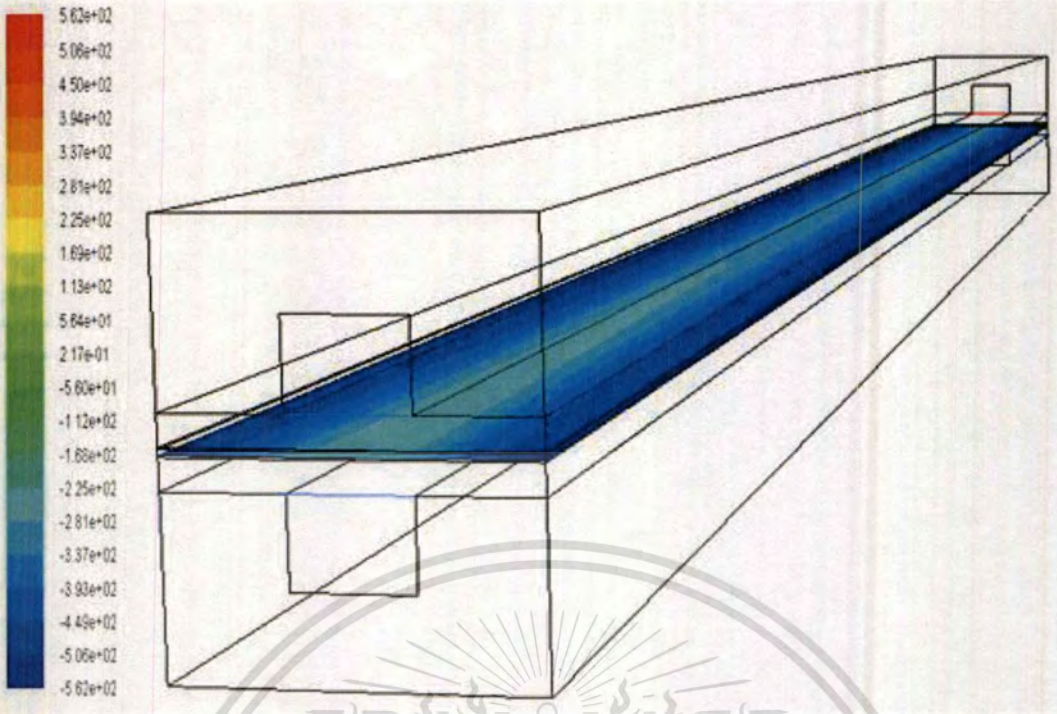

Figure 4.22 Back Diffusion Mass Source at the Cathode TPB for the case of very low humidity

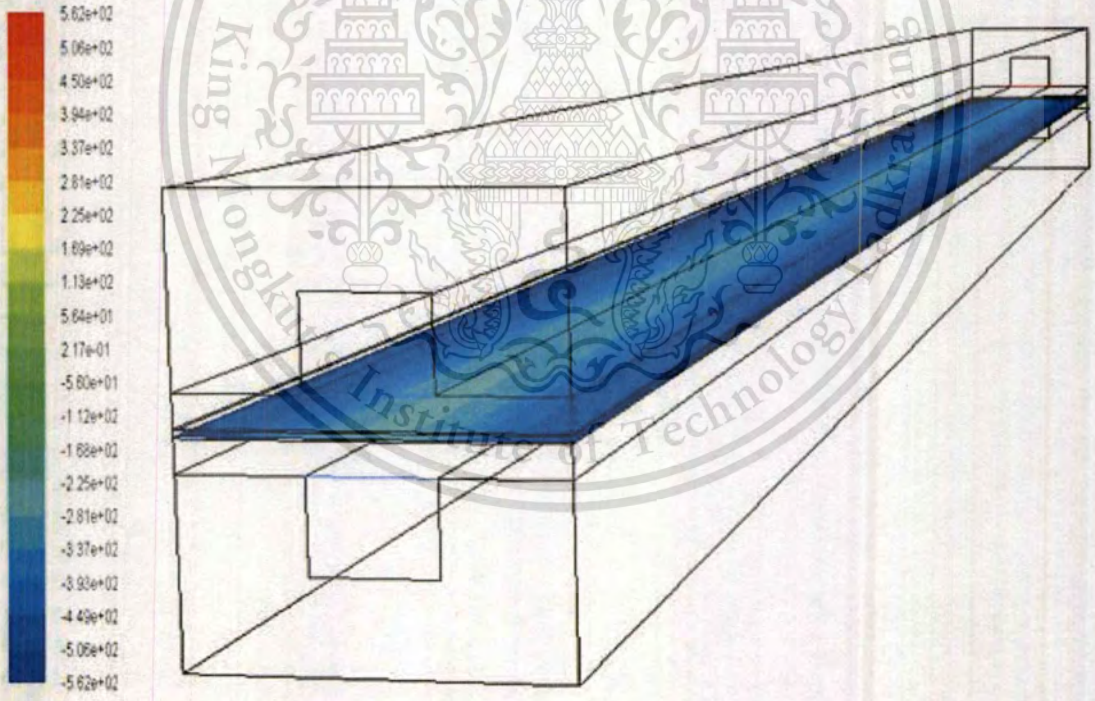

Figure 4.23 Back Diffusion Mass Source at the Cathode TPB for the case of low humidity

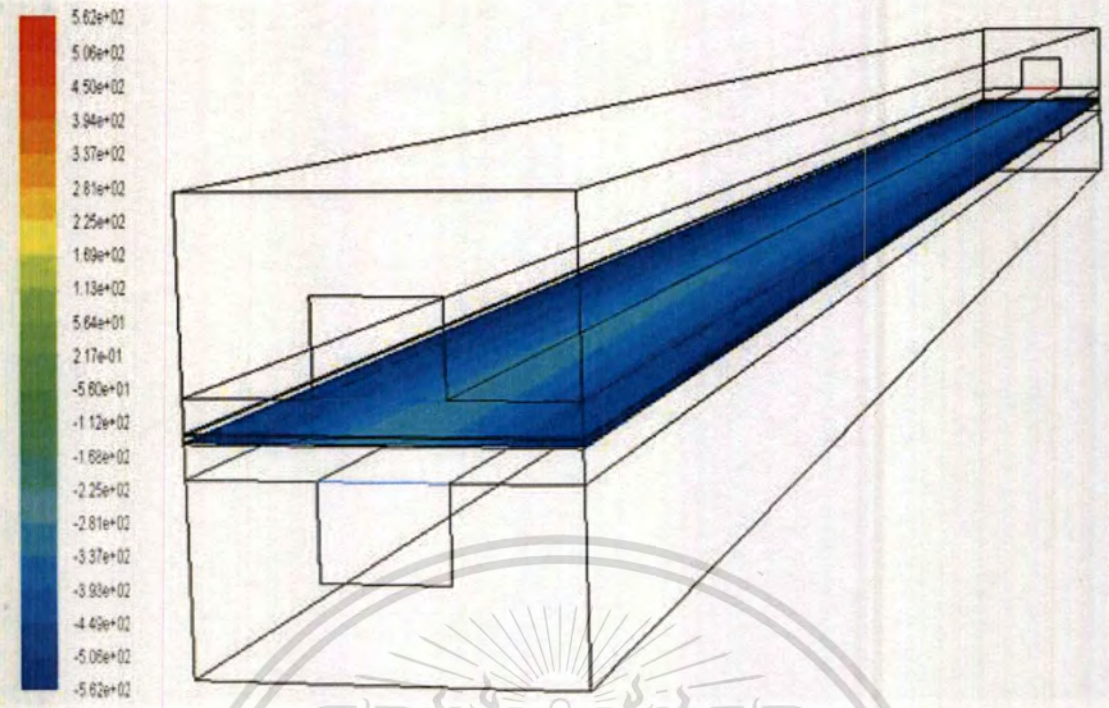

Figure 4.24 Back Diffusion Mass Source at the Cathode TPB for the case of high humidity

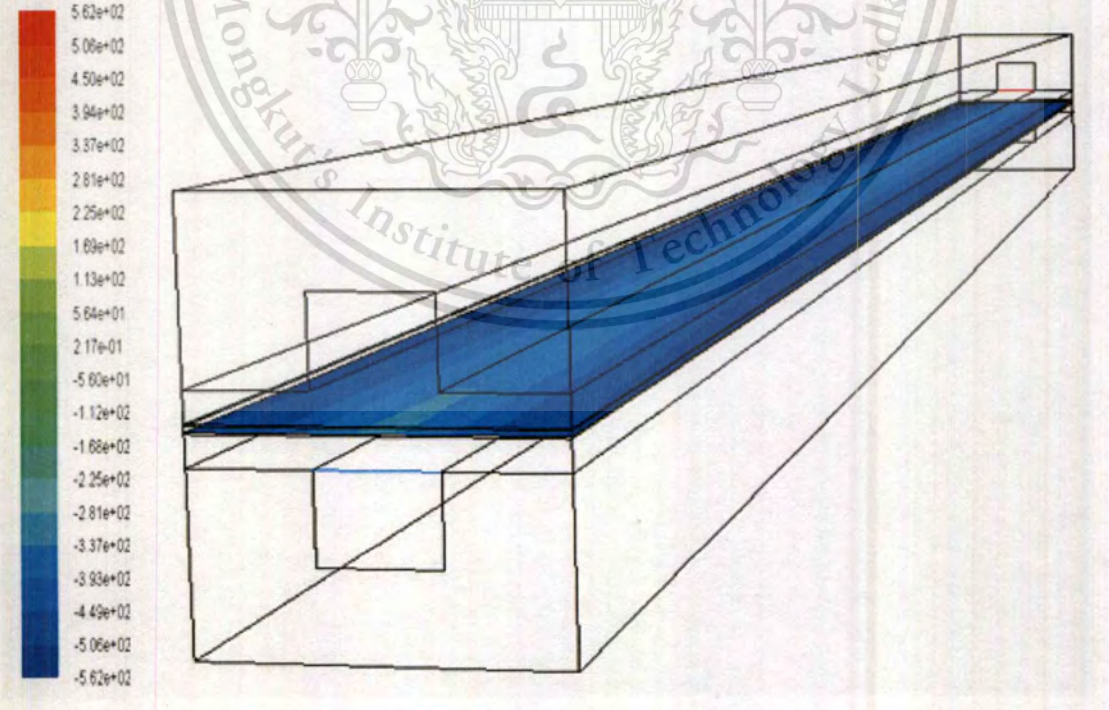

Figure 4.25 Back Diffusion Mass Source at the Cathode TPB for the case of very high humidity

As we know that the key issue of PEMFC is the ability in conducting the proton in the polymer electrolyte membrane. To represent the protonic transport capability of the membrane, the protonic conductivity for each case under this study is presented in figure 4.26 throughout to figure 4.33

At both anode and cathode TPBs, see figure 4.26- 4.33, we have found that the conductivity of proton increase gradually along the channel due to increasing in humidity. Although the concentrations of fuel and air in the anode and cathode channels, respectively, are low due to the dilution effect caused by the presence water vapour, the favourable effect of humidity on the protonic conductivity is far dominant. The cell performance is improved with increasing inlet humidity as seen in figure 4.34.

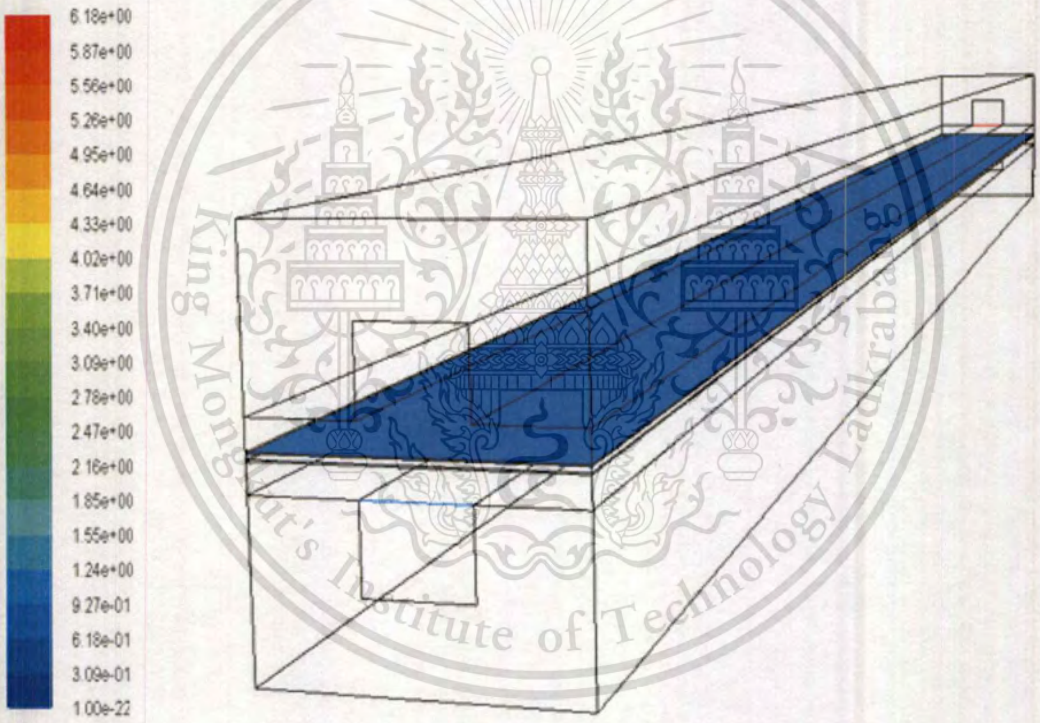

Figure 4.26 Protonic conductivity at the Anode TPB for the case of very low humidity

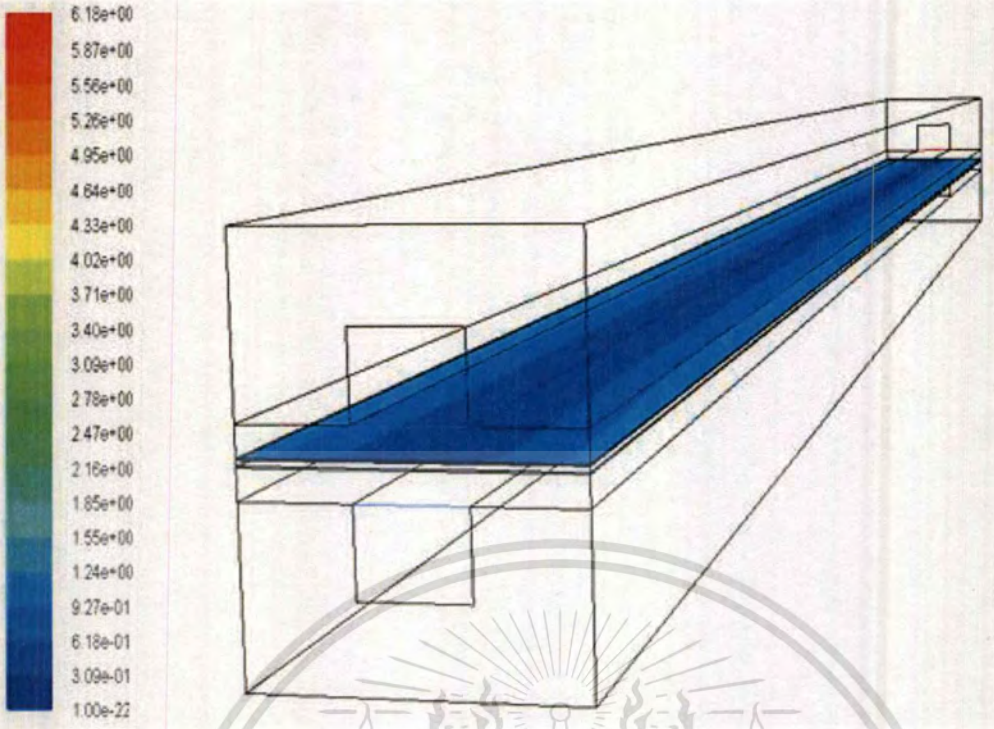

Figure 4.27 Protonic conductivity at the Anode TPB for the case of low humidity

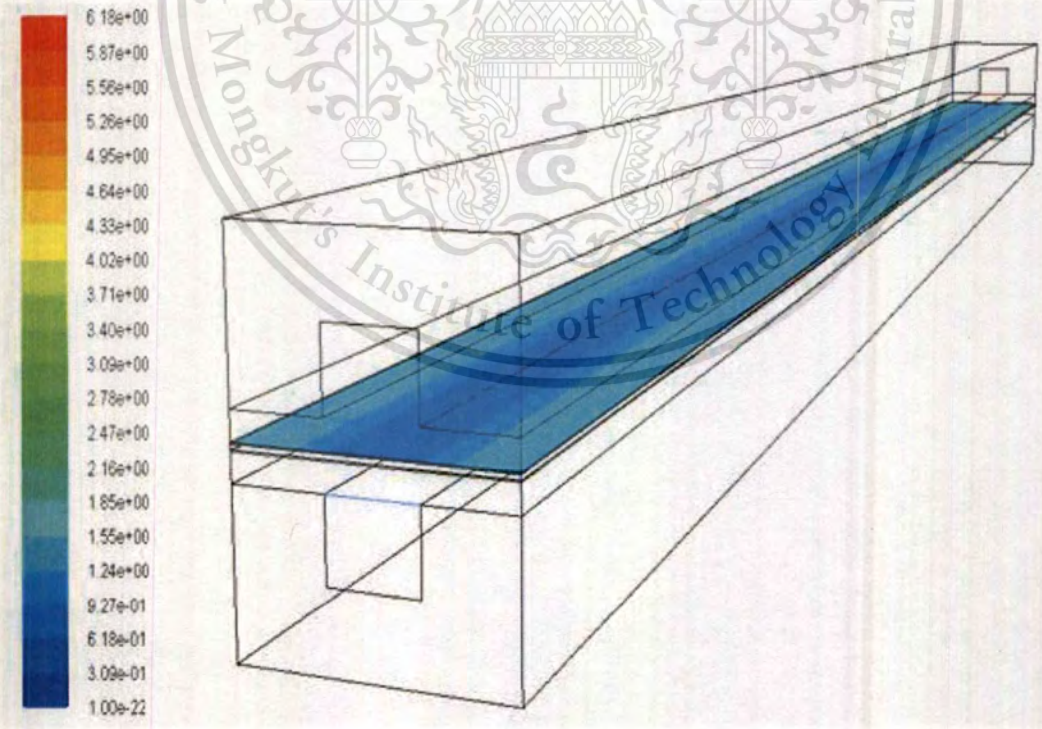

Figure 4.28 Protonic conductivity at the Anode TPB for the case of high humidity

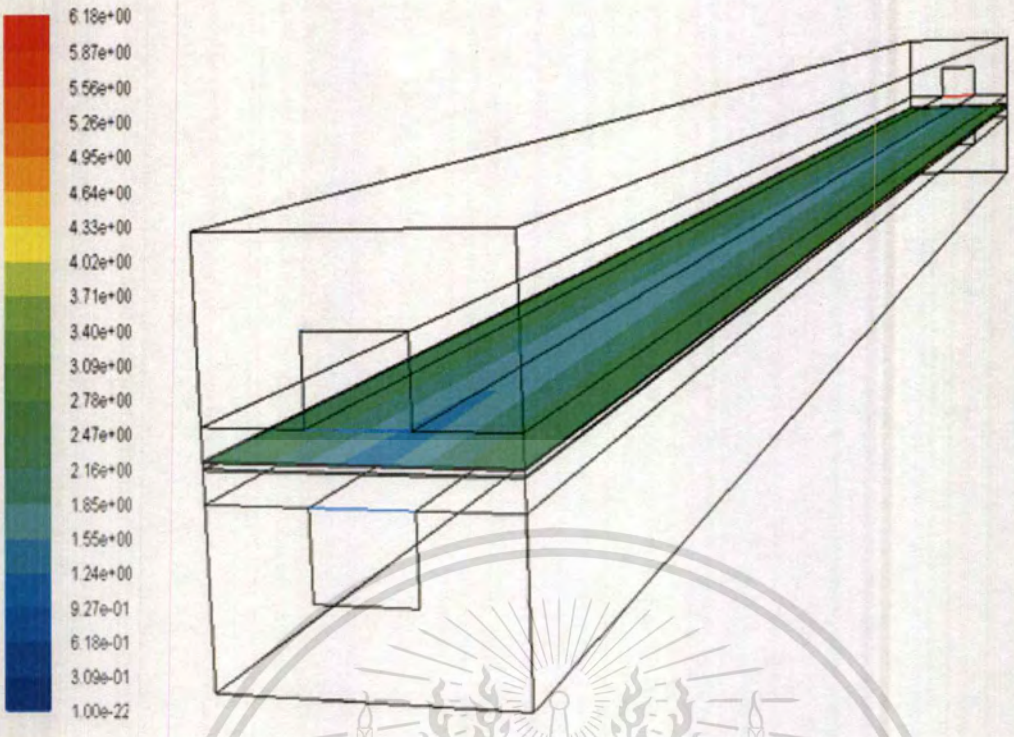

Figure 4.29 Protonic conductivity at the Anode TPB for the case of very high humidity

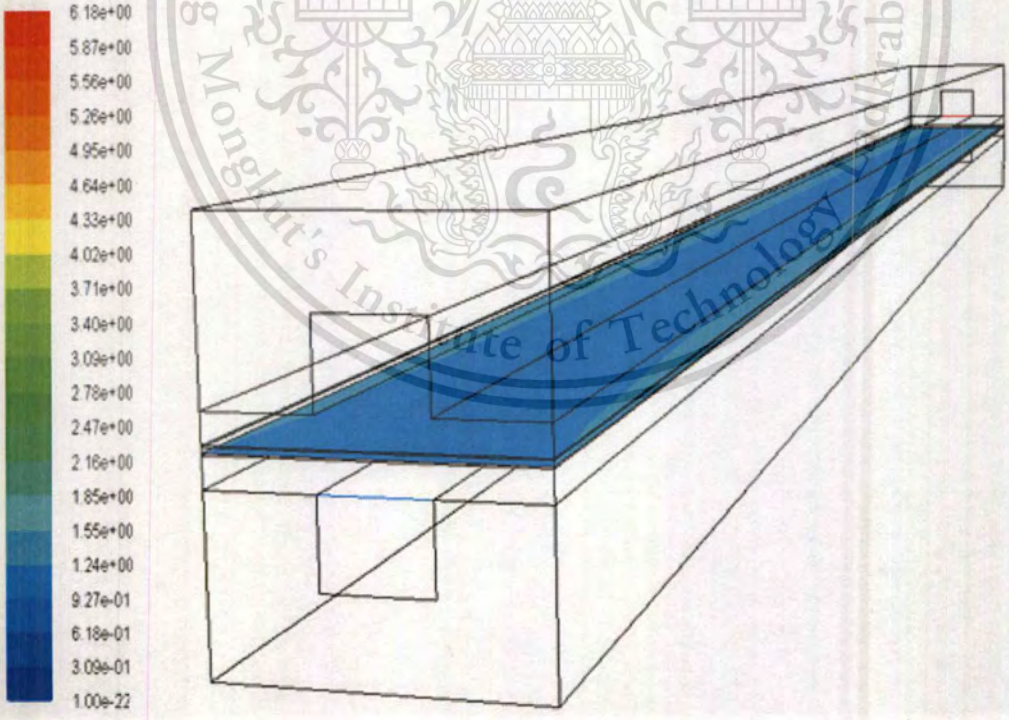

Figure 4.30 Protonic conductivity at the Cathode TPB for the case of very low humidity

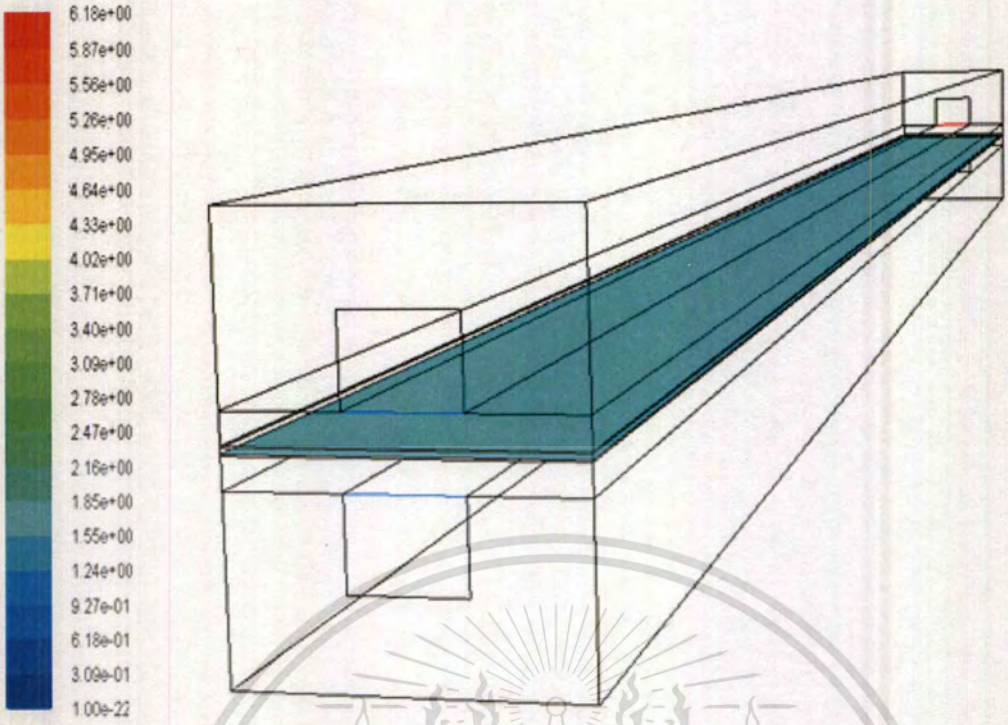

Figure 4.31 Protonic conductivity at the Cathode TPB for the case of low humidity

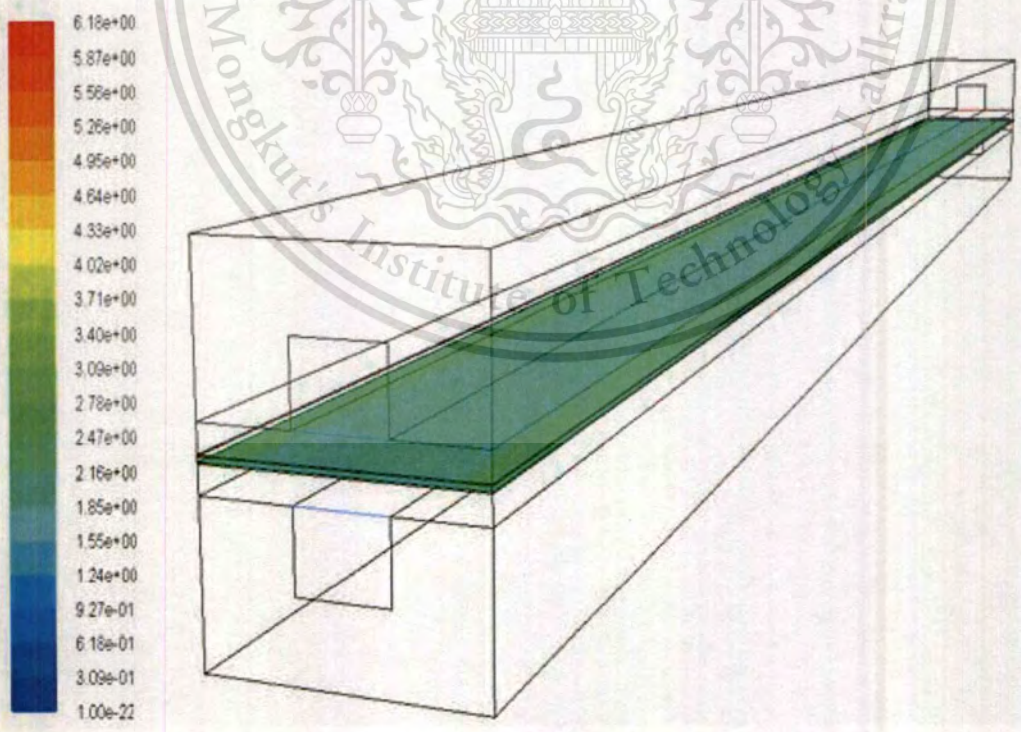

Figure 4.32 Protonic conductivity at the Cathode TPB for the case of high humidity

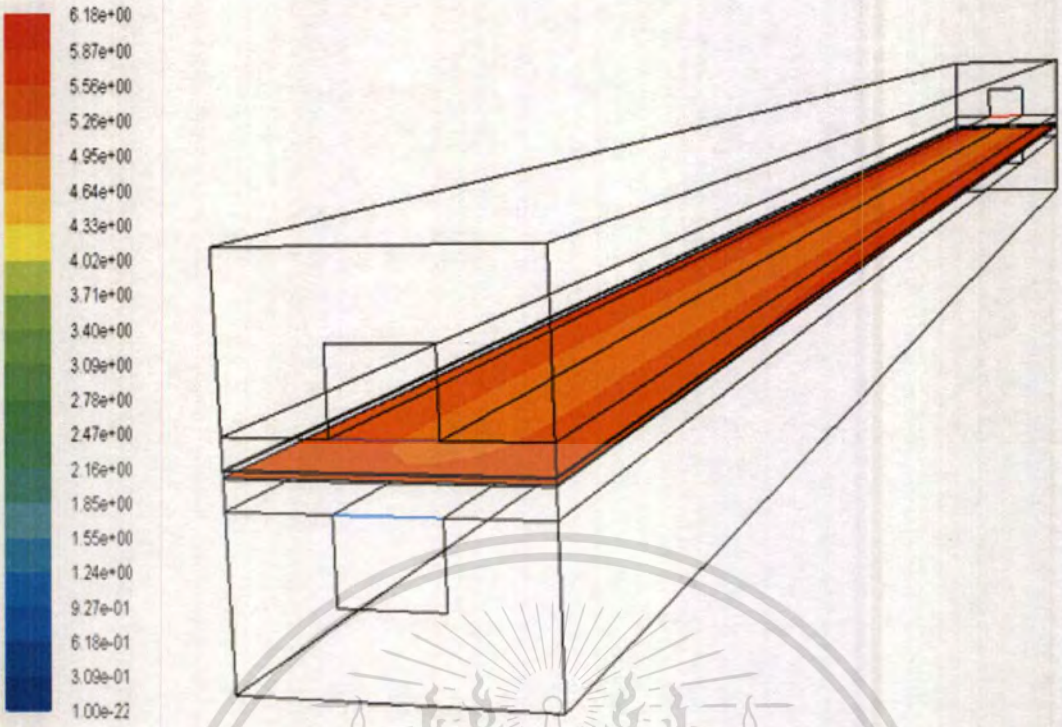

Figure 4.33 Protonic conductivity at the Cathode TPB for the case of very high humidity

In summary, all figures shown above has presented the interactive relationships among parameters such as temperature distribution, heat source and water transport source terms (electro osmotic drag and water back diffusion) and also protonic conductivity. For instance, the protonic conductivity is determined by water content and temperature (Eq. 2.116). An increase in protonic conductivity results in increasing osmotic drag source and consequently back diffusion mass source (thus, closely relate to improved electrochemical reaction). Moreover, the osmotic drag coefficient and water back diffusion sources are dependent to water content and its gradient, respectively (Eq. 2.105 and Eq. 2.110). High reaction rate is presented due to an increasing in temperature distribution as well.

Figure 4.34 shows the effect of inlet humidification on the Polarization Curve. From the simulation, we have found that an increasing in humidity at the inlet channel has a positive effect on the cell performance throughout the loading condition except at the open circuit condition.

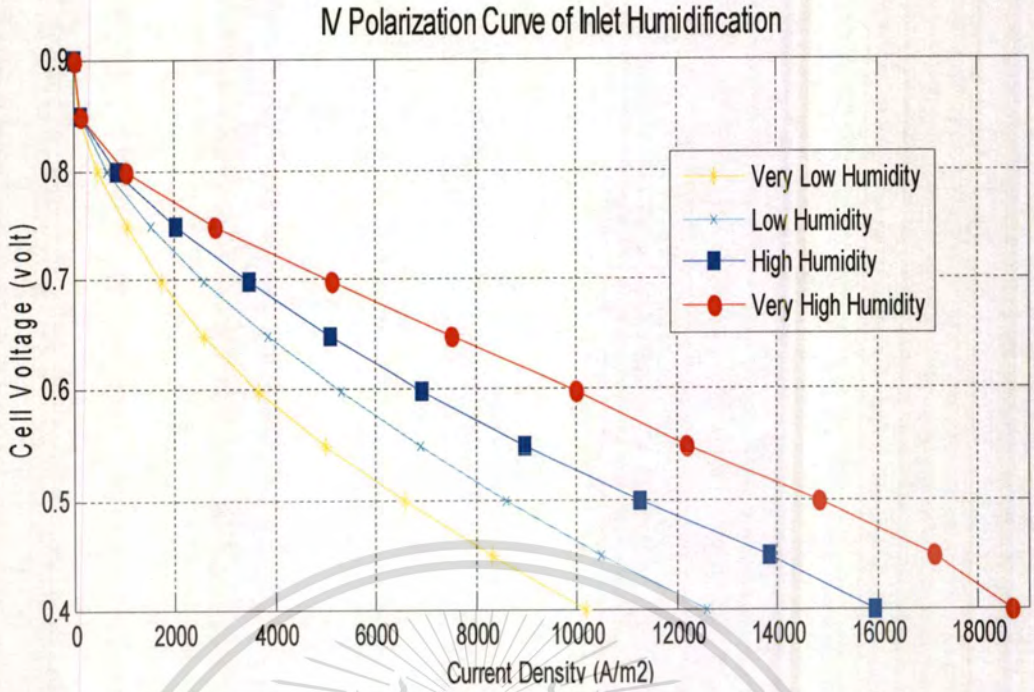

Figure4.34 IV Polarization Curve of Inlet humidification

4.2 Effect of Co and Counter Flow on Cell Performance

Figure 4.35 shows the comparison between IV Polarization Curve of Co-flow and Counter-flow patterns throughout the operation range. At low current operating condition, the result suggests that the co-flow pattern gives slightly higher cell voltage than the counter-flow pattern which is not observable from the graph. The effect of flow pattern is insignificant at this low current density range. On the other hand, at high current density, we have found that the counter-flow pattern gives better cell performance than the co-flow pattern. This is because the counter-flow pattern has lower concentration loss at high current density.

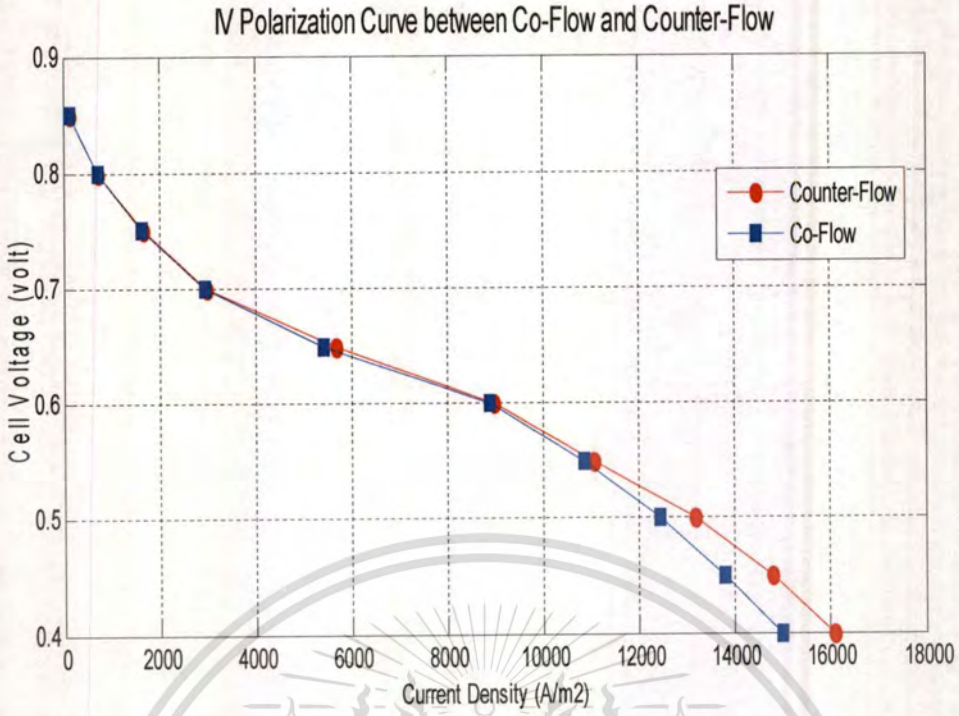

Figure 4.35 IV Polarization Curve between Co-Flow and Counter-Flow

Our approach in making a comparison of stack performance is on an 'identical output voltage' basis. With this approach the voltage drop or cell over-potential under different flow configurations and humidity values at both inlets are predefined where the current density for each case is calculated. This is however in contrast to other investigators where the current density is predefined and the cell output voltage is obtained from the calculation. The relationship between output cell voltage and current density, or in short, the performance curves obtained from these different approaches are, as expected, identical.

In this section, we have chosen the operating point for comparison at 0.4 volt (high current density condition). Apparently, greater current density under a predefined over-potential means less resistance electronically and less effort needed for mass transport, resulting in larger number of electrons and molecules of species at the TPB. Therefore, ones should find it is interesting to look at the cell performance at the same output voltage and relate the different values of current densities to the difference of controlled parameters they attempt to investigate.

As mentioned, the current density under identical voltage is also a meaningful way of comparison. At the same voltage losses, both co flow and counter flow configurations, have resulted in different electronic conductivity, as shown in the form of current density, see figure 4.35. Although this condition is beyond the validity range of the model, due to single-phase assumption as discussed in section 4.1, the effect of flow configuration can be qualitatively

determined. For instance, it can qualitatively determine the effectiveness of having counter-flow channel over the co-flow in the operation region of high current density.

The difference in efficiency of both flow configurations is obvious in this range, as seen in figure 4.35. Moreover, the results are discussed below.

Figures 4.36-4.37 show that the hydrogen concentration at the anode side, especially in case of counter-flow, has decreased gradually with the direction along the channel. In this case, greater amount of hydrogen as well as oxygen are consumed more than that of co-flow as a result of mass conservation Eq. 2.92 and species conservation Eq. 2.99. These source terms correspond to the consumption of hydrogen and oxygen at anode and cathode, respectively. This is due to higher electrochemical reaction rate, see also figures 4.38-4.39.The water concentration in the anode side has increased gradually along the channel mainly due to disappearance of hydrogen with additional effect of water back diffusion from the cathode side. Meanwhile the higher water concentration occurred at the cathode side due to the effect of electro osmotic drag and water formation from electrochemical reaction. When we compare the water concentration of co-flow and counter-flow configurations, the value at the cathode catalyst of the counter-flow is higher than that of the co-flow, which implies greater transport of water into this region as shown in figure 4.40-4.41.

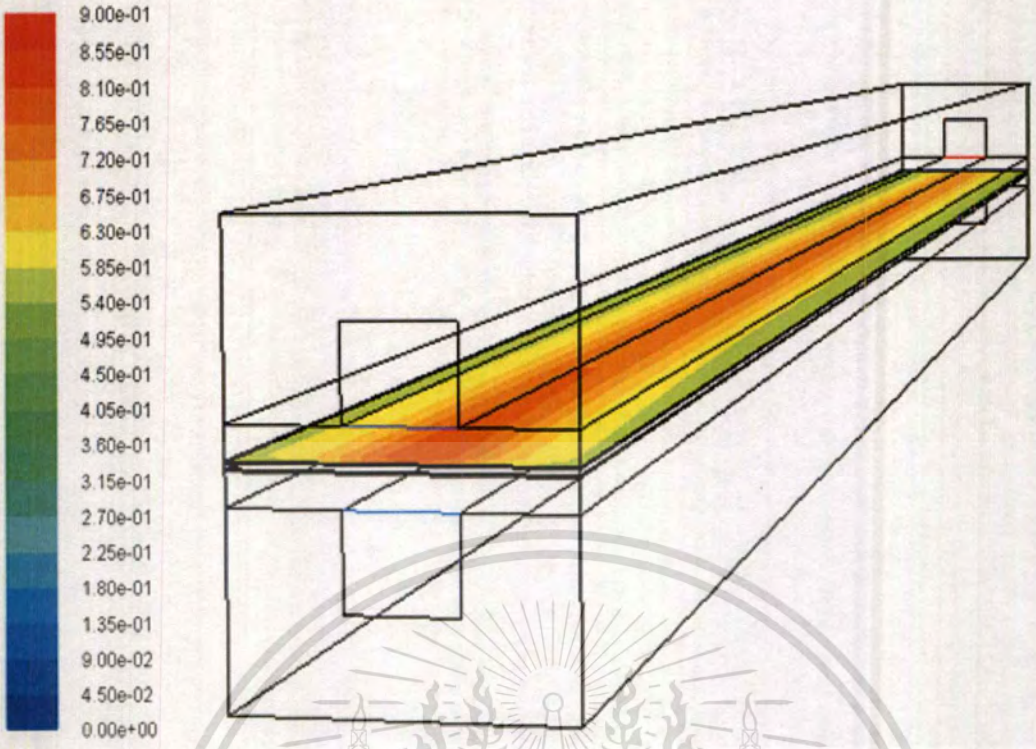

Figure 4.36 H_2 Mass fraction along the channel of Co-flow configuration

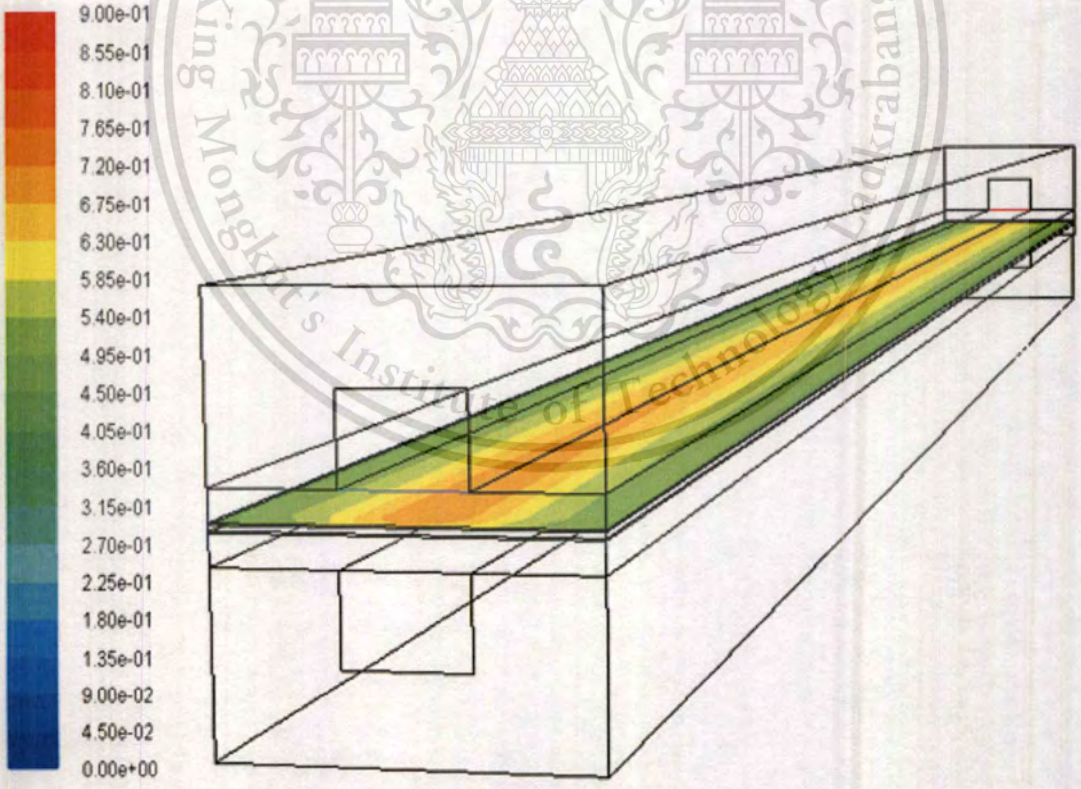

Figure 4.37 H_2 Mass fraction along the channel of Counter-flow configuration

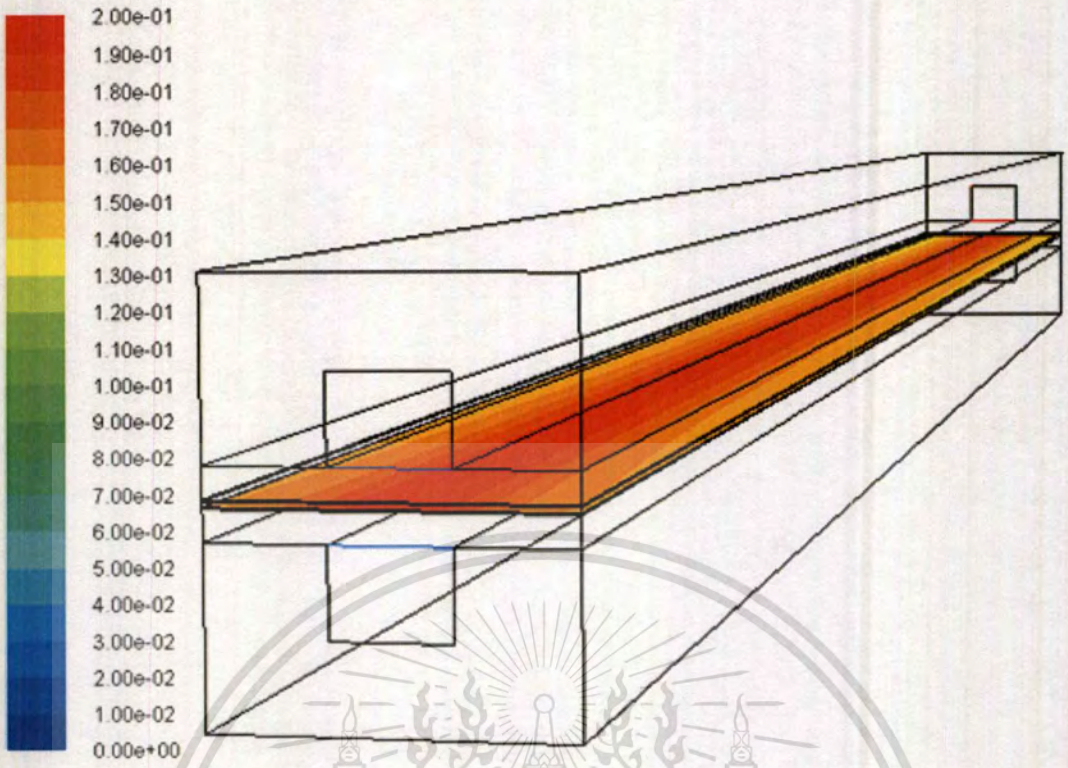

Figure 4.38 O_2 Mass fraction along the channel of Co-flow configuration

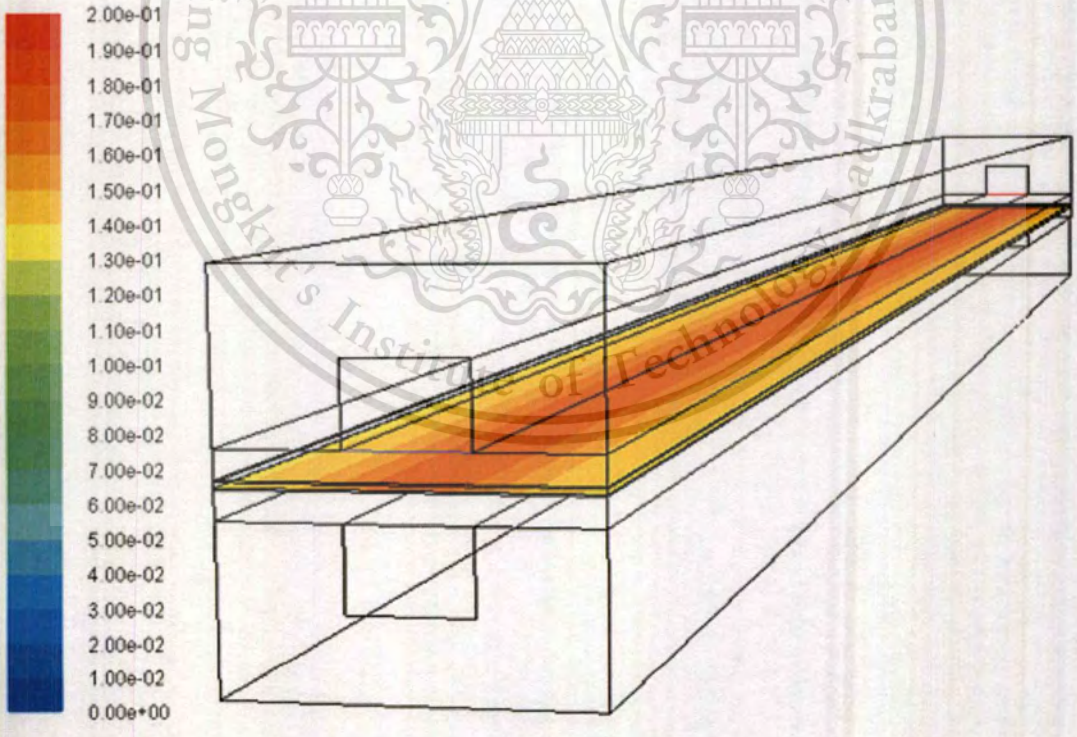

Figure 4.39 O_2 Mass fraction along the channel of Counter-flow configuration

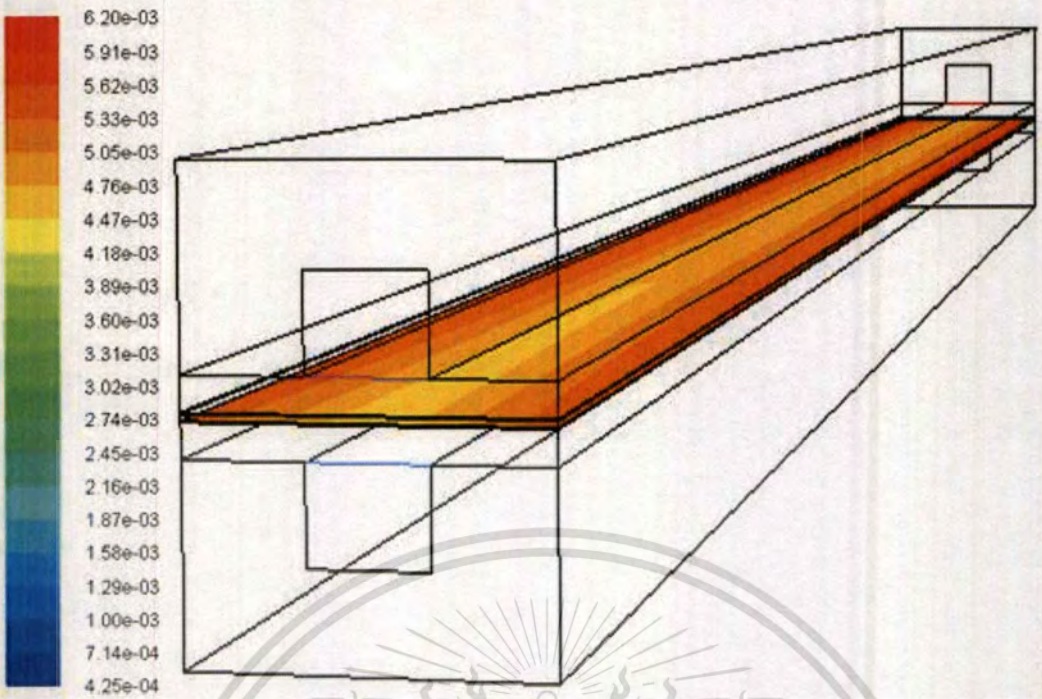

Figure 4.40 Molar Concentration of H_2O along the Channel of Co-flow configuration

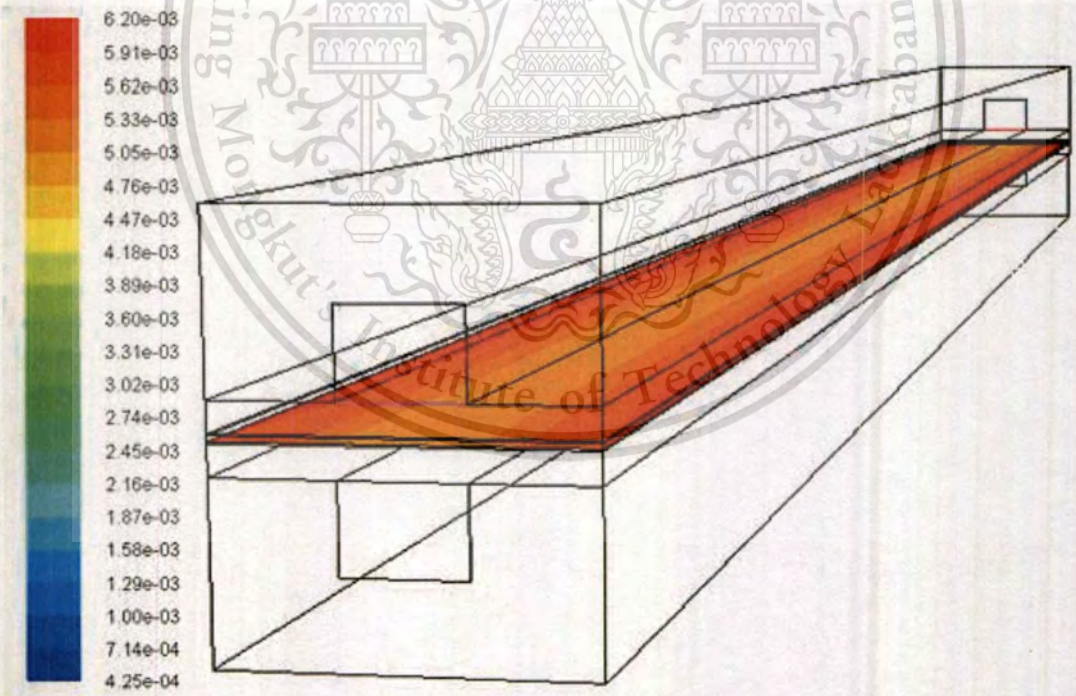

Figure 4.41 Molar Concentration of H_2O along the Channel of Counter-flow configuration

Figures 4.42-4.43 show the temperature distribution along the channel of both flow patterns for Co and Counter flow configurations. We have found that the counter flow pattern

yields relatively better temperature distribution in the high temperature area comparing with Co-flow pattern. Moreover, it is also found that high temperature occurs around the membrane, catalyst layer and gas diffusion layer especially on the cathode side (the highest) since the energy conservation is taken into account, see in Eq. 2.97 . As we know that the water production takes place in this area, thus this heat is a result of water formation.

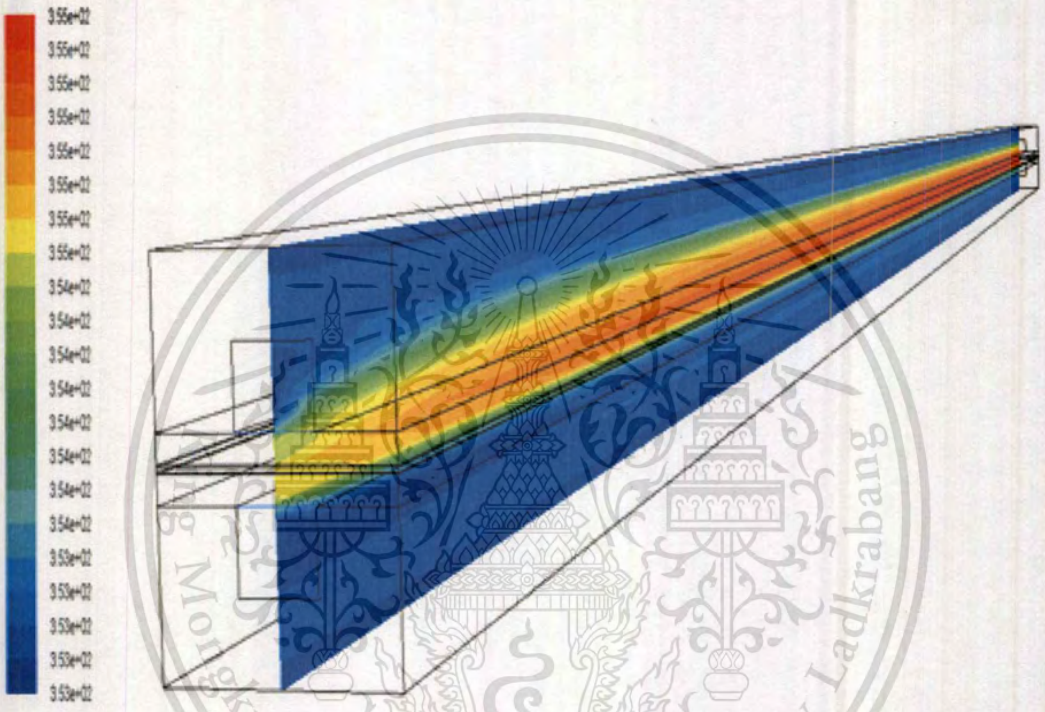

Figure 4.42 Temperature distribution along the channel of Co-flow

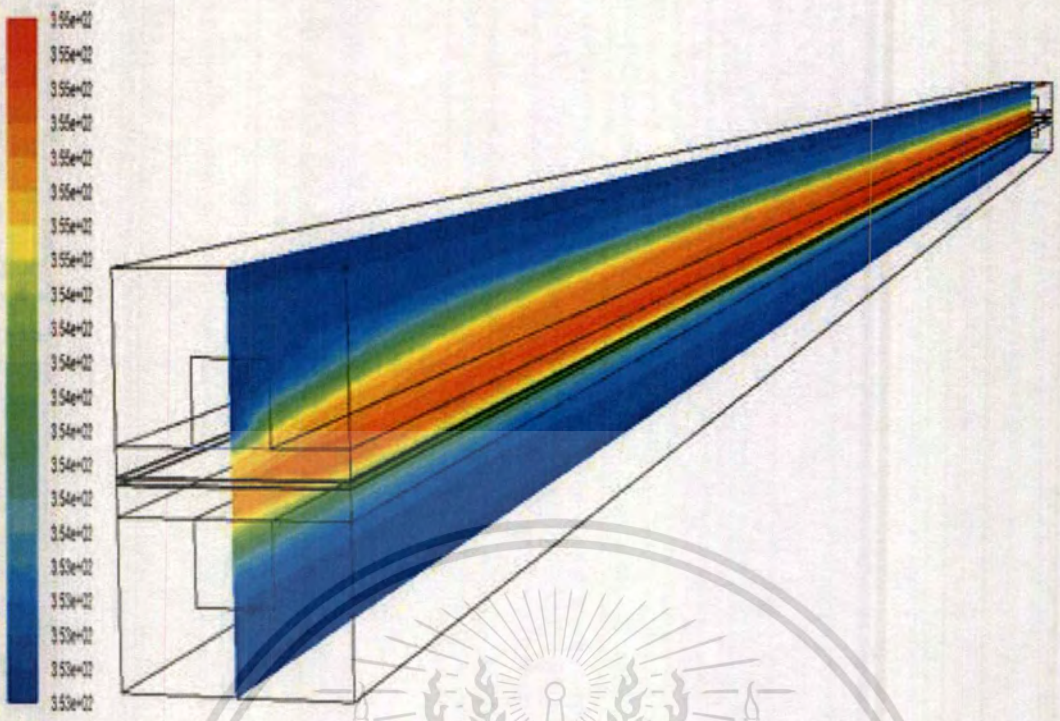

Figure 4.43 Temperature distribution along the channel of Counter-flow

At the high current density condition, we have also found that the Reaction Heat Source (w/m^3) of the Counter-flow pattern is higher than that of the Co-flow pattern due to both gas fuel and reactant are consumed at a greater rate than that of the Co-flow pattern as exothermic reaction which gain higher net enthalpy thus better reaction could be achieved as shown in Figure 4.44-4.45.

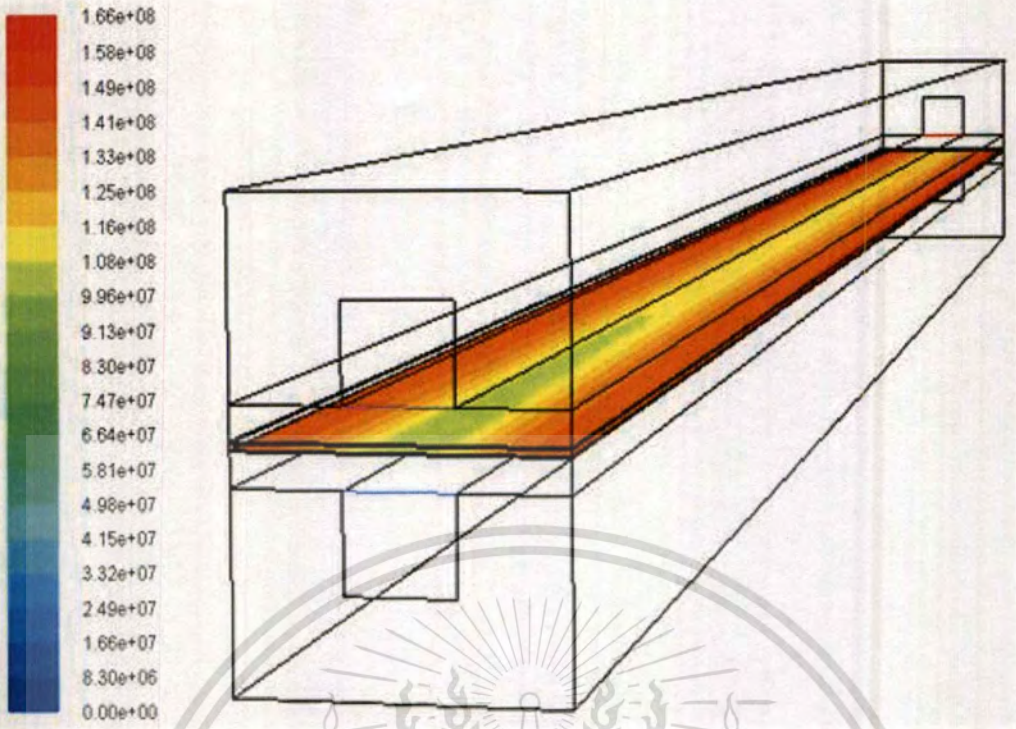

Figure 4.44 Reaction Heat Source of Co-flow configuration

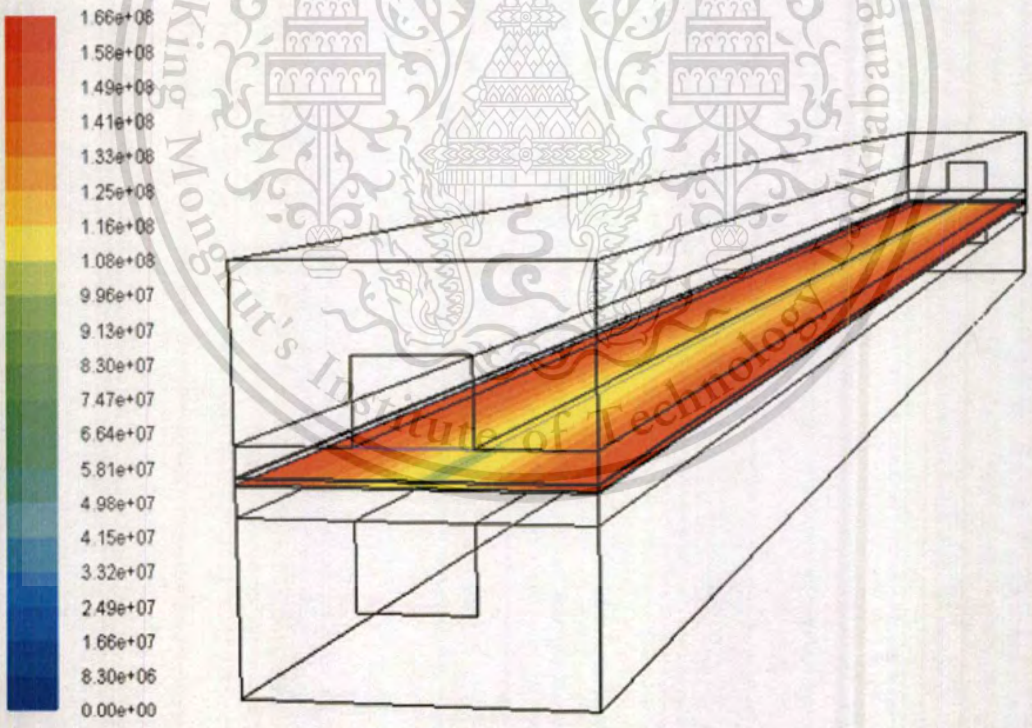

Figure 4.45 Reaction Heat Source of Counter-flow configuration

CHAPTER 5

CONCLUSION AND SUGGESTIONS

5.1 Conclusion

This research presented a three-dimensional computational analysis of a proton exchange membrane fuel cell, which included model validation, presented by IV Polarization Curve between Simulation and Experiment. It can be concluded that the model is valid in low and medium current density region but it over estimates the output voltage at high current density region, since the model is unable to simulate the blockage of liquid water along the fuel channel. As far as the effect of inlet humidification to cell performance is concerned, the simulation results showed that high reaction rate could be achieved for high inlet humidity for both anode and cathode sides as evident forms of protonic conductivity, temperature distribution, reaction heat source and also water transport source term (osmotic drag and back diffusion). The effect of Co and Counter flow on cell performance was also investigated. The study showed that the flow configuration did affect the cell performance, although insignificant effect was observed at low current density. At high current density, we have found that the counter-flow pattern apparently gives better cell performance than the co-flow pattern. This is because the counter-flow pattern has lower concentration loss at high current density. This is a result from the distribution characteristic of counter-flow configuration providing greater amount of hydrogen as well as oxygen being consumed more than that of co-flow. This led to higher electrochemical reaction rate. Meanwhile water concentration of counter flow was higher than co flow thus generating higher heat rate along the channel.

5.2 Suggestions

The single phase fully three dimensional simulation model was used in this work, which lead to our understanding in transport mechanism. Nevertheless, the model has some limitation in representing water flooding phenomena. In order to achieve closely the physical of PEMFC, the multiphase model should be employed. However, this simulation results may give the data necessary for further design.

REFERENCES

1. Barbir, F., "PEM fuel cell theory and practice," **California Elsevier Academic Press**, 2005.
2. Larminie, J., and Dick, A., "Fuel cell system explained," Chichester **John Wiley & Son** 2000.
3. Hontanon, E. , Escudero, M. J., Bautista, C., Garcia-Ybarra, P. L., and Daza, L., "Optimisation of flow-field in polymer electrolyte membrane fuel cells using computational fluid dynamics techniques," **Journal of Power Sources**, vol. 86, pp. 363–368, 2000.
4. Kumar, A., and Reddy, G.," Effect of channel dimensions and shape in the flow-field distributor on the performance of polymer electrolyte membrane fuel cells, " **Journal of Power Sources**, vol. 113, pp 11–18, 2003.
5. Shimpalee, S., Greenway, S., and Van Zee, J. W., "The impact of channel path length on PEMFC flow-field design," **Journal of Power Sources**, vol. 160, pp. 398–406, 2006.
6. Chang, A. C., St-Pierre, J., Stumper, B., and Wetton, B.,"Flow distribution in proton exchange membrane fuel cell stacks," **Journal of Power Sources**, vol. 162, pp. 340–355, 2006.
7. Bor Weng, F., Su, A., Bin Jung, G., Chiao Chiu, Y. and Hung Chan, S., "Numerical prediction of concentration and current distributions in PEMFC," **Journal of Power Sources**, vol.145, pp. 546–554, 2005.
8. Shimpalee, S.; Dutta, S.; Lee, W. K.; Van Zee, J. W. " Effect of humidity on PEM fuel cell performance part II - mumerical simulation **", Proceeding of ASME IMECH, TN, HTD**, Nashville,USA, 1999; Volume 364-1, pp. 367-374.
9. Shimpalee, S., Greenway, S., Spuckler, D., and Van Zee, J. W., "Predicting water and current distributions in a commercial-size PEMFC", **Journal of Power Sources**, vol. 135, pp 79–87, 2004.

REFERENCES (CONT.)

10. Shimpalee, S., and Van Zee, J. W., "Numerical studies on rib&channel dimension of flow-field on PEMFC performance," **International Journal of Hydrogen Energy**, vol. 32, pp. 842 – 856, 2007.

11. Zhuge,W.,Zhang, Y., Ming, P., Lao, X., Chen X., "Numerical simulation of three-dimensional gas/liquid two-phase flow in a proton exchange membrane fuel cell" **Energy Power Eng.** China, pp 305-310, 2007.

12. Pil Hyong,L., Sang Seok ,H.,Sang Soon, "Three-Dimensional Transport Modeling for Proton Exchange Membrane(PEM) Fuel Cell with Micro Parallel Flow Field", **Sensor**, pp.1475-1487,2008.

13. "Fuel Cell Handbook, 5th Edition", Report Prepared By **EG&G Services, Parsons**, Inc. And Science Applications International Corporation for the U.S. Department Of Energy, National Energy Technology Laboratory, October 2000.

14. Nguyen, P.T., "A Three-Dimensional Computational Model of PEM Fuel Cell with Serpentine Gas Channel", **MSc Thesis, University of Victoria**, 2003.

15. Nguyen T.V., White R.V., "A Water and Heat Management Model for Proton Exchange Membrane Fuel Cells", **Journal of Electrochemical Society**, 140(8), 2178-2186, 1993.

16. Mutafa.F.S "Dynamic modeling of water transport in Polymer Electrolyte Membrane Fuel Cell (PEMFC) designs", **MSc Thesis, Sabanci Univesity**, 2005.

17. Nguyen, P.T., Berning, T., Djilali, N., "Computational Model of A PEM Fuel Cell With Serpentine Gas Flow Cannel" ,**Journal of Power Sources**, 130,14-157,2004.

18. N. Jaruwasupant and Y. Khunatorn "Three-dimensional model and experiment of new flow field for proton exchange membrane fuel cell using CFDRC" **International Conference on Green and Sustainable Innovation**, Thailand, pp 563-571, 2006.

19. "PEM Fuel Cell Model Theory", **Fluent Fuel Cell Modules Manual**, Fluent Documentation.

REFERENCES (CONT.)

20. K. Suttanarak, N. Naksuk, J. Charoensuk., W. Pintrakoon, " Numerical Investigation on Water and Heat Generation in Proton Exchange Membrane Fuel Cell" **Proceeding of the 2nd Thammasat University International Conference on Chemical, Environmental and Energy Engineering**, Thailand, pp.275-280, 2009.

BIOGRAPHY

Name: Mr. Keerasut Suttanarak

Date of Birth: January 8, 1981

Place of Birth: Bangkok, Thailand

Education:

2000-2005 B. Eng. in Agricultural Engineering, Faculty of Engineering, Khon Kaen University (KKU)

2007-2010 M. Eng. in Automotive Engineering (International program), International College, King Mongkut's Institute of Technology Ladkrabang (KMITL)

Honour and Scholarship:

2007-2009 Full scholarship for study in the master degree from National Science and Technology Development Agency (NSTDA)

Publications:

1. K.Suttanarak, N.Naksuk, and J.Charoensuk, "Effect of gas humidification in cell performance of Proton Exchange Membrane Fuel Cell by Numerical Simulation", **Proceeding of the International Conference on World Renewable Energy and Congress 2009 –Asia,** Bangkok, Thailand, May 19-22, 2009. pp 793-798.

2. K.Suttanarak, N.Naksuk, and J.Charoensuk and W.Printakoon, "Numerical Investigation on Water and Heat Generation in Proton Exchange Membrane Fuel Cell", **Proceeding of the 2nd Thammasat University International Conference on Chemical, Environmental and Energy Engineering,** Bangkok, Thailand, March 3-4, 2009. pp 275-280.

3. K.Suttanarak, N.Naksuk, and J.Charoensuk, "Effect of Co and Counter Flow to Transport Phenomena for Proton Exchange Membrane Fuel Cell by Numerical Simulation", **Proceeding of the International Conference on Asian Simulation and Modeling 2009,** Bangkok, Thailand, January 22-23, 2009. pp 417-425.

Numerical Investigation on Water and Heat Generation in Proton Exchange Membrane Fuel Cell

Keerasut Suttanarak, Jarruwat Charoensuk
Department of Mechanical Engineering, Faculty of Engineering, King Mongkut's Institute of Technology Ladkrabang
E-mail: keerasut_ae@hotmail.com

Nirut Naksuk, Waravut Printakoon
National Metal and Materials Technology Center

Abstract

The objective of this research is to study the effect of Flow Configuration (Co and Counter flow) on water and heat generations and their transport by taking into account the concentration of hydrogen, oxygen and electrochemical reaction. In depth investigation is carried out by looking at the effect of electro osmotic drag, water back diffusion as well as heat generation between anode and cathode sides. At the operating potential, we have found that the effect of flow pattern at low current is insignificant. On the other hand, at high current condition, the Counter flow pattern gives higher rate of water and heat sources and thus yielding higher voltage than the Co flow pattern apparently due to decrease in the concentration loss.

Keywords: PEMFC, Flow characteristic, Water transport

1. Introduction

Proton Exchange Membrane Fuel Cell (PEMFC), with its zero emission and numerous future commercial prospects, is a promising future energy technology. To develop an efficient fuel cell system, it is necessary to understand its underline mechanisms such as non-uniform concentration, current density distributions, high ionic resistance due to dry membrane, or high diffusive resistance due to the flooding on the cathode. These phenomena can cause performance loss. Improving PEMFC performance has many way for example design of flow characteristic, optimal operating parameter also the water management are necessary. In this research we have carried out the study on effect of flow characteristic (Co and Counter flow) to water transport which lead to development of cell performance.

1.1 Electrochemical Reaction in Fuel Cell

Fuel cell uses reactant gases in electrochemical process to generate electricity. The reaction could be explained as follow.

A gas containing hydrogen molecule flows into the channel and is broken into protons and electrons at the catalyst layer (on the surface of the catalyst) as shown in Eq. (1). The protons are carried through the membrane while electrons as negative current go through external load and end up at the cathode side.

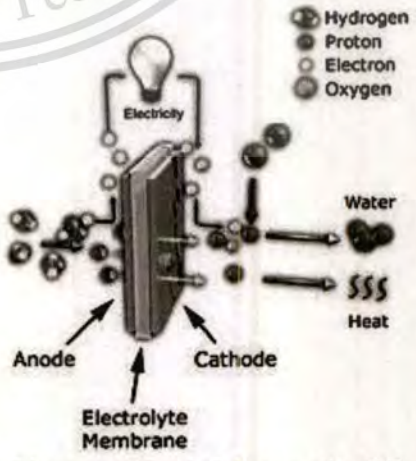

Fig. 1: Diagram of Fuel Cell operation [4]

At the cathode side, oxidation reaction takes place as oxygen molecules combine with electrons and protons (hydrogen ions) and forming water molecules in vapor form as shown in Eq. (2). This process is called reduction. Thus, the products from the reaction are water and electrons. This process is shown in Fig.1

$$H_2 \rightarrow 2H^+ + 2e^- \quad (1)$$

$$O_2 + 4e^- + 4H^+ \rightarrow 2H_2O \quad (2)$$

1.2 Fuel Cell Efficiency

Due to irreversible losses while delivering the electrical current, the cell potential is decreased from its open-circuit equilibrium. These losses are usually referred to as over potential, over voltage or polarizations. These include; i) the loss by equilibrium shift of the electro-chemical reaction or activation loss obviously observed at low current density, ii) the electronic resistance of the anode, cathode and other conducting material defined as ohmic loss which is linearly related to the amount of current drawn from the cell, and iii) the gas concentration gradient occurring across the electrode materials defined as concentration loss which prominently affect the cell performance at high current density.

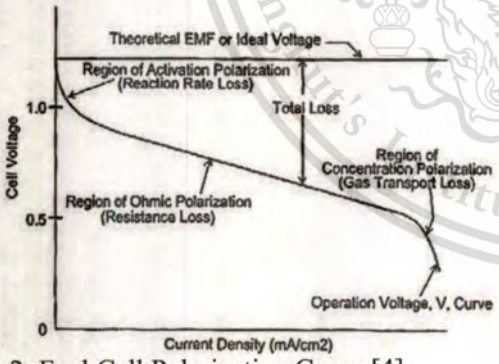

Fig. 2: Fuel Cell Polarization Curve [4]

2. Mathematical modeling and computational Domain

The simulation based on conservation equation of mass, momentum, energy, current and species implementing on CFD software. The key elements of modeling are transport phenomena in porous media, heterogeneous reaction in porous electrodes and coupling between mass transport, electrochemical and current potential fields.

The Computational Domain includes anode and cathode flow channels, anode and cathode current collectors, anode and cathode Gas Diffusion Layers, anode and cathode Catalyst Layers and Membrane as shown in fig 3 and fig 6. In case of co flow, fuel and the reactant flow in same direction as shown in fig 4. Conversely, fuel and the reactant flow in the opposite direction in the flow channels as shown in fig 5.

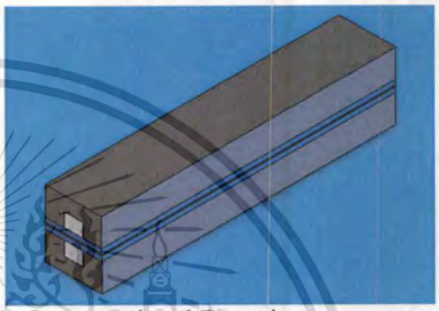

Fig. 3: Computational Domain

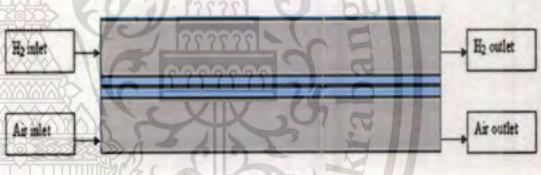

Fig. 4: Schematic of Co-flow

Fig. 5: Schematic of Counter-flow

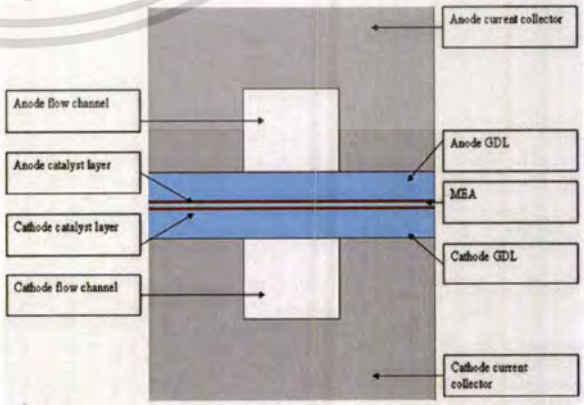

Fig. 6: Cross-section Schematic of PEM Fuel Cell

In this section, we will present all governing equations involved in the process. The mass conservation equation can be written as Mass conservation

$$\nabla.(\varepsilon\rho u) = s_m \quad (3)$$

where ε is porosity ρ is mixture density and u is velocity vector.

The s_m denotes source terms corresponding to the consumption of hydrogen and oxygen in the anode and cathode, and the production of water in the cathode

$$s_m = s_{H_2} + s_{aw} \quad : Anode\ side \quad (4)$$

$$s_m = s_{O_2} + s_{cw} \quad : Cathode\ side \quad (5)$$

Momentum conservation

$$\nabla(\varepsilon\rho uu) = -\varepsilon\nabla p + \nabla(\varepsilon\mu\nabla u) + s_u \quad (6)$$

where subscript 'a' and 'c' refer to the anode and cathode respectively.
Where p is pressure, μ is dynamic viscosity s_u denote source term based on Darcy's law

$$s_{ux} = -\frac{\mu u}{\beta_x},\ s_{uy} = -\frac{\mu u}{\beta_y}\ and\ s_{uz} = -\frac{\mu u}{\beta_z} \quad (7)$$

where β is the permeability And the energy conservation relation can be written as

$$\frac{\partial}{\partial t}(\varepsilon\rho h) + \nabla.(\varepsilon\rho uh) = \nabla.q + \varepsilon\frac{dp}{dt} - j_T\eta + \frac{i.i}{\sigma} + S_h \quad (8)$$

where h is mixture static enthalpy i is current density J_T is the transfer current η is electrode over potential σ is electrical conductivity S_h is latent heat of phase change and q is heat flux due to thermal conductivity. The species diffusion equation above can be written as

$$q = k\nabla T + \sum J_i h_i \quad (9)$$

where k is the thermal conductivity; T is the mixture temperature and J_i is species diffusion flux. The species conservation equation can be written as

$$\nabla(\varepsilon\mu C_k) = \nabla(D_k^{eff}\nabla C_k) + s_k \quad (10)$$

where C_k is Molar concentration of chemical species
D_k^{eff} is the effective diffusion coefficient and s_k denotes source term

$$s_k = -\frac{I(x,y)}{2F}M_{H_2}A_{CV} \quad :s_{H_2} \quad (11)$$

$$-\frac{\alpha(x,y)}{F}I(x,y)M_{H2O}A_{CV} \quad :s_{aw} \quad (12)$$

$$-\frac{I(x,y)}{4F}M_{O_2}A_{CV} \quad :s_{O_2} \quad (13)$$

$$-\frac{1+2\alpha(x,y)}{2F}I(x,y)M_{H2O}A_{CV} \quad :s_{cw} \quad (14)$$

where M_{H2}, M_{H2O} and M_{O2} are the molecular weight of hydrogen, water and oxygen respectively and $I(x,y)$ is the local current density F is Faradays constant $\alpha(x,y)$ is the local net water transfer coefficient per proton and A_{CV} is the specific surface area of control volume element in the domain.

The water management is a critical issue for the performance of a proton electrolyte membrane fuel cell. The transport phenomena of water can be described as follows.

First, the water molecules are transported through the polymer electrolyte membrane by the hydrogen protons and this process is called electro-osmotic drag. In addition to the molecular diffusion and electro-osmotic drag, water is generated in the cathode catalyst layer due to electrochemical reaction.

1) Electro-osmotic water flux going through the membrane can be calculated from the proton flux going through the membrane, given by the specified current density and Faraday law as

$$j_{H2O} = 2x\,n_d\frac{I(x,y)}{2F} \quad (15)$$

n_d is Electro-osmotic drag coefficient which depend on water activity as follow

$$n_d = 0.029\lambda^2 + 0.05\lambda - 3.4x10^{-19} \quad (16)$$

where λ represents water content of the membrane described as

$$\lambda = 0.043 + 17.81a_k - 39.85a_k^2 + 36a_k^3 \; ; 0 < a_k < 1 \quad (17)$$

$$\lambda = 14 + 1.4(a_k - 1) \; ; 1 < a_k < 3 \quad (18)$$

where a_k is water activity

$$a_k = \frac{x_{wk}\, p(x,y)}{p_{wk}^{sat}} \quad ; \; k \; is \; Anode \; or \; Cathode \quad (19)$$

where x_{wk} *and* p^{sat} are water mole fraction and saturation pressure at each electrode respectively therefore

$$\log_{10} p^{sat} = -2.1794 + 0.02953T - 9.1837x10^{-5}T^2 + 1.4454x10^{-7}T^3 \quad (20)$$

2) For the back diffusion flux, the water formation at the cathode results in a gradient in the water content between the cathode side and anode side of the membrane. For PEMFC, this gradient causes a water flux back to anode side which is superimposed to the electro-osmotic flux. This back diffusion is expressed as following water flux as

$$J_{H2O} = -\frac{\rho}{M} x D_w x \frac{d\lambda}{dz} \quad (21)$$

where ρ is the dry density of electrolyte, M is electrolyte equivalent weight, z is the direction through the membrane thickness and D_W is water diffusion coefficient therefore

$$D_w = D_\lambda \exp(2416x(\frac{1}{303} - \frac{1}{T_{cell}})) \quad (22)$$

where

$$D_\lambda = 10^{-10} \; ; \lambda < 2 \quad (23)$$

$$D_\lambda = 10^{-10}(1 + 2(\lambda - 2)) \; ; 2 \le \lambda \le 3 \quad (24)$$

$$D_\lambda = 10^{-10}(3 - 1.67(\lambda - 3)) \; ; 3 < \lambda < 4.5 \quad (25)$$

$$D_\lambda = 1.25x10^{-10} \; ; \lambda \ge 4.5 \quad (26)$$

The model assumptions we have adopted in this study are:

1) Steady state
2) Laminar flow
3) Isothermal
4) Incompressible fluid
5) Butler-volume equation is used to describe electrochemical reaction.
6) Reactant species include H_2, O_2, N_2 and H_2O (vapor) are considered.
7) The volume of liquid H_2O was assumed to be negligible in the domain.
8) The gravity effect is negligible

Table 1: Model parameters

Parameters	value
Channel width (*mm*)	0.8
Channel high (*mm*)	0.6
Channel length (*mm*)	125
Rip width (*mm*)	0.8
GDL thickness (*mm*)	0.21
Catalyst thickness (*mm*)	0.012
Membrane thickness (*mm*)	0.036
Operating pressure (*MPa*)	0.1
Operating temperature (*K*)	353

3. Results and Discussions

The Fig.7 (a) shows that the hydrogen mass fraction at the anode side, especially in case of counter flow, has decreased gradually with the direction along the channel. In this case, greater amount of hydrogen as well as oxygen are consumed more than that of co flow. This is due to higher electrochemical reaction rate; see also fig.10 (a) and fig.10 (b). The water mass fraction in the anode side has increased gradually along the channel mainly due to disappearance of hydrogen with additional effect of water back diffusion from the cathode side. Meanwhile the higher water mass fraction occurred at the cathode side due to the effect of electro osmotic drag and water formation from electrochemical reaction. When we compare the water mass fraction of co and counter flows, the value at the cathode catalyst of the counter flow is higher than that of the co flow, which implies greater transport of water into this region.

The water product is generated at Cathode side with certain amount diffuses back to the anode layer by water back diffusion. The osmotic drag force also crate significant amount of mass transfer of water from the anode side to the electrolyte layer. It is therefore worthwhile to observe these aspects of water sources at the cathode catalyst layer of both flow configuration (Co and Counter flow). We have also found that Reaction Heat Source of the Counter-flow pattern is higher than that of the Co-flow pattern due to both gas fuel and reactant are consumed at a greater rate than that of the Co-flow pattern, thus better reaction could be achieved as shown in Fig 8.

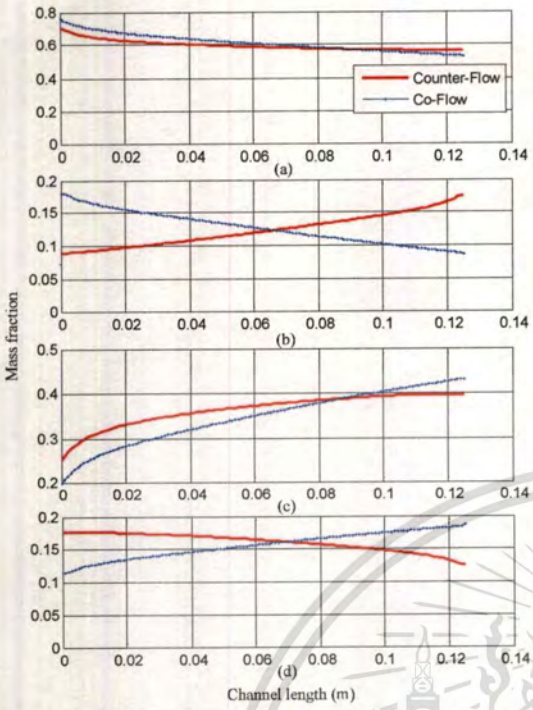

Fig. 7: Mass fraction along channel of co and counter flow at 0.75 volt
(a) Hydrogen mass fraction along anode-side channel
(b) Oxygen mass fraction along cathode-side channel
(c) Water mass fraction at anode catalyst layer
(d) Water mass fraction at cathode catalyst layer

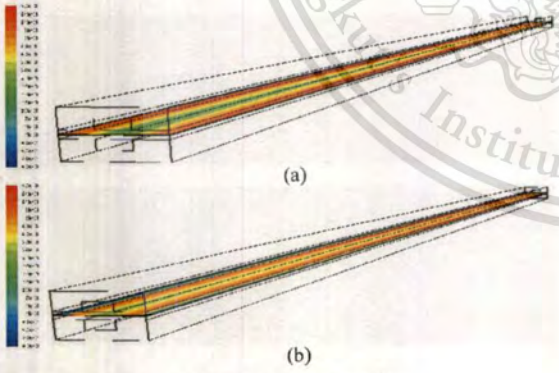

Contour of Reaction Heat Source (w/m^3)

Fig. 8: Reaction Heat Source along channel
(a) Reaction Heat Source of Co-flow configuration
(b) Reaction Heat Source of Counter-flow configuration

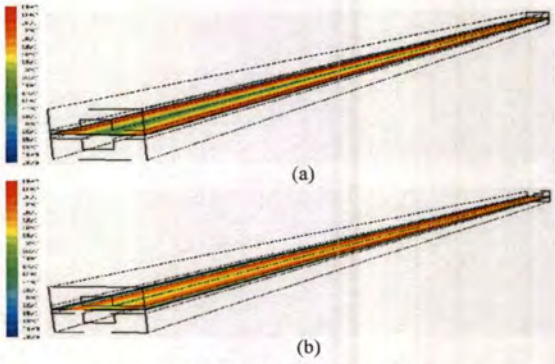

Contours of Osmotic Drag Source (kg/m^3s)

Fig. 9: Osmotic Drag Source along channel
(a) Osmotic Drag Source of Co-flow configuration
(b) Osmotic Drag Source of Counter-flow configuration

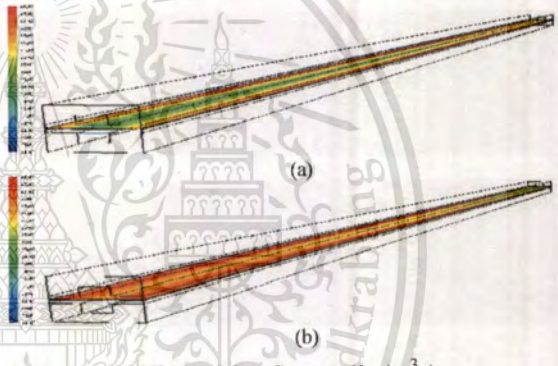

Contours of Diffusion Mass Source (kg/m^3s)

Fig. 10: Back Diffusion Mass Source along channel
(a) Back Diffusion Mass Source of Co-flow configuration
(b)Back Diffusion Mass Source of Counter-flow configuration

We have also found that the osmotic drag source of the Counter-flow pattern is higher than that of the Co-flow pattern as shown in Fig 9. This is caused by the hydrogen ion travelling through the membrane from anode side to cathode side at a greater transfer rate. We have also noticed that at the anode catalyst layer, the back diffusion mass source of the Counter-flow configuration is higher than that of the Co-flow. This is due to greater gradient in the water mass fraction between anode side and cathode side.

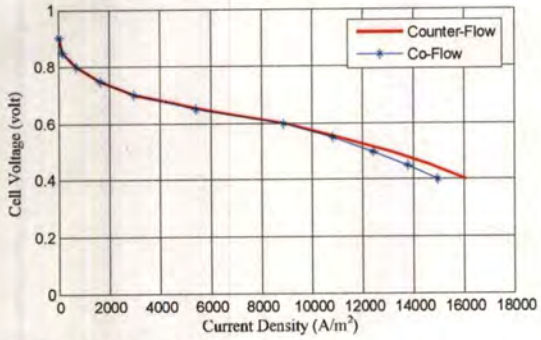

Fig. 11: IV Polarization Curve

The Fig 11 shows the comparison between IV Polarization Curve of Co-flow and Counter-flow patterns throughout the operation range. At low current operating condition, the result suggests that the co-flow pattern gives slightly higher cell voltage than the counter-flow pattern which is not observable from the graph. The effect of flow pattern is insignificant at this low current density range. On the other hand, at high current density, we have found that the counter-flow pattern gives better cell performance than the co-flow pattern. This is because the counter-flow pattern has lower concentration loss at high current density.

4. Conclusion

In this paper, numerical simulation is used as a tool to investigate the water transport in Proton Exchange Membrane Fuel Cell. It includes the study on hydrogen oxygen and water concentrations along the cathode and anode side flow channels. In order to achieve better understanding on the underlying mechanism, the source terms are considered which include reaction heat source, osmotic drag source and back diffusion mass source. It is found that these source terms for the counter-flow configuration are higher than those encountered in the co-flow configuration. Particularly, co-flow and counter-flow patterns were studied at the operating potential. The results showed insignificant effect of flow pattern at low current density. We also found that at high current density the counter-flow pattern had higher cell voltage than co-flow pattern obviously due to the reduction of concentration loss.

5. Acknowledgement

The author would like to thank Mr. Niwat Phoocharoen for well suggestion in using software and thank Electrochemical Materials and Systems Laboratory, National Metal and Materials Technology Center for the software package used in this research.

6. References

1. Barbir, F., "PEM fuel cell theory and practice," California Elsevier Academic Press, 2005.
2. Larminie, J., and Dick, A., "Fuel cell system explained," Chichester John Wiley & Son, 2000.
3. Kumar, A., and Reddy, G., "Effect of channel dimensions and shape in the flow-field distributor on the performance of polymer electrolyte membrane fuel cells," Journal of Power Sources, vol. 113, pp 11–18, 2003.
4. N. Jaruwasupant and Y. Khunatorn "Three-dimensional model and experiment of new flow field for proton exchange membrane fuel cell using CFDRC" International Conference on Green and Sustainable Innovation, November 29th – December 1st 2006 Chiang Mai, Thailand.
5. ZHUGE,W.,ZHANG, Y., MING, P., LAO, X., CHEN X., "Numerical simulation of three-dimensional gas/liquid two-phase flow in a proton exchange membrane fuel cell" Energy Power Eng. China, pp 305-310, 2007.
6. Pil Hyong,L., Sang Seok ,H.,Sang Soon, "Three-Dimensional Transport Modeling for Proton Exchange Membrane(PEM) Fuel Cell with Micro Parallel Flow Field", 2008.